Mechanical and Aerospace Engineering - Dissertations

College of Engineering and Computer Science

12-2012

Building Envelope Wind Pressure Manipulation for Application in Streamlined High-Rise Buildings

Sivaramprasad Sivakumar
Syracuse University

Abstract

This research investigates methods of manipulating building envelope wind pressure distribution for application in the natural ventilation of high-rise buildings. CFD simulations are employed to predict the wind pressure distribution around the building envelope. First, a 2-D CFD study is conducted to explore various techniques of manipulating the building envelope wind pressure distribution. This study indicates that the use of externally mounted flow-resistance devices is an effective method of manipulating the wind pressure distribution. It is demonstrated that this technique is well suited for application to buildings of streamlined cross-section (e.g. elliptical planform). Next, a 3-D CFD study is conducted in order to investigate the performance of the flow resistance device concept applied to a full-scale building. The results indicate that it is possible to significantly alter the pressure distributions at different heights of the building by utilizing continuous resistance devices. Manipulating the wind pressure distribution is shown to confer the ability to control the direction of the airflow exchange (i.e., intake v/s exhaust) in the interior zones of a building. The issue of partially polluted airflow exchange between occupied zones of a building is addressed, and a metric called ASHRAE-Equivalent Airflow is developed to assess the quality of ventilation provided under such conditions. A simple problem is formulated in order to demonstrate the application of this technique for the optimal control of natural ventilation. The results indicate that the resistance device concept may be well suited to meet the ventilation requirements in the building interior, especially when the demand for ventilation is non-uniformly distributed. This technique may be further augmented by allowing for control over the size of ventilation openings. Finally, a brief analysis of various energy consideration related to the application of natural ventilation is performed. It is seen that the energy consumption in a naturally ventilated

building may be minimized by appropriately controlling the amount of airflow exchange depending on the external conditions. In addition, the use of wind turbines mounted on the building periphery could be beneficial as the flow resistance medium device may offset a significant fraction of the electrical energy consumption in the building.

Building Envelope Wind Pressure Manipulation for Application in Streamlined High-Rise Buildings

By

Prasad Sivakumar

B.E., University of Mumbai, 2006

M.S., Syracuse University, 2008

A Dissertation

submitted in partial fulfillment of the requirements for the degree of

Doctor of Philosophy in Mechanical and Aerospace Engineering

Syracuse University

December 2012

Acknowledgments

I would like to begin by expressing my deep gratitude to my advisor Dr. Thong Dang for the immense support and guidance he has provided me during the course of my time at Syracuse University. The various discussions and interactions over these past few years have never failed to be a source of valuable knowledge and insight. His constant support, guidance and motivation are instrumental in my achievements here at Syracuse University and will no doubt continue to serve me well in my future endeavors.

I would also like to acknowledge the contributions of Dr. Harish Palanthandalam-Madapusi. His guidance and enthusiasm helped me make progress on my work and understand aspects of optimization and control, which were new topics for me. I would like to thank Dr. Arsen Melikov for his helpful suggestions regarding the computational analysis of a full-scale building.

I would like to thank Dr. H. Ezzat Khalifa, Dr. Jensen Zhang, Dr. Ed Bogucz, and Michael Pelken for taking the time and interest to sit on my committee. The constructive criticism and helpful insights they've provided over the years have contributed a great deal towards the final form of this work. I would also like to thank Dr. Eric Lui for taking the time to serve as the chair of my committee.

One of the highlights of my time in Syracuse has been working alongside exceptional graduate students. Interacting with them regarding matters both academic and otherwise has been interesting and a source of great pleasure. I would like to thank Ryan Dygert, Jackie Russo, Waleed Abdelmaksoud, and Nhan Phan for the various disccusions over the years and the assistance that they've provided me. I would like to thank Dustin Demetriou

Contents

List of Figures

List of Tables

1 Introduction

Energy consumption in buildings constitutes a large percentage of the total energy usage in the modern world. The buildings sector in the US accounts for approximately 40% of the total energy consumption [1]. A significant portion of building energy consumption is directed towards the cooling, heating and ventilation of interior spaces. According to the US Department of Energy, approximately 40% of the total energy consumption of buildings is directed towards the supply and conditioning of the ventilation airflow. On account of the recent focus on energy efficiency, there has been increased interest in investigating methods to decrease energy consumption in buildings.

Many conventional buildings currently operate on the principle that the whole building should be heated (or cooled) all year round. The drive to reduce energy consumption has led to the investigation of alternative ventilation strategies, such as the use of local heating/cooling when comfort conditions are exceeded, turning off HVAC systems and opening windows when ambient conditions allow for thermal comfort, and implementing hybrid ventilation strategies incorporating sophisticated control systems [2].

Another method for reducing energy use in buildings is by utilizing natural ventilation. For suitable climates, application of natural ventilation can result in significant savings in energy consumption of buildings associated with ventilating interior spaces. In addition, naturally ventilated buildings also have lower capital and operational costs. According to the US Environmental Protection Agency (EPA), sick building syndrome (SBS) is a phenomenon in which building occupants experience adverse health and comfort effects on account of time spent inside buildings. Inadequate ventilation rates, and chemical &

biological contaminants from indoor and outdoor sources have been hypothesized to contribute towards causing instances of SBS. It has been reported that application of natural ventilation can improve the indoor air quality (IAQ) in the interior of a building, and therefore, reduce instances of sick building syndrome (SBS) [3]. This improvement in IAQ has been correlated with improved occupant productivity, which can result in additional monetary savings [4, 5, 6].These factors provide compelling reasons to further investigate application of natural ventilation.

Natural ventilation relies on pressure differences generated across a building envelope on account of naturally occurring phenomena such as wind and buoyancy to drive ventilation airflow through the building. Natural ventilation can be classified into two types depending on the driving forces involved; wind-driven ventilation and buoyancy driven ventilation. Wind driven ventilation is illustrated in Figure 1, which is originally published in [7].
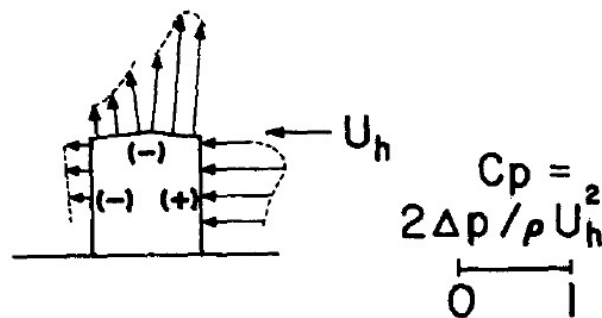
Figure 1: Pressure coefficient distribution for cross-ventilation

The wind pressure distribution on a building facade is determined by factors such as the building shape, wind direction, and the proximity of other buildings. In general, the wind pressure is high on the windward side of a building facade, and it is low on the leeward side. This pressure difference drives ventilation airflow from the windward side to the leeward side of the building. This type of ventilation configuration is known as cross-ventilation.

The second regime of naturally ventilated flows is that of buoyancy (or stack) driven ventilation. As illustrated in Figure 2, temperature differences between the interior and the exterior of a building (or between two interior zones) lead to different hydrostatic pressure gradients.
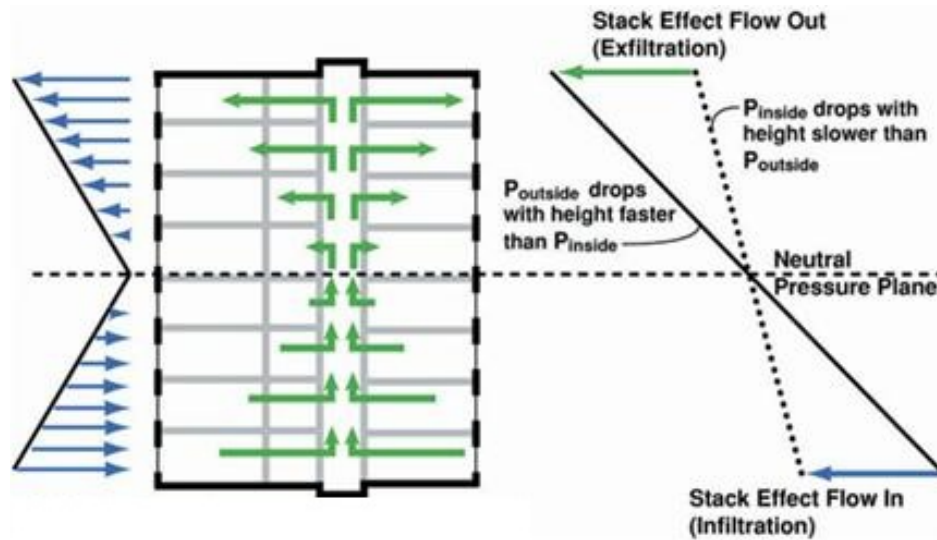
Figure 2: Buoyancy-driven ventilation (image taken from www.buildingscience.com)

This mechanism can be explained as follows. The hydrostatic pressure gradient can be expressed as,

$$\frac{\partial p}{\partial z} = -\rho g \tag{1}$$

where g is the gravitational acceleration, and ρ is the air density, which is a function of the air temperature. Therefore, as the temperature of the air changes (and hence the density), so does the hydrostatic pressure gradient. Hence, if the interior temperature of the building is different from the ambient temperature, the internal and external pressure gradients will be different. Therefore, at different heights along the building, the pressure difference between the interior and the exterior of the building (or between two zones) varies. This

can give rise to airflows from the high pressure side to the low pressure side. The direction of this induced airflow may be reversed along the height of the building.

At certain times during a year, these two flow regimes may both be significant factors influencing the airflow exchange with the ambient. Under such situations, these regimes may either reinforce each other, or they may be in opposition to each other. At other times during the year, one flow regime may dominate over the other (e.g., high wind speed, and small temperature difference between indoor and outdoor).

There are two purposes for which natural ventilation may be employed. The first is for the purpose of achieving satisfactory indoor air quality in the building interior. This is primarily the mode of operation during the heating season, where outside temperatures are low. If the pollutant emission characteristics of a particular indoor environment are known, it is possible to calculate the minimum amount of fresh (outdoor) airflow that needs to be supplied in order to maintain acceptable air quality in a zone. Airflow rates larger than this minimum amount will lead to better IAQ in the building. However, during the heating season, it may be necessary to heat the ventilation air in order to maintain the indoor temperature within acceptable levels. Therefore, bringing in large amounts of airflow may not be ideal on account of the increased energy expenditure to condition this airflow. Hence, under these circumstances, an optimal balance needs to be found between the amount of energy required to condition the ventilation airflow, and the level of IAQ in the building interior. One possible method of defining this balance is by minimizing the amount of energy required to condition the supply airflow, while maintaining a minimum acceptable level of IAQ (e.g., such as that corresponding to a zone ventilated following ASHRAE Standard 62 guidelines).

The second purpose for which natural ventilation is utilized is for maintaining thermal comfort during the cooling season. There are several factors that influence an occupant's perception of thermal comfort such as temperature, humidity, air velocity and levels of clothing. Apart from the occupants themselves, there are various other heat loads within a building such as lighting, computers and other electrical appliances. Under these conditions, the goal of the natural ventilation system is to remove the heat gains within the building and maintain the indoor temperature within the comfort range. When the ambient temperature is near the comfort range, the usual strategy for achieving this goal is by bringing in large amounts of outside airflow. However, care needs to be taken to ensure that the indoor air velocities are not very high, as this will cause uncomfortable draft conditions. Typically, the recommended maximum value for indoor air velocity is 0.8 m/s [8]. Another strategy that is employed for this purpose is night cooling. In this, large amounts of outside airflow are brought in during the unoccupied period (night-time) in order to cool the thermal mass of the building. This thermal mass then acts as a heat sink during the occupied period of the building operation [9].

1.1 Problem Definition

Green buildings are designed to interact with the outdoor environment in order to create an acceptable Indoor Environment Quality (IEQ), both in terms of thermal comfort and Indoor Air Quality [10]. To this end, one of the many important aspects of green building design is the strong interaction between the building envelope pressure distribution and the interior space in the building. In particular, the distribution of IEQ can be a strong function of the "controlled" air leakage distribution between indoor and outdoor along the

building envelope, as the main driving mechanism of the air leakage flow is the local pressure difference between the local outside building envelope and the local indoor pressure level.

The present research is focused on wind-driven natural ventilation. The air exchange between the building interior and the surroundings is determined by the wind pressure distribution around the building envelope. For a given wind speed and direction, the static pressure distribution around the envelope is fixed, and therefore, so is the air exchange pattern with the interior. The amount of intake/exhaust airflow can be varied by changing the sizes of openings to the ambient; however, the distribution pattern of the airflow cannot be changed. In many situations, it may be desirable to change the distribution pattern of the indoor airflow. For example, changing occupancy patterns within the occupied zones of a building dictate that the amount of airflow supplied to different zones vary with time. It may not be possible to satisfy such changing ventilation requirements given a particular fixed wind pressure distribution. It is therefore useful to have the ability to manipulate the wind pressure distribution around the building periphery, based on the occupancy.

For the purposes of this research, the underlying assumption is that the wind pressure is the dominant factor driving the ventilation flow, and that the effect of buoyancy is not significant. In order to judge the validity of this assumption, it is first necessary to quantify the conditions under which the stack effect is negligible. This may be determined by using the dimensionless parameter known as the Archimedes number, defined as,

$$Ar = (g\beta)\left(\frac{H\Delta T}{U_\infty^2}\right) \tag{2}$$

where g is the gravitational acceleration (m/s^2), β is the thermal expansion coefficient of

air $(1/K)$, H is the stack height (m), ΔT is the prevalent temperature difference (K), and U_∞ is the ambient wind speed. If the Archimedes number is of the order of 1 or larger, then this means that the effects of buoyancy cannot be neglected.

Figure 3 shows variation of the Archimedes number with wind speed under conditions of different temperature differences, for two stack heights. For a stack height of 10 m, it can be seen that even for conditions that favor buoyancy (i.e., large temperature difference and low wind speed), the Archimedes number is relatively small ($\sim$ 0.3), and therefore, the effects of buoyancy may be neglected. As the wind speed increases, the effects of buoyancy become increasingly negligible, as indicated by the small values of the Archimedes number. For a stack height of 100 m, it is seen that the effects of buoyancy are much more significant. For a temperature difference of 10 K, and a wind speed of 3 m/s, the Archimedes number is approximately 3.5, which means that buoyancy is very important in determining the flow field. Even though the Archimedes number decreases as the wind speed increases, for this stack height, it may still not be appropriate to neglect the effects of buoyancy for large temperature differences.
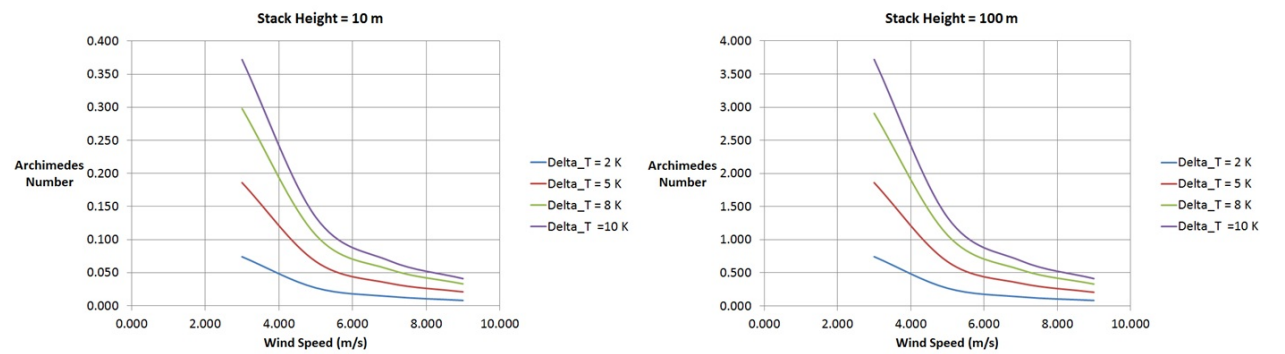
Figure 3: Variation of Archimedes number with wind speed)

Therefore, in situations where the temperature difference and stack height are relatively

small, the effects of buoyancy likely to be small in comparison to those of the wind. Further justification for this statement is provided in section 3.4, where the potential for building envelope wind pressure manipulation is discussed. In addition, if the internal heat gains in a building are small (e.g., residential building), then the temperature difference between the ambient and the interior is not likely to be very large. Furthermore, in some existing naturally ventilated buildings, the designers have isolated blocks of floors vertically from each other in order to reduce the effective stack height, and thus reduce the magnitude of the stack pressures. This is done with the intention of diminishing the risk of potentially strong updrafts, however, the same principle can be applied to ensure that wind-driven ventilation is the predominant mode of ventilation.

Therefore, in some applications, there is justification for the assumption that wind pressure can be taken to be the sole factor driving airflow across the building envelope. Accordingly, we are then interested in investigating how we can use this resource effectively to satisfy ventilation requirements that are dependent on the demand. The primary goal of the ventilation system considered is maintaining acceptable IAQ within the building interior, i.e., the building is assumed to be operating in the heating season, where relatively small amounts of airflow are brought in from the ambient in order to minimize the energy expenditure involved in conditioning the supply airflow.

The goals of this research can then be presented as follows:

1.2 Research Objectives

1. Investigate techniques of manipulating building envelope wind pressure distribution around standalone high-rise buildings of streamlined cross-section.

2. Apply technique to study how the airflow distribution in naturally ventilated buildings may be controlled.

For the first research objective, Computational Fluid Dynamics (CFD) simulations are performed to investigate various possible techniques for manipulating building envelope wind pressure distribution. First, preliminary 2-D simulations are conducted to study different techniques and investigate the effect of various relevant parameters on the envelope pressure distribution. This is followed by a 3-D CFD study of a full-scale building where the effect of a particular pressure manipulation technique is studied in detail.

For the second objective, the multi-zone modeling software CONTAMW is used to simulate the airflow and contaminant distribution with the building interior. Changes in the airflow distribution resulting from the modification of the building envelope pressure distribution are studied, and the utility of the concept is gauged. Simple optimization routines (using MATLAB) are performed in order to obtain "optimal" solutions to various ventilation configurations. It should be noted that the scenarios considered are assumed to be quasi-steady. This means that changes in internal/external conditions occur much more slowly than the time taken to setup a new ventilation configuration. In addition, the effect of the thermal mass of the building is assumed to be small.

It should be emphasized that the use of the word "control" in this objective does not refer to the use of classical control techniques per se. Instead, this work should be understood as

an exploratory investigation of how building envelope pressure manipulation may be used for the purpose of manipulating the airflow distribution in a naturally ventilated building.

1.3   Roadmap

The structure of this thesis is as follows. In chapter 2, existing work related to wind-driven ventilation and the control of natural ventilation is reviewed. In chapter 3, we discuss various potential means of manipulating building envelope wind pressure distribution and their associated advantages and drawbacks. This is followed by a detailed examination of the resistance device pressure manipulation technique, in 2-D as well as 3-D. In chapter 4, we examine how this concept impacts the airflow distribution in the interior of a building, and how this may be useful for the purposes of natural ventilation. We also assess the influence of inter-zonal partially polluted airflows with a building, and develop a metric that allows us to quantify the quality of ventilation provided in a naturally ventilated building. A simple control problem is also explored in order to demonstrate the utility of this concept. In chapter 5, we discuss various issues related to the topic of energy consumption for natural ventilation. We also discuss the potential for energy extraction by the use of building mounted wind turbines. Finally, the main conclusions of this work are stated in chapter 6, and potential avenues for further research are discussed in chapter 7.

2 Literature Review

2.1 Current implementations of natural ventilation

Traditionally, natural ventilation systems have been used in residential buildings, and low-rise office buildings, schools etc. There are several examples of application of natural and hybrid ventilation in office buildings, particularly in Europe. The application of such techniques to high-rise buildings has historically been limited. Recently however, there has been increased interest in the application of energy efficient ventilation strategies in high-rise buildings, and there have been a number of high-rise buildings built that either are purely naturally ventilated or use natural ventilation for a significant portion of the year, as part of a hybrid ventilation ("mixed-mode") system.

An example of such a building is the Swiss Re Building (30 St. Mary Axe) shown in Figure 4(a), located in London. This 41 story building utilizes a hybrid ventilation scheme, in which the cooling needs of the building are designed to be met by natural ventilation for 40% of the year. The natural ventilation for this building is primarily wind-driven. The building is divided into a number of zones, which can be naturally or mechanically ventilated independent of each other, depending upon the ventilation requirements. It is estimated that the energy consumption is about half that of conventionally air-conditioned office towers of similar size.

The Commerzbank headquarters (Figure 4(b)) located in Frankfurt is another example of a mixed-mode building. This 50 story building has been designed to utilize natural ventilation for at least 60% of the year. The building has a central atrium that rises from
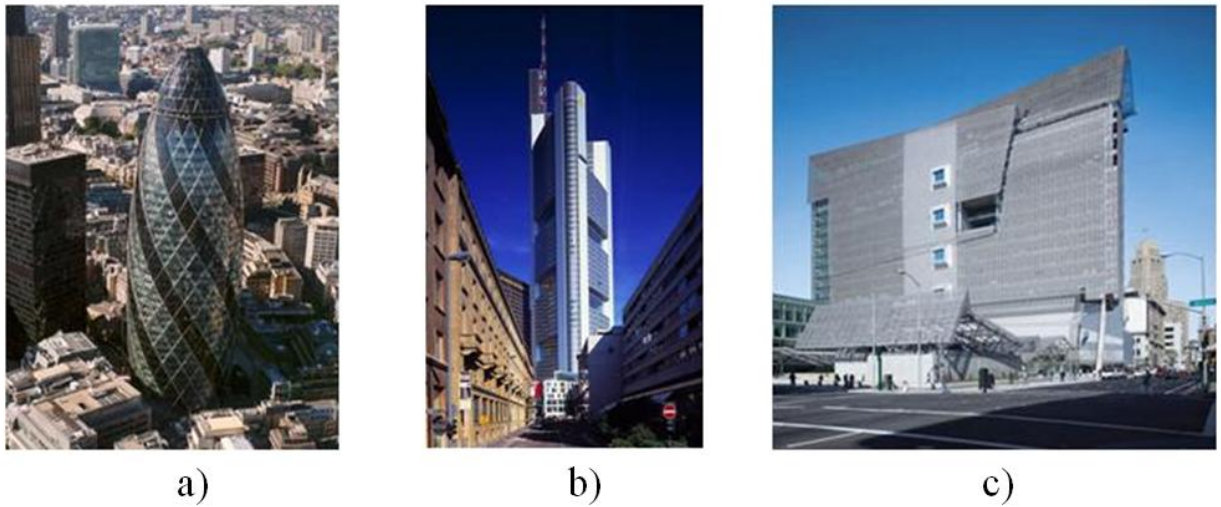
Figure 4: Examples of natural/mixed-mode buildings: (a) Swiss Re Building, London (b) Commerzbank Tower, Frankfurt (c) Federal Building, San Francisco

the ground to the top of the building, and therefore, the stack effect plays an important role in the natural ventilation system for this building. However, in order to reduce the powerful updrafts that may be generated on account of a single unbroken column (as this could cause discomfort to the building occupants), the atrium is divided into 4 segments of 12 floors each. The ventilation air enters each of the spaces at the lower end on the windward side, and exits through openings on the leeward side at the upper end of each section. Etheridge and Ford [11] also recommend such segmentation as desirable in implementation of natural ventilation systems for tall office buildings. The San Francisco Federal Building (Figure 4(c)) is an example of a fully naturally ventilated building. The mode of ventilation is wind-driven cross-ventilation, which is aided by the high aspect ratio of the building footprint (105 m x 19 m). The shallow depth (relative to its width) of this building also allows for sunlight to penetrate well into the building interior, allowing for natural day lighting, which is another favorable aspect of naturally ventilated systems.

Typical characteristics of NV and mixed-mode buildings are described in a report by the Center for the Build Environment [12]. NV buildings typically have a narrow depth, which allows for better cross-ventilation, as well as penetration of sunlight. The windows used in such buildings are small in dimension, and may be operable by the occupants. Ventilation airflow rates may be high during the cooling season, and small in the heating season while meeting IAQ requirements. The same paper notes that based on simulations, it has been reported that the energy savings for a hybrid ventilation system may range from 13% to 79% based on the prevalent climate in the building location (compared to a conventional building).

The buildings discussed above are all located in regions of temperate climate. Natural ventilation is best suited for application under such conditions. However, even in regions where temperature extremes are present, it may still be possible to utilize natural ventilation during certain periods over the course of a year when the outside temperatures are moderate (e.g., fall/spring) [12]. Natural ventilation may be least suitable for locations with climates where high humidity may be a concern. Studies have been conducted to investigate the potential suitability of climates for application of natural ventilation, and try to formulate methods that can help assess this suitability. An example of such a method is one that was developed as part of the URBVENT project [13]. This technique estimates the potential for free-cooling available at the building site, and compares it to specific reference sites (where natural ventilation suitability is known a priori).

DeDear and Brager [14] discuss the implications of revisions to ASHRAE Standard 55 made in 2002, which relate to issues of thermal comfort in buildings. Older versions of the standard recommended that the temperature be maintained within certain strict limits to

ensure the thermal comfort of the occupants. It was usually not possible to satisfy this goal without the use of a conventional HVAC system, even in temperate climates. In developed countries such as the U.S, there is widespread adoptance of conventional HVAC systems, which aim to maintain indoor temperature levels within a narrow range. However, the authors discuss several studies which indicate that in naturally ventilated buildings, occupants are willing to accept, and may in fact, prefer a wider variation in the indoor temperatures. This is especially the case in other parts of the world (e.g., Europe, developing countries), in which the use of conventional ventilation systems is not as widespread as in the U.S. In these countries, people may have control over their local environment (e.g., operable windows) and may therefore, be willing to tolerate a larger range of temperatures. In fact, higher temperatures may be desirable as long as there is some breeze flowing. For example, the authors report the results of a Danish study in which it was found that for a fixed air speed of 0.2 m/s, the occupants in a particular building preferred an indoor temperature of 28º C, as compared to 26º C. The perception of thermal comfort is not determined solely by fundamental physics and human physiology, and the psychological factors influencing it are not well understood. Therefore, this prompts the use of an adaptive thermal comfort standard, as adopted in ASHRAE Standard 55, which allows for higher indoor temperatures in naturally ventilated buildings in summer, as well as in warmer locations. Nicol and Humphreys [15] also discuss this issue and make similar recommendations.

However, there remain questions about the suitability of natural ventilation for North American climates. Axley and Emmerich [16] have developed a technique to analyze the suitability of a given climate for natural ventilation. Based on a steady-state analysis of the heat balance within occupied buildings, they estimate the portion of a year when the

outdoor temperature allows the use of natural ventilation such that thermal comfort requirements are met. They performed this analysis for a number of climatic conditions in North America, and they indicate that it may be possible to use natural ventilation in many areas in North America for a large percentage of the year. In particular, it has also been reported that coastal California is well suited for application of natural ventilation on account of its climate [17].

Emmerich and Crum have conducted a simulation study comparing the performance of natural, purely mechanical, and hybrid ventilation systems in office buildings located in different climatic regions around the U.S. (namely, Boston, Los Angeles, Miami, Minneapolis and San Francisco). [18]. A building model was developed in CONTAMR, a multi-zone modeling program used for conducting the simulations. Different control strategies for the ventilation systems were considered, and the effect on overall performance as well as energy consumption was investigated. The results of the simulations indicate that the natural ventilation system works best in San Francisco, where both thermal comfort and IAQ requirements are met with minimal requirements for conditioning (heating) the supply airflow. The performance of the NV system was not as good in Los Angeles, Boston and Minneapolis, leading to high temperatures in Los Angeles, and high energy requirements for conditioning the supply airflow in the latter two cities. The NV system performed very poorly in Miami, as for a large percentage of the year, the temperatures in the building were well above the thermal comfort range, and the humidity levels were high.

Heiselberg has discussed the effects of parameters such as pressure distribution on external surfaces, airflow exchange with the ambient as well as between zones in the context of hybrid ventilation [19].

The Natvent study conducted in several European nations aims to reduce energy consumption in buildings by providing solutions to problems commonly encountered in the application of natural ventilation. Liddament et al. discuss various case studies involving buildings surveyed in this study that use natural and hybrid ventilation in a variety of climatic locations, while identifying shortcomings and suggesting possible remedial actions [20]. In order to ensure energy efficient ventilation is provided while maintaining acceptable IAQ, they make several recommendations such as implementing demand control ventilation, minimizing pollutant sources, increasing building envelope airtightness to minimize infiltration and to reduce amount of ventilation airflow provided during non-occupancy periods. They also emphasize the importance of reducing solar heat gains and efficient incorporation of thermal mass in order to maintain thermally comfortable conditions indoor. Common problems encountered in naturally ventilated buildings included overheating in the occupied spaces due to improper estimation of the thermal heat loads, faulty control strategies (e.g., winter heating left on during the summer), outdoor pollution and noise, and operational faults associated with control actuators.

Pasquay studied the performance of three naturally ventilated buildings with double façades in Germany over the period of a year [21]. He concludes that it is reasonable to employ natural ventilation in buildings with such façades, and that they can indeed realize energy savings. In addition, he states that completely naturally ventilated buildings may be possible, as long as one is able to accept a few days where the indoor and outdoor temperatures are approximately the same, which may not be ideal for thermal comfort.

Ring and Brager have conducted a survey of three office buildings in California which employ conventional HVAC systems, and in addition, allow occupant control over window

openings [22]. They report that granting control over the openings allows for an improved perception of air quality within the occupied spaces. According to them, the occupants also reported an undesirable increase in the levels of outdoor noise and air pollution.

2.2 Wind driven natural ventilation

There have been extensive efforts dedicated towards characterizing the effect of wind on building façades and wind-driven ventilation. A lot of work has been dedicated towards studying wind driven natural ventilation by performing wind tunnel studies of building models. These studies typically aim to characterize the distribution of the wind pressure coefficient C_P over the building surface. C_p is defined as,

$$C_P = \frac{P - P_\infty}{\frac{1}{2}\rho V_\infty^2} \tag{3}$$

where P is the static pressure measured at a particular point on the building surface, P_∞ and V_∞ are the reference pressure and reference velocity measured well upstream of the building model, and ρ is the air density. The building model is usually placed on a rotating platform so that the effect of different wind incidence angles can be studied.

Examples of such studies can be found in [7, 23, 24, 25]. While such studies can give an idea about the range of ventilation rates that can be induced, it should be noted that these studies fail to give any details about the flow pattern within the interior of the building. It is important to locate window openings appropriately on the building envelope in order to maximize the potential for wind-driven ventilation and thermal comfort [26]. Different

window opening configurations give rise to different air distribution patterns in the interior, and this can result in varying Indoor Environmental Quality (IEQ) in the building interior [27].

Using the data from such experiments, flow rates across the building envelope are related to the incident wind speed and direction, typically, using a power-law equation of the form,

$$Q = C\left(\Delta P\right)^{n} \tag{4}$$

The above relation relates the pressure differential across an opening to the flow rate through it [28, 29, 30]. By varying the coefficient and the exponent, this form of equation can be used to determine the flow rate across small, crack-like openings in the building envelope as well as larger openings, such as custom-provided ventilation ports. Equations of this type are used to model airflow elements in multi-zone modeling software packages such as CONTAMW, COMIS, AIOLOS etc.

Theoretically, the exponent in Equation 4 should lie between 0.5 and 1. An exponent value of 0.5 is used when the flow across an opening is turbulent, while a value of 1 is used when the flow is laminar [3, 31]. Typically, the value of the exponent is chosen to be approximately 0.65 [28, 31, 32]. These equations do a reasonable job of predicting the airflows across small openings in the building envelope, cracks etc. However, when applied to large openings (such as doorways), when the effect of thermal stratification is important, the results can be inaccurate.

In CONTAMW, this type of equation is used to model one-way flow through openings [32].

If two zones at different temperatures are connected by a large opening, then, on account of the stack effect, a positive pressure difference may exist at the top of the opening and there may be a negative pressure difference at the bottom (or vice-versa). The two-way flows associated with such large openings make it difficult for power-law equations of this type to model the flow accurately. In situations where the zones under consideration are approximately isothermal, two-way flows induced may be small, and therefore, the prediction error associated with using these models may be reduced.

In the present work, the ventilation openings under consideration in the model are not large openings (such as typical windows). Such openings are impractical for implementation in high-rise buildings on account of the high wind pressures likely to be experienced, along with safety issues. Instead, the openings are assumed to be similar to the ventilation ports shown in Figure 5 (originally published in [33]), which are found in the Uptown München tower located in Munich, Germany. These ports are much smaller than conventional windows, therefore, the power-law equation discussed previously may be suitable to model the airflow through such openings.

As mentioned previously, an important factor affecting the amount of airflow induced is the incident wind direction. For example, if the wind is aligned normal to the major axis of a streamlined building, it is trivial to set up a cross-ventilation flow pattern as one side of the building envelope is at a higher pressure as compared to the other side (see Figure 1). For such wind-driven cross-ventilation, it should be noted that there is little control over how the airflow is distributed in the interior, that is, it is difficult to control which zones receive airflow from the ambient, and which zones exhaust airflow to the ambient. However, when the wind is at small angles relative to the major axis, then the driving wind pressure

Figure 5: Examples of ventilation ports in the Uptown München tower

differences between opposite sides of a building are likely to vary along the length of the major axis in both magnitude and direction in a significant way. In this case, it may be necessary to utilize techniques to vary and/or reverse this pressure difference in order to provide the required ventilation airflow. Self-regulating inlet openings, in which the opening areas change according to the local pressure difference, are therefore very useful to ensure reliable performance in naturally ventilated systems. Regardless of wind direction, when wind speeds become low, the ventilation airflow rates will decrease accordingly. Therefore, this is often considered as a worst-case scenario when considering wind-driven ventilation. However, Axley reports that a few studies indicate that such very low wind speed scenarios are not only infrequent at many locations, but that even if they do occur, the duration of low wind speed is small [34]. Similarly, Linden also states that considering worst case scenarios may lead to placing unnecessarily stringent demands on buildings, which may not necessarily be reflected in real-life situations [35].

Irwin et al. discuss various methods by which the wind loading on tall buildings may be reduced [36]. Their primary motivation is to reduce the structural demands on the building façade resulting from the incident wind. They recommend softened (more aerodynamic) corners, tapers and setbacks as effective techniques to mitigate vortex shedding and the resultant stress on the building frame. They also discuss the utilization of high wind speeds typically present at higher floors of the building to implement wind driven natural ventilation. They concede that the induced wind pressure may far exceed the pressure required to provide adequate ventilation, however, they state that this may be offset by utilizing smaller openings to the ambient and/or double-skin façades. Under such circumstances, it may be beneficial to be able to reduce the magnitude of the pressure loading on the building envelope.

There has been a lot of effort dedicated to understanding the interaction of wind and buildings. Though large sections of the literature deal with characterizing wind pressure distribution on building façades, manipulating the wind pressure distribution is a subject that has not been addressed in the literature. Such manipulation of wind pressure distribution can be potentially advantageous when dealing with variation in wind direction and ventilation demands. Another potential application of such techniques is the control of structural load, which is not addressed here. The aerospace industry has long used methods of circulation control to manipulate the pressure loading on airfoils, and in principle, the problem of building envelope wind pressure distribution is a similar problem, for certain types of buildings.

2.3   Ventilation Control

There is a substantial body of work related to development of efficient control strategies for conventional ventilation systems. In recent years, there has been an increased focus on control of natural (and hybrid) ventilation systems. Aggerholm discusses the implementation of hybrid ventilation systems in several European buildings [37]. He reports that hybrid ventilations systems can maintain satisfactory indoor environmental conditions provided that appropriate control techniques are applied. These control strategies may either be implemented using a centralized controller, or alternatively, appropriate control actions can be performed by the occupants to change the local conditions as desired. However, he recommends that there should be an option for an occupant to override the actions of the automatic controller in order to maintain the required local environment. He reports that it may be possible to achieve satisfactory performance by allowing for occupant control in individual offices, but for open floor plan offices (and during non-occupied hours), it is essential to have an active control system. Carrilho da Graça et al. described the development of a control strategy for the naturally ventilated San Francisco Federal Building [38]. The system implemented employs a rule-based control logic that controls window openings based on the prevalent weather conditions.

Mahdavi and Proglhof [39] have discussed the implementation of a model-based control system for natural ventilation. They developed an empirical relationship between the number of air changes per hour in a test chamber and the opening size of a window located in the chamber based on a small number of test measurements. This model was then used to simulate the performance of an office room under varying outdoor conditions and the results were compared to airflow rate measurements from the room. They report that the

relative difference between the measured and simulated airflow rates was between 25%-40%. They state that the error may be reduced by increasing the size of the sample data set that was used to develop the empirical relationship.

The use of model-predictive control has also been investigated for optimal control of heating systems and thermal comfort [40, 41, 42]. Other approaches for dynamic control include the use of fuzzy logic controllers for the purpose of optimal control of both natural and conventional ventilation systems [43, 44, 45, 46]. Kolokotsa et al. [47] have developed a state-space model using system identification methods in order to use predictive control techniques. Dounis and Caraiscos [48] have written a comprehensive review of the current control methods implemented in building management systems.

Ward et al. state that the linear, time-invariant (LTI) models commonly found in conventional building control systems are not well suited for application in buildings where natural ventilation is widely used [49]. They propose an alternative scheme where a model based on physical principles is used as the basis for non-linear, data driven system identification. This identified model is then used by an optimization process to determine the control action that will best satisfy the control objectives.

An important factor impacting the thermal comfort of occupants in the building is the actions taken by the occupants themselves in the shape of opening or closing of windows. If an occupant is placed in a situation of thermal discomfort, given the option, he will take an action so as to remedy the situation. Rijal et al. investigated the effects of window adjustment on the thermal conditions within the building interior [50]. An adaptive algorithm for controlling window position was developed by observing occupant behavior. Applying this simulation to a simulated office indicated the possibility for improved thermal

comfort, reduced occupant window adjustment and reduced heating energy consumption.

Model-predictive control is a technique that has been applied for the control of both conventional and naturally ventilated buildings. This method involves the development of a building model to predict the future behavior of the indoor environment, thus allowing the evaluation of possible ventilation strategies. For example, the relationship between window opening size and the airflow through it would be a suitable model for someone seeking to control the amount of airflow received by space. The model can be a mathematical formulation of the system behavior, a simulation-based model, or alternatively, the model can also be derived by analyzing existing data related to building performance and extracting a model (e.g., training a neural network).

There are two challenges with developing an optimal control system for natural ventilation. First, to determine optimality, an objective function or performance metric that captures the goals of the ventilation is needed. Although this issue has been addressed to some extent in the literature [51, 52], this is still largely an open area of research. Second, in natural ventilation, due to significant inter-zonal airflows, control decisions cannot be made separately for each zone. Instead, the control problem must be treated as a centralized coupled control problem for the whole building. Accounting for the effect of the coupled inter-zonal airflows in the control decision-making process is challenging and has largely been ignored in existing control strategies. In addition, most existing control strategies for natural ventilation focus on thermal comfort and do not consider indoor air quality (IAQ), or alternatively, consider IAQ as a constraint (i.e., provide a minimum acceptable ventilation level). Although this approach is feasible in mild weather conditions as large amounts of outdoor air can be brought into the building and thus IAQ is not a concern, in

cold weather conditions only a small amount of air can be bought into the building and hence IAQ must also be considered. IAQ is also a concern at times when the outdoor air is polluted.

3   Concept Evaluation using CFD

In this section, methods of manipulating the building envelope pressure distributions for a
family of building geometries are discussed. In particular, the focus is on building
geometries that have curved surfaces (e.g. circular and elliptical shapes), allowing for the
use of "circulation" control techniques to manipulate the envelope pressure distribution.
Buildings with "aerodynamic shape" (e.g. elliptical shape) are the best suited for the
application of circulation control technique. Building shapes with sharp corners (e.g.,
rectangular and square shapes) where the flow separation points are fixed at the 90-degree
corners do not belong in this category.

3.1   Exploration of Pressure Manipulation Techniques

The flow field around tall buildings in the presence of wind can be treated as an
aerodynamic problem around bluff bodies (e.g., cylindrical/square shapes) or streamlined
bodies (e.g., elliptical shape) [7]. Manipulation of the pressure distribution around
streamlined-body shapes to control lift (force normal to wind direction) and drag (force
parallel to wind direction) and flow separation have been exploited by the aerospace
industry for decades by both semi-active (e.g., mechanical flaps/slats) and active (e.g., flow
blowing/suction) flow-control techniques. For example, the flow field around a cylinder can
be manipulated via flow control techniques.

Figure 6 shows several streamline patterns around a cylinder which are altered using
synthetic (zero net mass flux) jets [53]. In this figure, the flow is from right to left. A
synthetic jet is a periodic blowing/suction scheme with a small and zero net mass flux
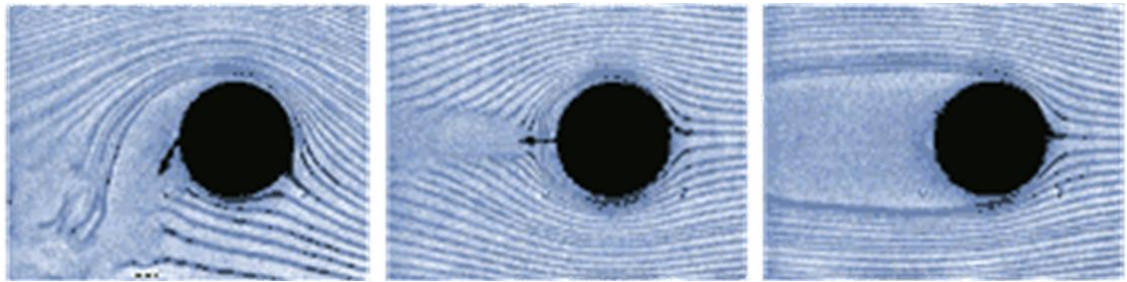
Figure 6: Flow around cylinder with flow control

applied at a proper frequency. The flow pattern on the right is the case without any flow control, showing a large separated region behind the cylinder. The case in the middle is with a synthetic jet pointing in the horizontal direction, and the streamline pattern looks much like that of an ideal fluid, i.e., there is no flow separation at the rear of the cylinder. Finally, the case on the left is with a synthetic jet pointing downward, and the streamline pattern corresponds to a flow around a cylinder with circulation. These figures clearly show that the streamline pattern around a cylinder can be manipulated to modify the pressure loading around the circumference. Therefore, this may be a potential method for controlling the wind pressure distribution around a building of circular cross-section. However, it should be noted that this method requires an external power source in order to energize the jet of air. In addition, this technique may not work in scenarios where the wind has large random fluctuations.

Next, consider the case where the building indoor air distribution is designed to depend on the magnitude of the building envelope pressure loading, which is not adequate when the wind speed is below a certain value. Another method to handle such a scenario is to employ the so-called Coanda-jet flow control technique (steady flow blowing). Figure 7 shows the streamline pattern around the building with a Coanda jet applied at the trailing edge with a wind blowing in the horizontal direction, which is originally published in [54]. It can be

seen that the streamline pattern is drastically modified, and a large pressure differential is created across the two sides of the building, which may then be adequate for satisfying the building air distribution demands. Note that in the case of no blowing, the streamlines would be symmetrical around the horizontal line and the pressure loading would be zero.
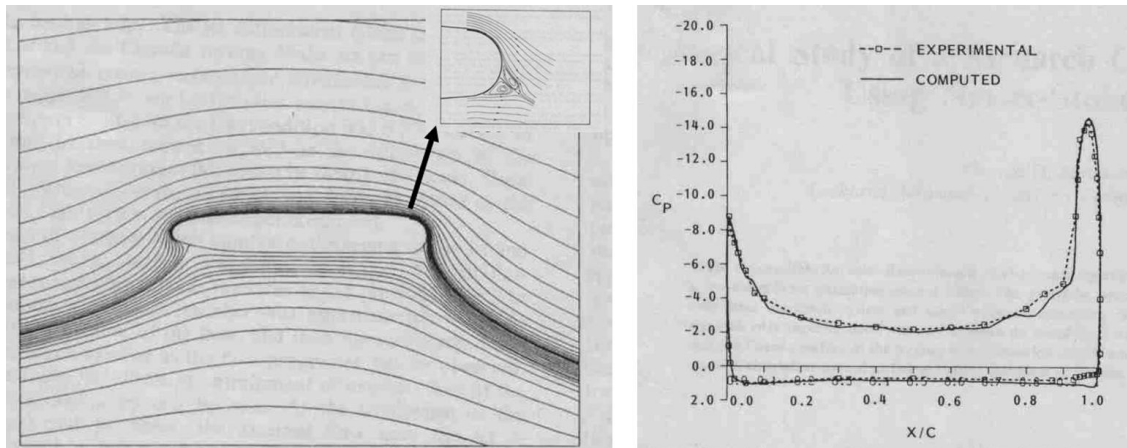
Figure 7: Building envelope pressure loading with Coanda jet

In buildings where natural ventilation is employed, blowing and suction are already present in the system. Specifically, air infiltration through controlled leakage (e.g. windows and small openings) can be interpreted as discrete (single opening) or continuous (several opening) suction holes, while the exhaust air (i.e. usually on the order of one air change per hour (ACH)) can be energized to provide high-momentum blowing for flow control purpose. It is clear that one may be able to manipulate the building envelope flow field by properly controlling these blowing/suction holes by altering their flow areas (or by opening/closing). It should be noted that for the amount of airflow intake/exhaust considered here (i.e., on the order of 1 ACH), the effect of blowing/suction will not affect the envelope pressure distribution unless the stream of air is sufficiently energized. This is especially the case when the wind speeds are high (~ 10 m/s) as is the case in the present research. Therefore, the processes of air intake/exhaust associated with natural ventilation

do not affect the pressure distribution around the building perimeter at the airflow rates considered in this work.

An important parameter which measures the strength of blowing is called the jet momentum coefficient (C_μ), and is defined as,

$$C_\mu = \frac{\dot{m}_j V_j}{\frac{1}{2}\rho_\infty V_\infty^2 C} \qquad (5)$$

where ρ_∞ indicates the density of the free-stream air, V_∞ is the free-stream velocity, $\dot{m}_j$ is the mass flow rate of the jet (per unit width), V_j indicates the jet velocity and C is the chord length of the building.

Dimmock has conducted a study investigating the effectiveness of jet flaps in manipulating the pressure distribution around a 12.5% thick elliptical cross-section airfoil [55]. A jet flap is a stream of energized air which is blown from a slot at the trailing edge of an airfoil. As the elliptical section is symmetrical, the pressure distribution over its upper and lower surfaces is the same at zero angle of attack. Figure 8 presents the variation of the lift coefficient with the jet momentum coefficient as reported in this study.

Dimmock reports that using the jet flap technique with a jet momentum coefficient of around 0.02 causes a pressure loading of the order of 1 wind dynamic pressure to develop across the upper and lower surfaces. Therefore, this technique may be feasible to introduce a pressure loading across similar building cross-sections. As mentioned previously, the ventilation air that is exhausted can potentially be used for flow blowing purposes. It is then of interest to investigate the scenarios under which this technique may be feasible. As
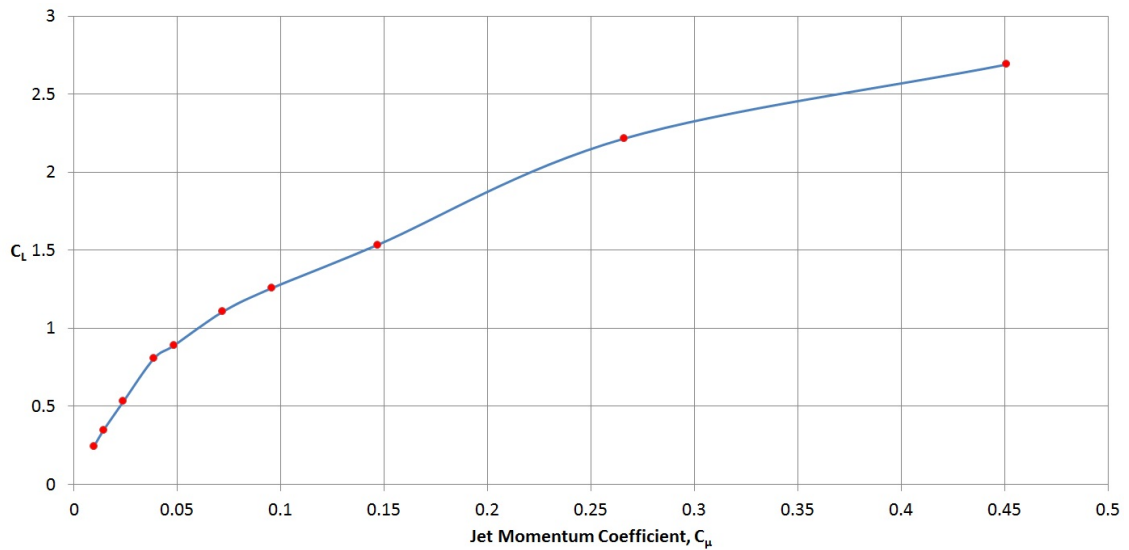
Figure 8: Variation of lift coefficient with jet momentum

a preliminary calculation, assume that the rate at which the air is exhausted into the surrounding is equivalent to 1 ACH (based on a cross-sectional area of 785 m^2, and a 3 m ceiling height). It is then necessary to calculate how the jet velocity should vary as a function of wind speed, in order to obtain a particular jet momentum coefficient. Figure 9 shows the variation of the jet momentum coefficient as a function of the jet velocity, for different wind speeds.

It is seen that for wind speeds of around 1-2 m/s (2.2-4.5 mph), the jet velocity required to obtain a jet momentum coefficient of 0.02 is not very high. For such low wind speeds, it is potentially feasible to obtain much larger values of C_μ, which can lead to significant pressure loading being developed across the building envelope. Therefore, this method may be useful for the purpose of increasing the amount of ventilation airflow provided under low wind speed conditions, where the driving wind pressure is insufficient to meet the ventilation requirements. However, as wind speeds increase, the jet velocity required to obtain even a coefficient of 0.02 becomes very high. The power requirements for the
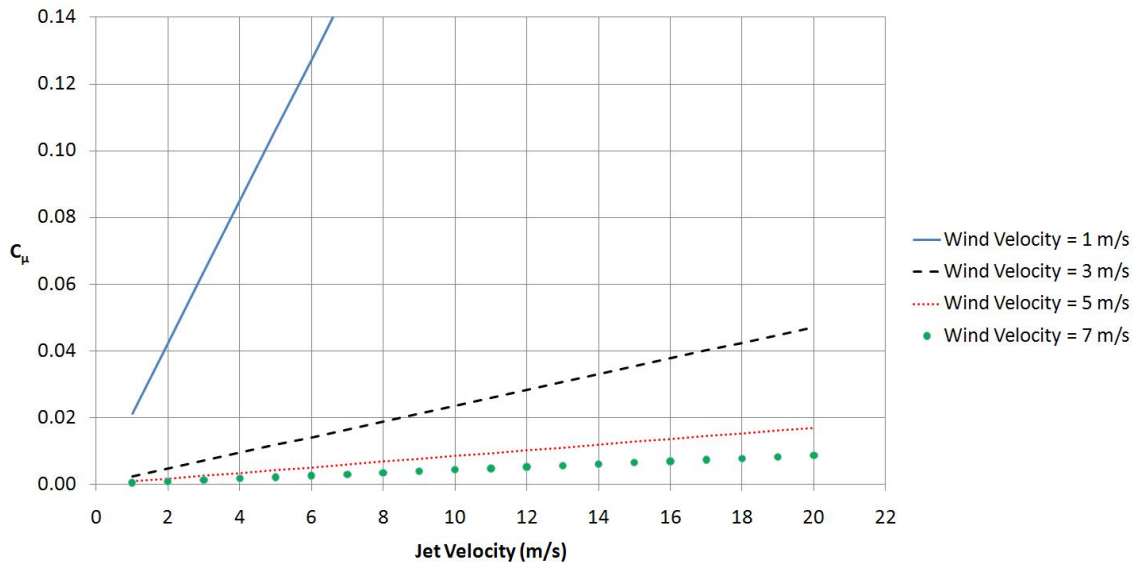
Figure 9: Variation of jet momentum coefficient with jet velocity

purpose of energizing this air will become prohibitively large, and hence, this technique will not be useful under high wind conditions.

A promising technique to manipulate the building envelope static pressure distribution is the use of flow resistance devices. Flow resistance devices can range from simple implements like screens and meshes to complicated devices such as Vertical Axis Wind Turbines (VAWT). Such devices have the effect of removing energy from the wind, which in turn alters the building envelope static pressure distribution. It should be noted that mounting VAWT's around the building perimeter also allows for harvesting energy from the wind, which may be used to offset a part of the building energy consumption. Figure 10 illustrates a proposed concept for integrating VAWT's in a building of streamlined (elliptical) cross-section (This concept is discussed[56]).

These VAWT's (an alternative option is the use of screens) can be mounted on rails so that they may be moved around the building perimeter to locations where they may have the

Figure 10: Concept illustrating integration of VAWT's in a streamlined building

desired impact on the envelope pressure distribution. Alternatively, many such devices may be fixed at multiple locations, but with the provision that they can be made inactive (e.g., by moving them into the building interior or by varying the flow resistance).

There are a few examples of building integrated wind turbines in full scale operation. A notable example of building integrated wind power technology is the World Trade Center building in Bahrain, shown in Figure 11. This building consists of two towers, connected by three bridges. A horizontal axis wind turbine (29 m in diameter) is attached to each bridge. The buildings are designed in such a way that the airflow between them is accelerated as it passes through the gap between the buildings, which allows for greater extraction of energy from the wind. It is estimated that these turbine can provide 10-15 % of the total electrical power consumption of the buildings.

Another prominent example of building mounted wind power techniques is the Pearl River

Figure 11: World Trade Center Building, Bahrain (image taken from www.popsci.com)
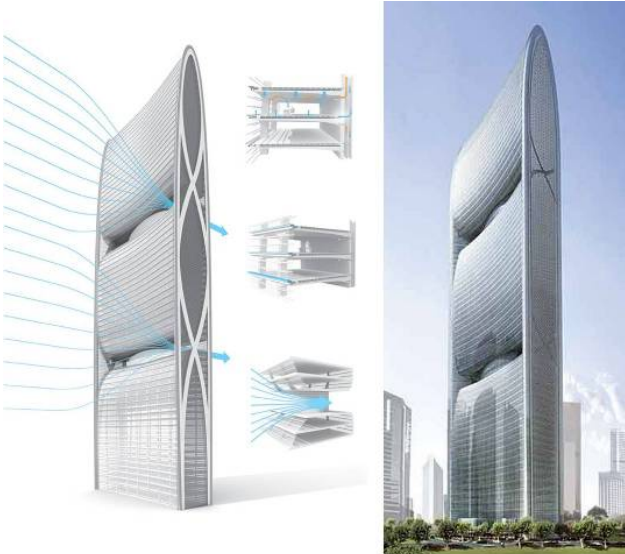
Figure 12: Pearl River Tower, Guangzhou (image taken from www.plusultratech.com)

Tower in Guangzhou, China, seen in Figure 12. This 310 m tall building has four vertical axis wind turbines located in the central space, which is again shaped in such a way that the incoming flow is accelerated. In addition to wind power, this building also incorporates photo voltaic cells for producing solar power. As part of a design study, Land discusses several possible strategies for integration of wind energy harvesting techniques in buildings[57].

3.2   CFD model information

For the first task of the problem description, the feasibility of manipulating the wind pressure distribution on a building envelope is investigated. For this purpose, Computational Fluid Dynamics (CFD) is used to model the aerodynamics of building cross-sections. In this section, the CFD model used to evaluate the performance of the resistance device concept is described and preliminary results are presented.
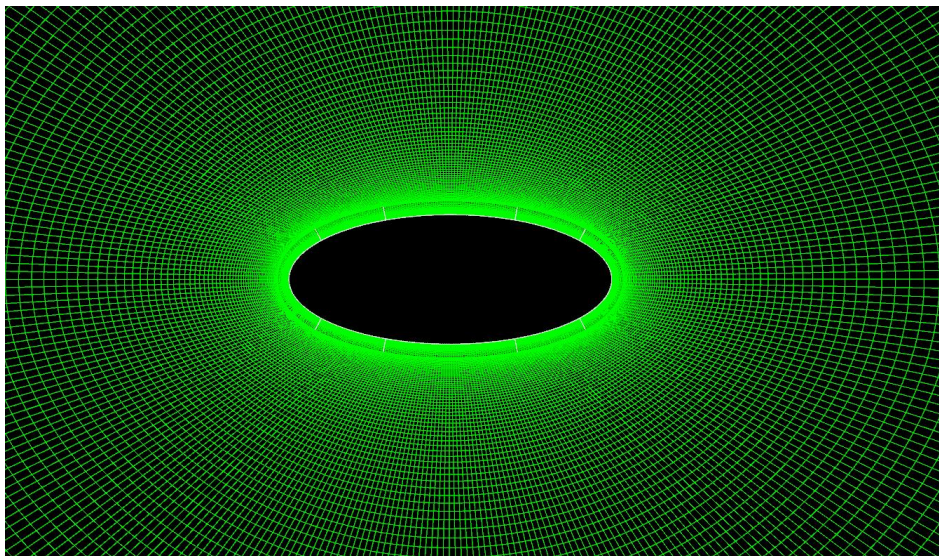
Figure 13: Example of a structured O-mesh

The flow domain is discretized using an O-grid mesh generated using the commercial grid generation package Gridgen. An O-mesh is a structured grid containing quadrilateral (in 2-D) or hexahedral (in 3-D) elements that wraps around the body to discretize the flow domain. An example of an O-mesh generated around an elliptical body is shown in Figure 13.

Fluid flow is governed by the basic physical principles of conservation of mass, conservation of momentum and conservation of energy. These principles can be represented either by partial differential equations, or the equivalent integral form. CFD consists of approximating these (continuous) equations by suitable discretized forms, and solving them numerically using a computer. A multitude of methods that may be employed to achieve this goal are described in various textbooks on the subject [58, 59]. The CFD solver used for this work (Ansys Fluent 13) uses a technique called the "finite volume method". In this method, the integral forms of the governing equations are discretized at each computational cell, and the resulting set of equations are solved in order to obtain the desired flow variables. In the current problem, the equations to be solved describe:

1. Conservation of mass

2. Conservation of momentum

3. Turbulence model

The general conservation equation for any fluid property ϕ can be described according to the following equation,

$$\frac{\partial(\rho\phi)}{\partial t} + \frac{\partial(\rho u_i \phi)}{\partial x_i} = \frac{\partial}{\partial x_i}\left(\Gamma_\phi \frac{\partial\phi}{\partial x_i}\right) + S_\phi \tag{6}$$

where ρ is the fluid density, u_i is the fluid velocity component in the i-direction, Γ_ϕ is the diffusion coefficient, and S_ϕ is the source term. We can obtain specific equations by selecting a diffusion coefficient an appropriate value for ϕ. For example, the equation for conservation of mass is (setting ϕ equal to 1),

$$\frac{\partial \rho}{\partial t} + \frac{\partial(\rho u_i)}{\partial x_i} = 0 \tag{7}$$

For incompressible flow, where the fluid density is constant, the above equation becomes,

$$\frac{\partial u}{\partial x} + \frac{\partial v}{\partial y} + \frac{\partial w}{\partial z} = 0 \tag{8}$$

where u, v and w are the velocity components in the x, y and z directions. The momentum equations can similarly be obtained by setting ϕ to the corresponding values.

The Reynolds numbers for the cases considered in the present work are on the order of 10^7, which falls in the turbulent range. There are a large range of length scales in turbulent flows, ranging from the large length scales on the order of the characteristic length scale of the problem, to very small scales where viscous dissipation occurs. In order to simulate all these scales directly, it is necessary to have an extremely fine computational grid. However, for complex engineering problems, such as the present work, the computational requirements for this approach are extremely prohibitive, and therefore, this method is infeasible. Hence, we follow another approach, which involves solving ensemble averaged equations, known as the Reynolds Averaged Navier Stokes (RANS) equations. For conservation of mass and momentum, these equations are,

$$\frac{\partial \rho}{\partial t} + \frac{\partial(\rho u_i)}{\partial x_i} = 0 \tag{9}$$

$$\frac{\partial(\rho u_i)}{\partial t} + \frac{\partial(\rho u_i u_j)}{\partial x_i} = -\frac{\partial p}{\partial x_i} + g_i + \frac{\partial}{\partial x_j}\left[\mu\left(\frac{\partial u_i}{\partial x_j} + \frac{\partial u_j}{\partial x_i} - \frac{2}{3}\delta_{ij}\frac{\partial u_i}{\partial x_i}\right)\right] + \frac{\partial}{\partial x_j}(-\rho\overline{u_i' u_j'}) \quad (10)$$

where u_i and u_i' are the mean and fluctuating velocity components in the i direction, p is the static pressure, g_i is the body force, μ is the molecular dynamic viscosity and δ_{ij} is the Kronecker delta function ($\delta_{ij} = 1$ if $i = j$, $\delta_{ij} = 0$ if $i \neq j$).

These equations contain an extra term $(-\rho\overline{u_i' u_j'})$ as compared to the instantaneous Navier-Stokes equations. This term is known as the Reynolds stress tensor. The presence of this term means that the number of equations is less than the number of unknowns, and therefore, presents a closure problem. In order to ensure closure, a turbulence model is used to introduce additional equations that solve for the extra variables introduced.

In this research, the Spalart-Allmaras turbulence model is used, which is a one equation model that solves a transport equation for the kinematic (eddy) viscosity. The transported variable ($\tilde{\nu}$) is identical to the turbulent kinematic viscosity except in the near-wall (viscosity-affected) region. The transport equation for this variable is,

$$\frac{\partial(\rho\tilde{\nu})}{\partial t} + \frac{\partial}{\partial x_i}(\rho\tilde{\nu}u_i) = G_\nu + \frac{1}{\sigma_{\tilde{\nu}}}\left[\frac{\partial}{\partial x_j}\left(\mu + \rho\tilde{\nu}\right)\frac{\partial\tilde{\nu}}{\partial x_j} + C_{b2}\rho\left(\frac{\partial\tilde{\nu}}{\partial x_j}\right)^2\right] - Y_\nu + S_{\tilde{\nu}} \quad (11)$$

where G_ν is the production of turbulent viscosity, Y_ν is the destruction of turbulent viscosity, ν is the molecular kinematic viscosity, and $\sigma_{\tilde{\nu}}$ and C_{b2} are model constants. The turbulent viscosity (μ_t) is computed according to,

$$\mu_t = \rho\tilde{\nu}f_{\nu 1} \quad (12)$$

with the viscous damping function f_{v1} given by,

$$f_{v1} = \frac{\chi^3}{\chi^3 + C_{v1}^3} \tag{13}$$

and

$$\chi = \frac{\tilde{\nu}}{\nu} \tag{14}$$

The turbulence production term (G_ν) is given by,

$$G_\nu = C_{b1}\rho\tilde{S}\tilde{\nu} \tag{15}$$

where

$$\tilde{S} = S + \frac{\tilde{\nu}}{\kappa^2 d^2} f_{v2} \tag{16}$$

and

$$f_{v2} = 1 - \frac{\chi}{1 + \chi f_{v1}} \tag{17}$$

where d is the distance from the wall, S is a scalar measure of the deformation tensor, and C_{b1} and κ are model constants. The destruction term is modeled according to,

$$Y_\nu = C_{w1}\rho f_w \left(\frac{\tilde{\nu}}{d}\right)^2 \tag{18}$$

where

$$f_w = g \left[\frac{1 + C_{w3}^6}{g^6 + C_{w3}^6}\right]^{\frac{1}{6}} \tag{19}$$

$$g = r + C_{w2}(r^6 - r) \tag{20}$$

$$r = \frac{\tilde{\nu}}{\tilde{S}\kappa^2 d^2} \tag{21}$$

where C_{w1}, C_{w2} and C_{w3} are model constants. The values for the model constants are obtained on the basis of the curve fitting of experimental data. For the present work, the values of the model constants are as follows:

$C_{b1} = 0.1355, C_{b2} = 0.622, \sigma_{\tilde{\nu}} = \frac{2}{3}, C_{\nu 1} = 7.1, C_{w1} = \frac{C_{b1}}{\kappa^2} + \frac{(1+C_{b2})}{\sigma_{\tilde{\nu}}}, C_{w2} = 0.3, C_{w3} = 2.0, \kappa = 0.4187$

Further details regarding the workings of the CFD solver may be obtained from the user guide for Ansys Fluent 13 [60]. The governing equations are discretized using a second-order upwind scheme, and the discretized equations are solved using an implicit solver in Fluent 13. The results are presented in terms of the pressure coefficient as defined in Equation 3.

In this study, buildings of the following cross-sections are considered: circular, rectangular with circular ends, and elliptical. These cross-sections are illustrated in Figure 14. In the figure, the lines projecting normal to the cross-sections represent the resistance media which are used to manipulate the building envelope wind pressure distribution. In the CFD simulations performed, these are modeled as porous jumps, which give rise to a discontinuity in the static pressure (or a drop in total pressure). It should be noted these devices may be turned off if it is desired that they have no effect on the envelope pressure distribution.
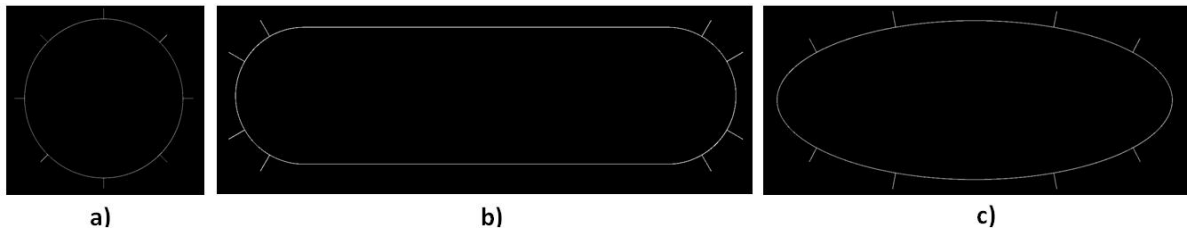
Figure 14: Building cross-sections investigated: a) Circular b) Rectangular with circular ends c) Elliptical

3.3   CFD model validation

Wind driven ventilation is dependent upon the wind pressure distribution around the building facade. Obtaining reliable estimates for the air exchange across the envelope is therefore dependent on accurate simulation of the wind pressure distribution around the building envelope. A major part of the present study is focused on studying the wind pressure distribution around an elliptical cross-section building of 40% thickness. However, experimental data for the combination of this cross-section and the relevant Reynolds number was not found in the literature for the purposes of validating the CFD model for the ellipse.

Therefore, the similar problem in the aerospace field, of computing the lift developed by an airfoil is considered instead. In particular, given that the elliptical cross-section considered is 40% thick, it is also necessary to perform validation using a thick airfoil. The lift generated by an airfoil is dependent on the pressure distribution over its surface. As in the wind-driven ventilation scenario, it is therefore necessary to accurately predict the pressure distribution over the airfoil surface if it is required to compute the lift. Therefore, the objective in validating the airfoil CFD model is to show that using this CFD model, it is possible to predict the pressure distribution accurately, and therefore, by extension, that

this methodology is sufficiently accurate in predicting building envelope wind pressure distribution.
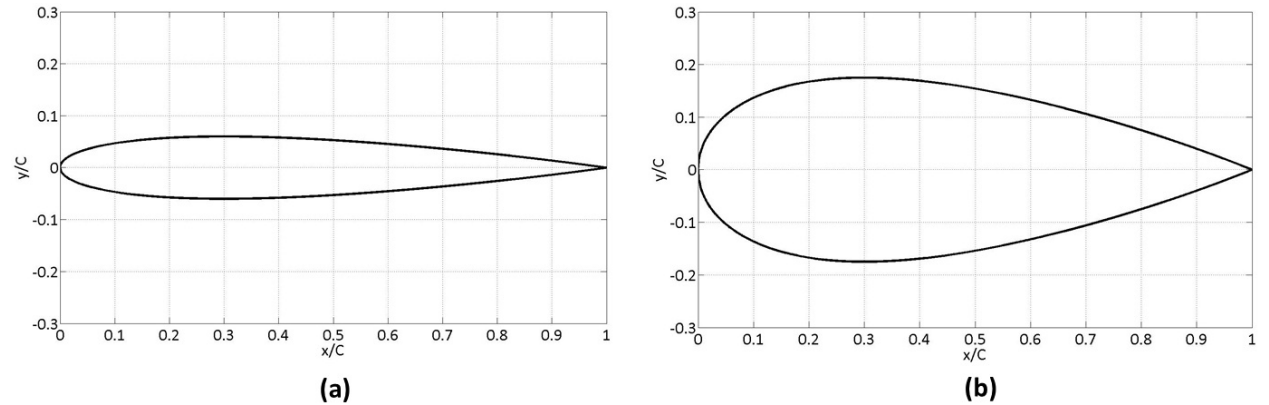
Figure 15: Airfoil sections chosen for validation study: a) NACA 0012 b) NACA 0035

For the purposes of validation, 2-D CFD calculations using two symmetrical airfoil sections are performed, namely, the NACA 0012 section, which is a 12% thick airfoil, and the NACA 0035 section, which is a 35% thick airfoil. Figure 15 shows the airfoil sections plotted in non-dimensional co-ordinates. The x-axis on these plots represents the ratio of the distance along the airfoil chord (x) normalized to the chord length (C). The y-axis represents the thickness of the airfoil section at a particular location along the chord (y), non-dimensionalized again by the chord length.

For the NACA 0012 airfoil, the pressure coefficient distribution is compared with published experimental results obtained from [61] for different angles of attack. Pressure coefficient data was not found in the literature for the NACA 0035 airfoil. Instead, the variation of the lift coefficient as a function of angle of attack is compared with experimental data

obtained from [62]. The lift coefficient is defined as,

$$C_L = \frac{L}{\frac{1}{2}\rho V_\infty^2 A} \tag{22}$$

where L is the lift, i.e., the force acting on the airfoil in the direction normal to the free-stream, ρ is the air density, V_∞ is the free-stream velocity, and A is the planform area of the airfoil. The lift force L is given by,

$$L = \oint p\mathbf{n} \cdot \mathbf{k}dA + \oint \tau_w \mathbf{s} \cdot \mathbf{k}dA \tag{23}$$

$$\mathbf{s} \cdot \mathbf{n} = 0 \tag{24}$$

where p is the static pressure on the airfoil surface, n is the unit normal vector (pointing into the airfoil), k is the unit vector normal to the free-stream, τ_w is the viscous shear stress magnitude on the airfoil surface, s is the unit vector along the airfoil, and A is the planform area of the airfoil. Note that the contribution of the viscous force towards the lift is small compared to the contribution of the pressure force, and lift can be understood as an integrated value of the pressure distribution around the airfoil surface. Therefore, as the purpose of the validation is to demonstrate that it is possible for CFD to capture pressure distributions accurately, in the absence of pressure data, it is reasonable to compare available lift (coefficient) data instead. For both airfoils, the flow Reynolds number is approximately 5×10^6.

Figure 16 shows the comparison between experimental and CFD results for the pressure coefficient distribution around the NACA 0012 airfoil for different angles of attack. It is seen that the CFD model is capable of predicting the pressure distribution around the
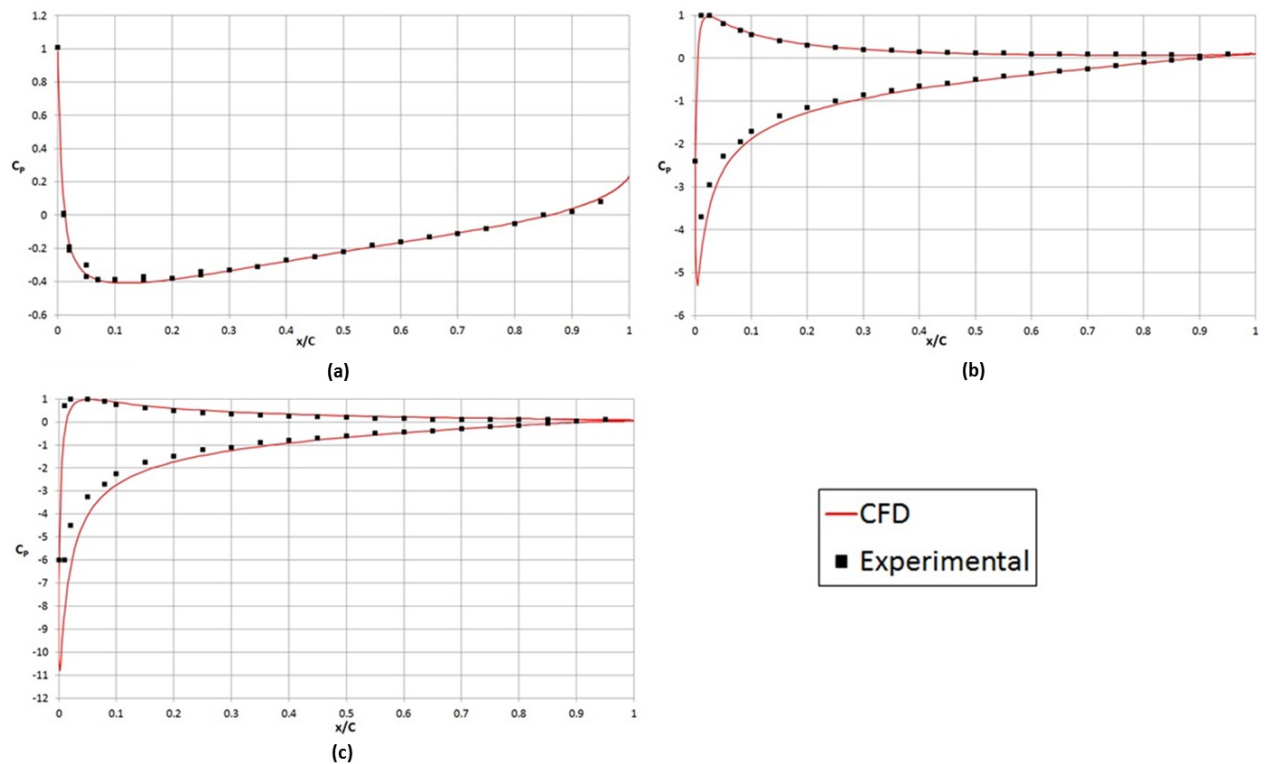
Figure 16: C_p **distribution for NACA 0012 airfoil at different angles of attack: a)** 0^0 **b)** 10^0 **c)** 15^0

airfoil accurately. Despite the relatively high angle of attack (15^0) where stall occurs, the CFD model is able to capture the pressure distribution with good accuracy.

Figure 17 shows the comparison between experimental and CFD results for the variation of the lift coefficient with angle of attack for the thick NACA 0035 airfoil section. The lift coefficients computed using the CFD simulations show good agreement with the experimental values. There are small discrepancies seen at higher angles of attack, and this may be on account of the flow separation which is likely to occur under such conditions. This airfoil has larger thickness than the NACA 0012, and therefore, we expect more flow separation to occur for a given angle of attack.
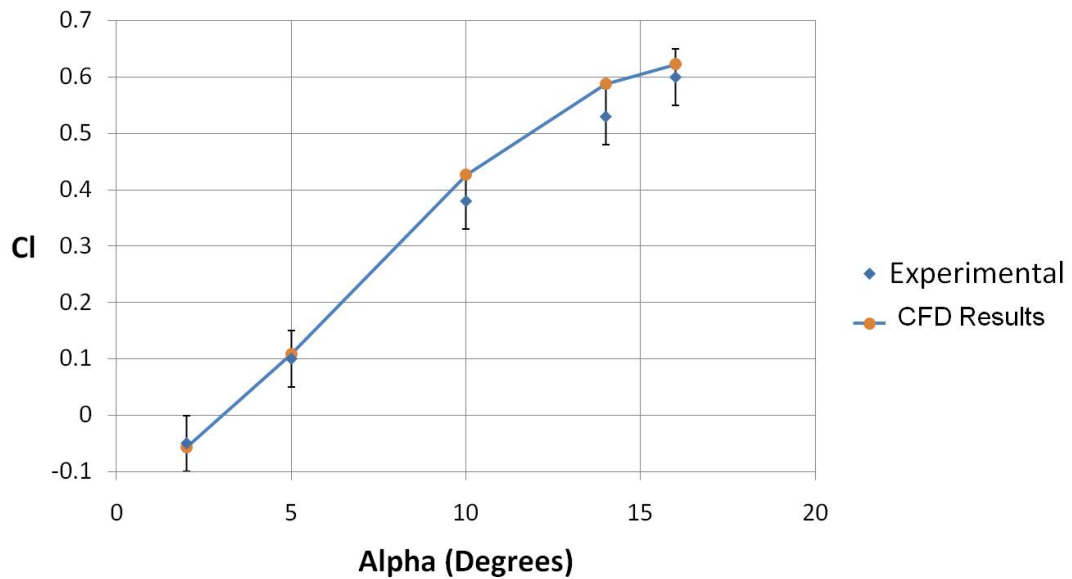
Figure 17: Variation of lift coefficient with angle of attack for NACA 0035

Another factor that may be significant in influencing the pressure field around building envelopes is flow unsteadiness. One of the buildings considered in this study is of a circular cross-section. It is well known that vortex shedding is an important factor determining the flow around a cylinder. Therefore, in order to capture the pressure distribution around such a cross-section correctly, it is necessary to capture the unsteadiness present in this flow. For this purpose, unsteady CFD simulations were performed to see whether the vortex shedding phenomenon could be captured accurately. Figure 18 shows the variation of the lift coefficient with respect to time. Here, we see that the periodic variation in the lift coefficient, which indicates that the vortex shedding phenomenon is captured by the simulation.

The Reynolds number based on the cylinder diameter is 2×10^7. The period of vortex shedding is observed to be approximately 12 seconds. Therefore, the corresponding Strouhal number for this flow is 0.29. Roshko has conducted experiments studying the flow
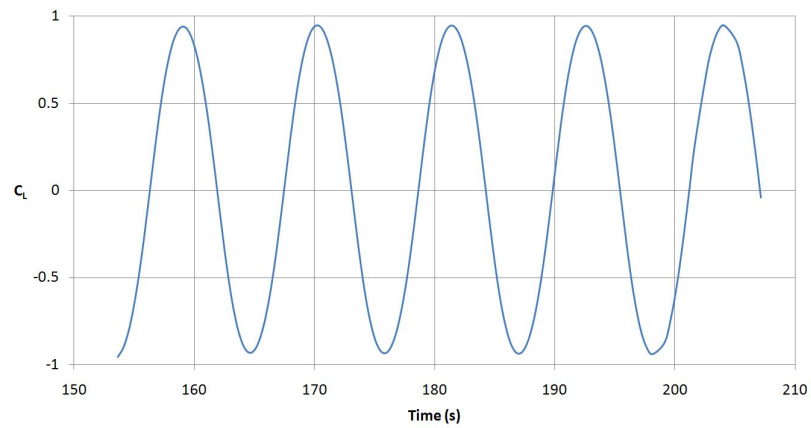
Figure 18: Variation of lift coefficient with time for circular cross-section
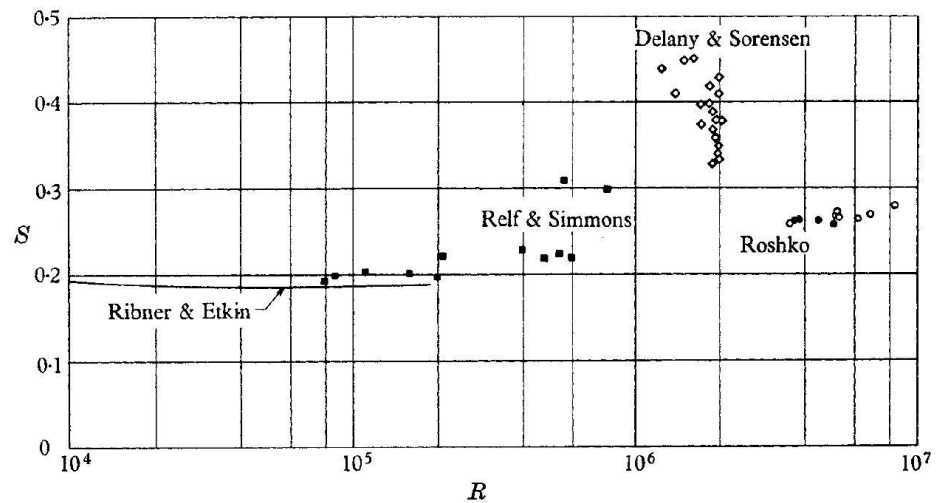
Figure 19: Strouhal number of vortex shedding frequency

past circular cylinders at very high Reynolds numbers [63]. The variation of Strouhal number with Reynolds number for a circular cylinder is presented in Figure 19. He reports that above a Reynolds number of 3.5×10^6, vortex shedding is observed with a Strouhal number of 0.27.

Next, we look at a CFD validation of the jet flap concept discussed previously. The validation data is obtained from an investigation of the jet flap concept conducted by

Dimmock [55]. This experiment studies an elliptical cross-section airfoil with a jet located at the trailing edge of the ellipse. The ellipse major axis is 0.2 m and the thickness of the airfoil is 12.5% of the chord. This ellipse is shown in Figure 20.

Figure 20: Elliptical cross-section airfoil with jet flap

The impact that the jet flap has on the pressure distribution depends on the parameter known as the jet momentum coefficient (C_μ), defined in equation 5. For the purposes of validation, several cases are run with different jet momentum coefficients, and the lift coefficients for each case are compared with the data published in [55]. The jet momentum coefficient is varied by changing the exit velocity of the jet while keeping the free-stream velocity fixed. In all the cases considered, the wind is at 0º angle of incidence with respect to the major axis of the ellipse.

Figure 21 shows the variation of the lift coefficient (C_L) with the jet momentum coefficient. The lift coefficients calculated using the CFD data show very good agreement with the experimental results. Note that since the simulations were conducted at 0º angle of attack with a symmetrical airfoil, the lift coefficient for the baseline case (i.e., no jet) is zero. It can be seen that even for small jet momentum coefficient values (~ 0.05), it is possible to obtain lift coefficients on the order of 1. The lift coefficient can be interpreted as an integrated value of the pressure distribution over the airfoil. Therefore, it is interesting to observe the extent to which the jet flaps modify the pressure distribution over the surface of the airfoil.
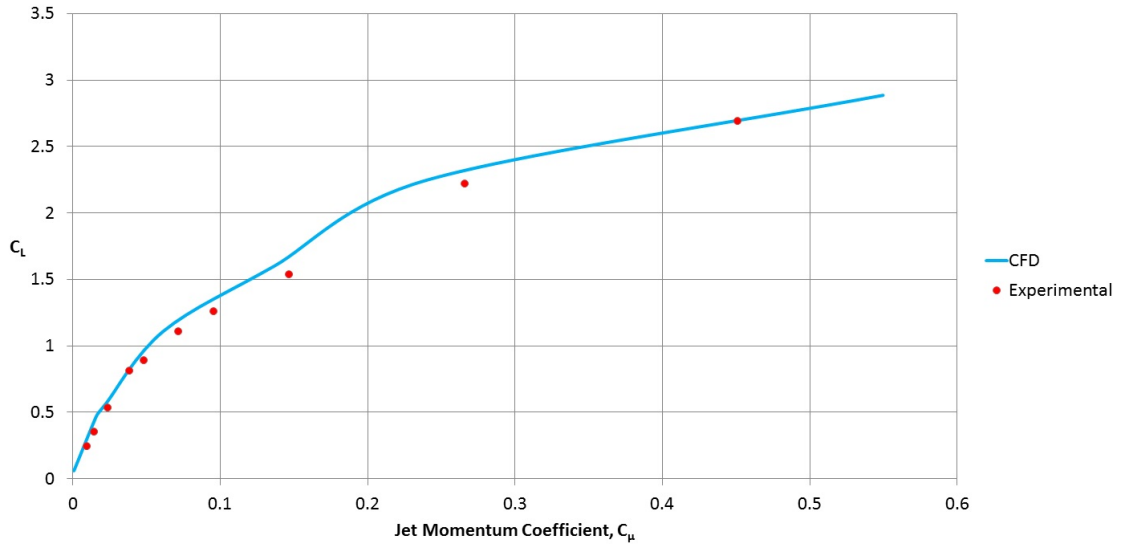
Figure 21: Variation of jet momentum coefficient with jet velocity
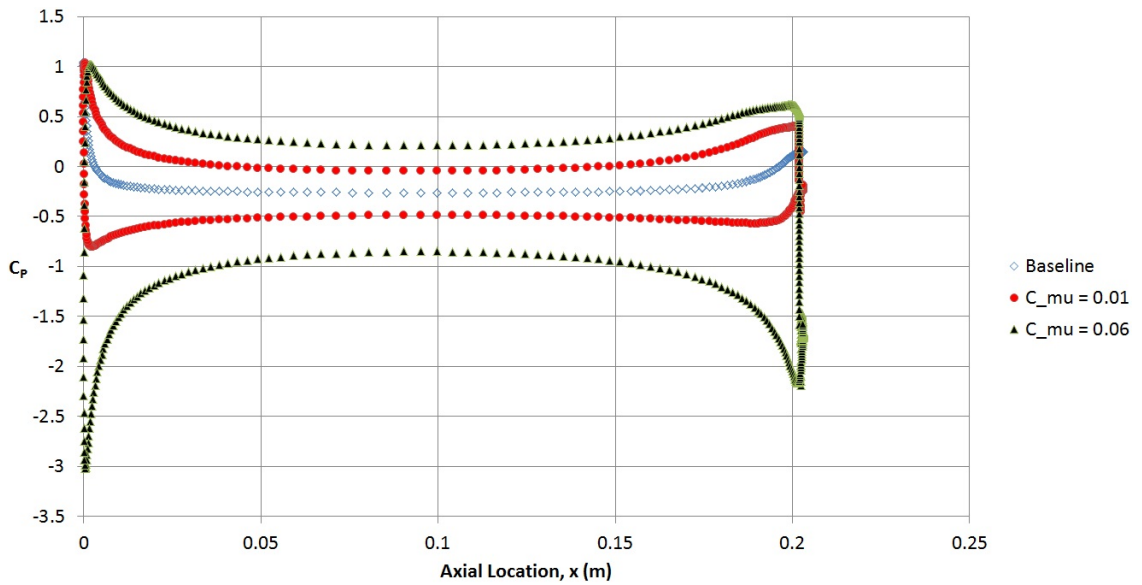
Figure 22: Variation of airfoil surface pressure coefficient distribution with jet momentum coefficient

Figure 22 compares the pressure coefficient distributions for two different jet momentum coefficients with the baseline distribution (i.e., no jet). Since this case is at 0° angle of attack, for the baseline scenario, the upper and lower surfaces of the airfoil have identical

pressure distributions, and the overall pressure coefficient distribution curves collapse into one. It is readily apparent that the jet flaps modify the pressure distribution on the airfoil significantly. For the low jet momentum coefficient case, it is seen for that a large percentage of the chord of the airfoil, it is possible to maintain a relatively constant pressure difference of about half of the wind dynamic pressure. Towards the trailing edge and especially towards the leading edge, this pressure difference is increased significantly. Similarly, for the high jet momentum case, the pressure difference in the central region of the airfoil is about one wind dynamic pressure. For this case, near the leading edge, the pressure difference increases to as much as four wind dynamic pressures. Therefore, in situations where the wind speed is lower than that necessary to provide the required amount of ventilation airflow, this concept may be employed in order to increase the pressure loading on the building, which may be used for providing adequate ventilation airflow. In addition, these results indicate that even though the angle of incidence of the wind is 0°, it may still be possible to set up a cross-ventilation pattern by using this technique.

In the aerospace field, it is a difficult problem to predict the drag on an airfoil, as this depends on capturing viscous effects accurately. In contrast, capturing the pressure distribution on an airfoil (and by extension, lift coefficients) is relatively easy, as these are largely determined by inviscid flow phenomena. The primary focus of the present work is on wind-driven natural ventilation, and for this purpose, it is necessary to estimate the building envelope pressure distributions accurately. Based on these results, it can be seen that using CFD simulations, it is possible to accurately capture such wind pressure distributions.

3.4   Investigation of flow resistance device concept

In this section of the study, the use of flow resistance devices to control wind pressure loading is investigated. In the CFD simulations, these devices are modeled as porous jumps, which give rise to a discontinuity in the static pressure. The magnitude of the pressure drop is given by Equation (25),

$$\Delta P = K(\frac{1}{2}\rho V^2) \tag{25}$$

where K is the resistance pressure drop coefficient. For this study, unless otherwise specified, the value of K is taken to be 0.9. This value is chosen based on the following reasoning. The Betz limit determines the maximum amount of energy that may be extracted from the wind by a stand-alone turbine (i.e. a turbine immersed in an infinite stream). Based on an analysis performed using the free-stream wind magnitude, it is seen that the Betz limit corresponds to a pressure drop coefficient of approximately 0.9. However, it should be noted that on account of the shape of the building cross-section, locally, the local wind speed can be much larger than the free-stream value (e.g. on the so-called suction surface of the building envelope), and therefore, the operation of the turbine can be well within the Betz limit. In addition, The Betz limit is not relevant for devices such as screens or meshes. The pressure coefficients for these devices may be as large as desired.

3.4.1   Effect of building cross-section

In this study, the effectiveness of the resistance devices for manipulating envelope pressure distribution for the three cross-sections shown in Figure 14 is investigated. To begin, the elliptical cross-section building is considered. There are several real life examples of high-rise buildings of elliptical or similar streamlined cross-sections. A few examples of such buildings are shown in Figure 23. Note the "smoothness" of the building envelope surface from the glass window construction, which implies an "aerodynamic" shape. The dimensions of the buildings are chosen such that they have approximately equal cross-sectional areas. The ellipse major axis is 50 m, and its minor axis is 20 m, giving it a thickness ratio of 0.4. The rectangular cross-section has a total length of 55 m and a thickness of 15 m, and the circular cross-section has a diameter of 32 m.

These dimensions were chosen so that they are similar to the dimensions of the Highcliff tower in Hong Kong, shown in Figure 23. This is a 252 m tall high-rise residential building consisting of large apartments. As this tower is residential, it possesses characteristics relevant to the present work, such as open floor plans (as compared to typical office buildings) and non-uniform occupant distributions. Therefore, this tower was chosen as a model for the selection of both the building cross-section as well as interior floor plans to be investigated. An example floor plan for the Highcliff tower is shown in Figure 24.

First, the general flow field around the baseline case with the flow-resistance turned off, and a case with two flow-resistance devices turned on having K values of 0.9 is described. They are shown in Figure 25 as VAWT's. The VAWT on the upper side of the building is located at approximately $x/L = 0.1$ measured from the front of the building (called U10 device), while the VAWT on the lower side of the building is located at approximately x/L

Figure 23: Example of streamlined cross-section high-rise buildings

= 0.7 measured from the front of the building (called L70 device). In the baseline case, the angle-of-attack is taken to be $\alpha = 10^0$.

Since the Reynolds numbers involved are very high, it is reasonable to assume that the flow is independent of Reynolds number. Hence, the results obtained from the simulations at a wind speed of 9 m/s (or 20 mph) apply for other wind speeds if we work with non-dimensional quantities. The pressure coefficient C_p around the building envelope is defined according to Equation 3. In this parametric study, the variation in building
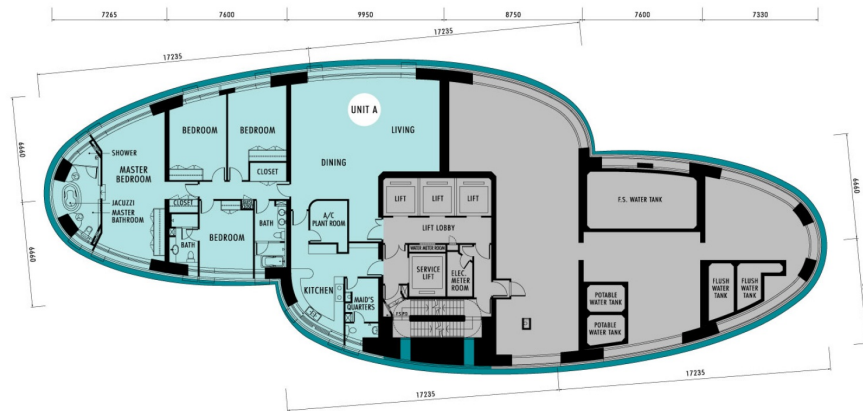
Figure 24: Example floor plan of Highcliff residential tower (dimensions in mm)(image taken from www.highcliff.com.hk)
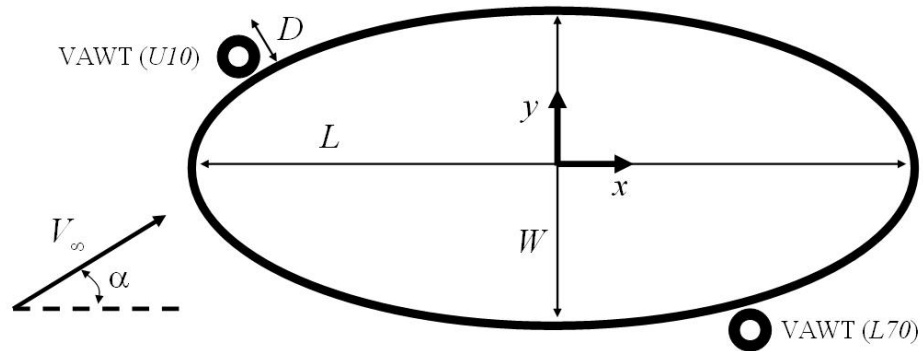
Figure 25: Resistance device configuration

pressure loading due to the presence of the resistance device(s) is investigated. The pressure loading is defined as the pressure difference between the lower and upper surfaces at a given x location. Note that this quantity is relevant when cross ventilation in the y-direction is of interest. In the CFD model, the two flow-resistance devices U10 and L70 can be activated simultaneously or individually. Table 1 summarizes the four cases illustrated in this paper. Also, it is not expected that more than one resistance device is used on each surface, as the second resistance device placed downstream of the first one would be in the separated region and hence ineffective.

Case	U10 Device	L70 Device
Baseline	Off	Off
Case 1	On	Off
Case 2	Off	On
Case 3	On	On

Table 1: Summary of cases run for elliptical building
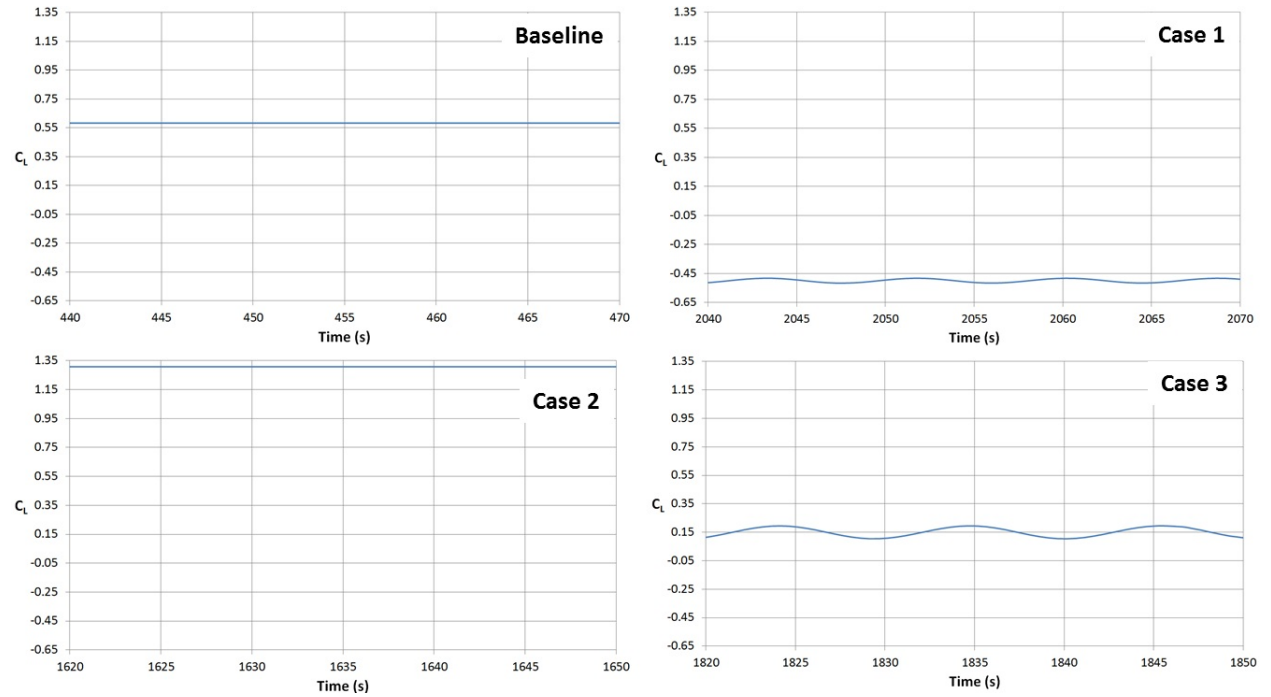
Figure 26: Variation of C_L with time for elliptical building

When the resistance devices are activated, the removal of energy from the wind can result in large flow separation, which in turn can trigger large-scale periodic flow-oscillation due to vortex shedding. This unsteady-flow phenomenon was simulated via CFD. The cases shown in Table 1 are simulated with the unsteady solver running with a time step of 0.05 s. For reference, the flow time (defined as the building major axis divided by the free-stream wind speed) in this scenario is about 5.5 seconds. Therefore, the time step chosen is about a 100 times smaller than the flow time. The presence of vortex shedding is identified by

monitoring the lift coefficient acting on the building as a function of time. The CFD results
shown in Figure 26 demonstrate that the baseline case and Case 2 are steady (no vortex
shedding), while Cases 1 and 3 exhibit vortex shedding. For these cases, the CFD results
show that the period of vortex shedding is approximately 10 s, corresponding to a Strouhal
number of 0.2 (based on the building's width). Another interesting observation is the
variations in magnitude and direction of C_L, which have impacts on both ventilation and
structural load.
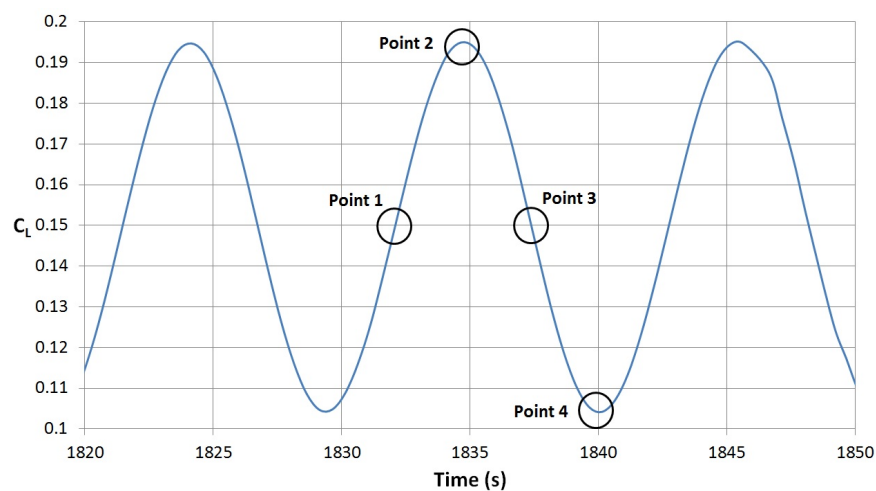
Figure 27: Points at which pressure coefficient distributions are compared for case 3

The results for Case 3 are then investigated in more detail. Four points along the vortex
shedding cycle are chosen, as shown in Figure 27. The instantaneous pressure coefficient
distribution around the building envelope at these points are then compared to each other.
Figure 28 shows that the pressure distributions at these points are similar to each other.
These pressure distributions are approximately the same as the time-averaged distribution.
Similar results (not shown here) are obtained for Case 1 as well. Hence, it is concluded
that the effect of vortex shedding for this building cross-section (at 10° angle of attack) is
minimal. Therefore, all subsequent studies involving the elliptical cross-section are
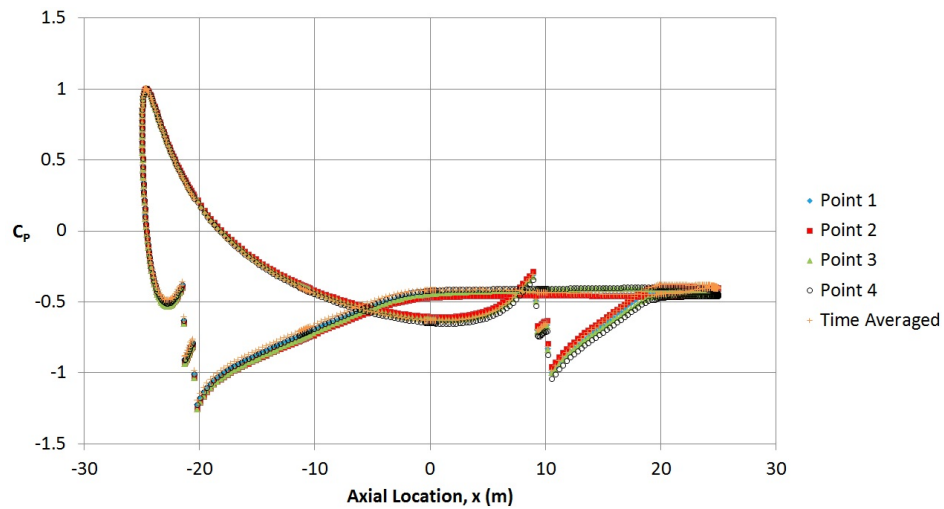
Figure 28: Comparison of pressure coefficient distributions for points shown in Figure 27

performed as steady CFD simulations.

Figure 29 displays the static pressure contours for the cases considered for the elliptical building. It is readily apparent the presence of the resistance devices significantly alters the pressure distribution around the building envelope. In particular, the low pressure region present on the upper surface in the baseline case disappears in case 1. A low pressure region is in fact introduced on the lower surface in case 1. In case 2, we see that the region of low pressure on the upper surface increases in size as compared to the baseline case. For case 3, we see that the pressure distributions along the upper and lower surfaces are approximately equal in magnitude for a large section of the building perimeter.

Figure 30 shows the distributions of C_p around the building perimeter for these four cases. Note that these curves show a pressure jump at the location where the flow-resistance device is turned on. The baseline case is considered first. The plot shows that the pressure loading crossover point is at approximately x/L = 0.65. In the front part of the building
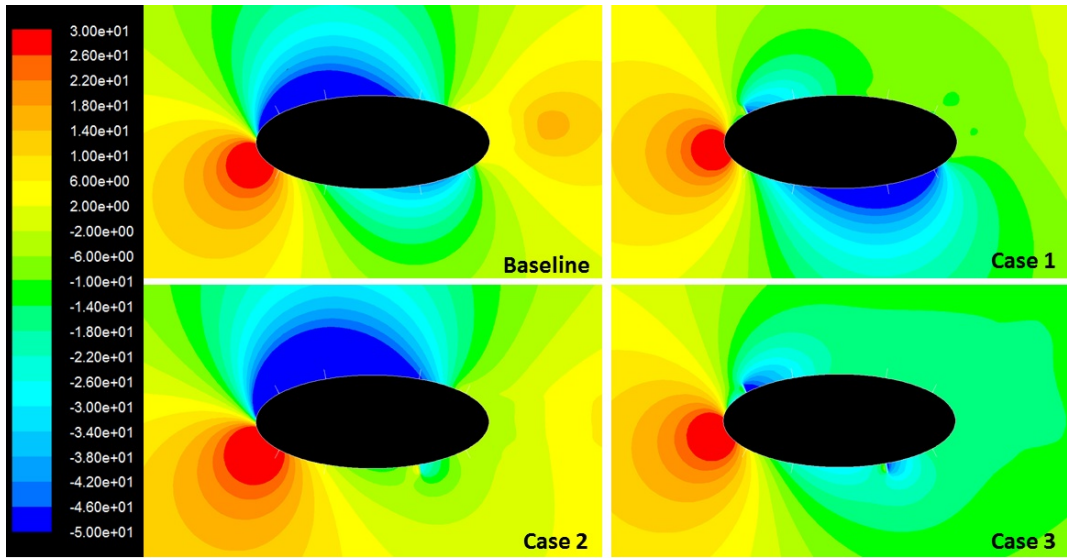
Figure 29: Static pressure contours (in Pa) for elliptical cross-section building
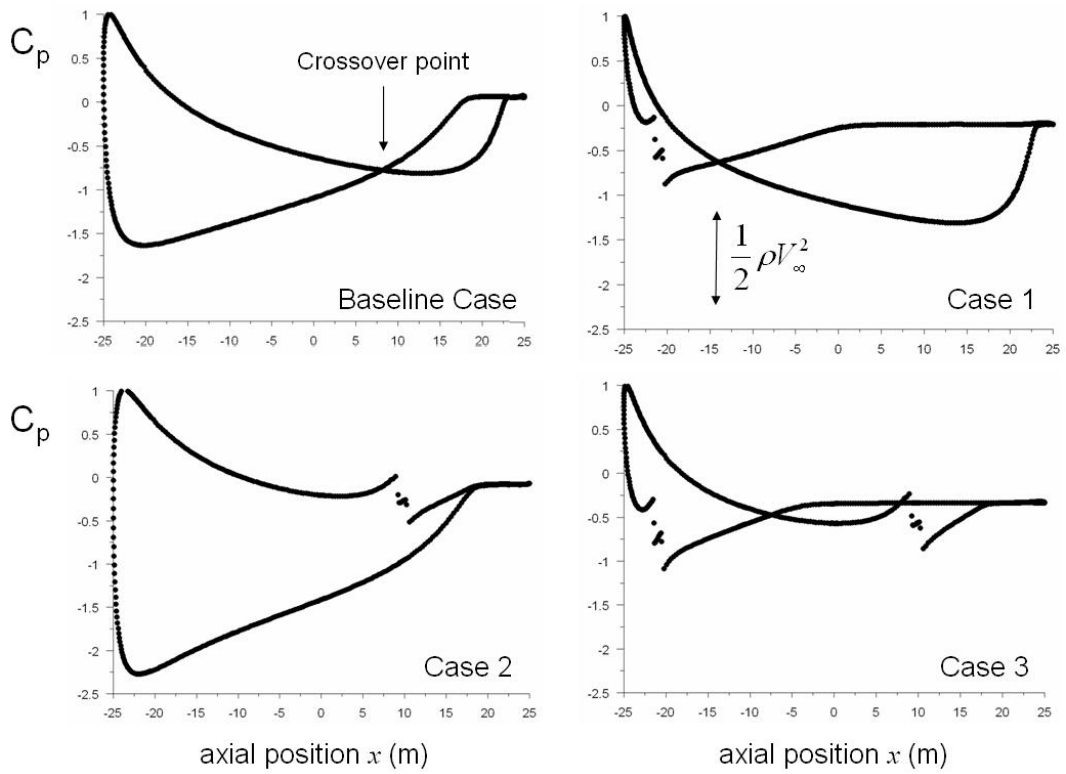
Figure 30: Effect of resistance devices for elliptical building

(from front to crossover point), a positive pressure loading exists (i.e. low pressure on the upper surface and high pressure on the lower surface), while a negative pressure loading occurs in the rear part of the building (from crossover point to rear).

Next, the effects of activating the flow-resistance device(s) are examined. It is seen from these results that, by properly turning on/off the two flow-resistance devices, the pressure distribution along the building envelope can be significantly altered. For example, in Case 1 where device U10 is turned on, the crossover point begins to move upstream to the position $x/L = 0.25$. On the other hand, in Case 2 where device L70 is turned on, the opposite effect takes place; the crossover point moves all the way to the back, and the entire building is subjected to a positive pressure loading. Finally, when both devices U10 and L70 are turned on (Case 3), the pressure loading is significantly reduced, and two crossover points appear (one at $x/L = 0.35$, and the other at $x/L = 0.65$). Clearly, for naturally ventilated buildings, these variations in the pressure distribution on the building envelope will result in large changes in intake/exhaust airflow distributions around the building. This study demonstrates that, by externally mounting the flow-resistance devices such that the positions of these devices can be changed (e.g. via rail mounted), it is possible to manipulate to a large extent the ventilation distribution within the building.

From Figure 30, it can be seen that the difference in the value of the pressure coefficient between the pressure and suction sides can be around 1 and 2 (i.e., ΔC_p can lie between 1 and 2). This means that for a wind speed of 6 m/s (13.5 mph), the pressure difference between the two sides can range from 22 Pa to 44 Pa ($\Delta C_p \times \frac{1}{2}\rho V_\infty^2$). Referring to Table 1, it is seen that this driving wind pressure can be much greater than the stack pressure under certain conditions. For instance, for a stack height of 20 m and a temperature

difference of 5^0 C, the pressure difference is approximately 5 Pa. Wind speeds of this magnitude are not uncommon depending on the location.

For instance, a wind rose of the San Francisco area (as shown in chapter 4) reveals that wind speeds of this magnitude (or greater) can be expected for around 50% of the year (refer Chapter 4). This means that under such climatic conditions, the influence of the stack pressure can be considered negligible in comparison to wind pressure acting on the building envelope, and the problem can be assumed to one of purely wind-driven ventilation.

Figure 31 shows the contours of velocity magnitude for the cases considered. The effects of the resistance device are again readily apparent. The most prominent effect is the presence of a large wake region downstream of the resistance device locations, especially for cases 1 and 3.
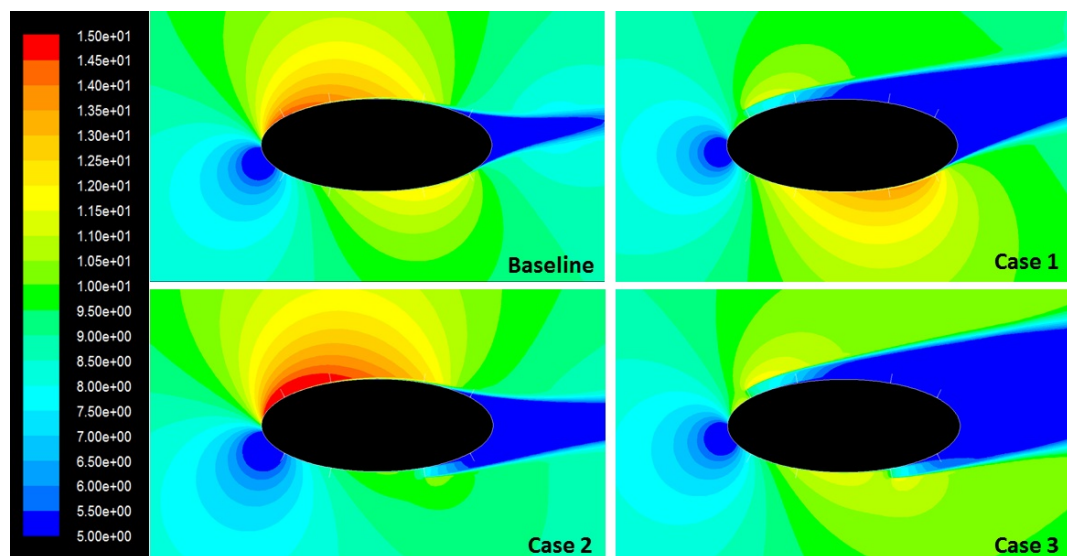
Figure 31: Velocity magnitude contours (in m/s) for elliptical cross-section building
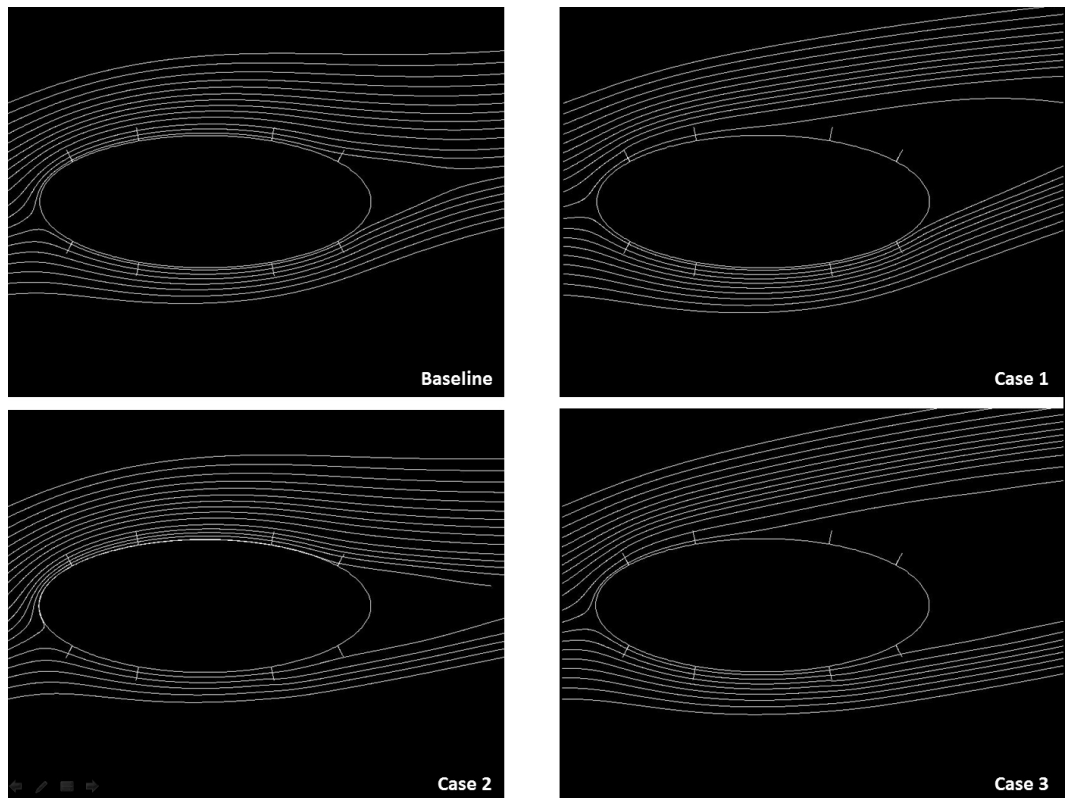
Figure 32: Pathlines for elliptical cross-section building

Figure 32 shows the pathlines around the elliptical building for the cases considered here. We see that the resistance devices impact the flow pattern around the building perimeter significantly. For instance, comparing the baseline case and case 1, we see the change in streamline curvature that occurs in case 1, as the flow separates downstream of the resistance device. Finally, further details about the flow field around the building can be obtained from Figure 33, which plots the velocity vectors around the building.

Next, the effect of the resistance device concept on the rectangular building cross-section shown in Figure 14 b) is considered. Figure 34 shows the configuration of the resistance devices for the cases run. The baseline case, in which no resistance devices are activated, is taken to be the reference case. Cases 1, 2 and 3 have resistance devices activated at the
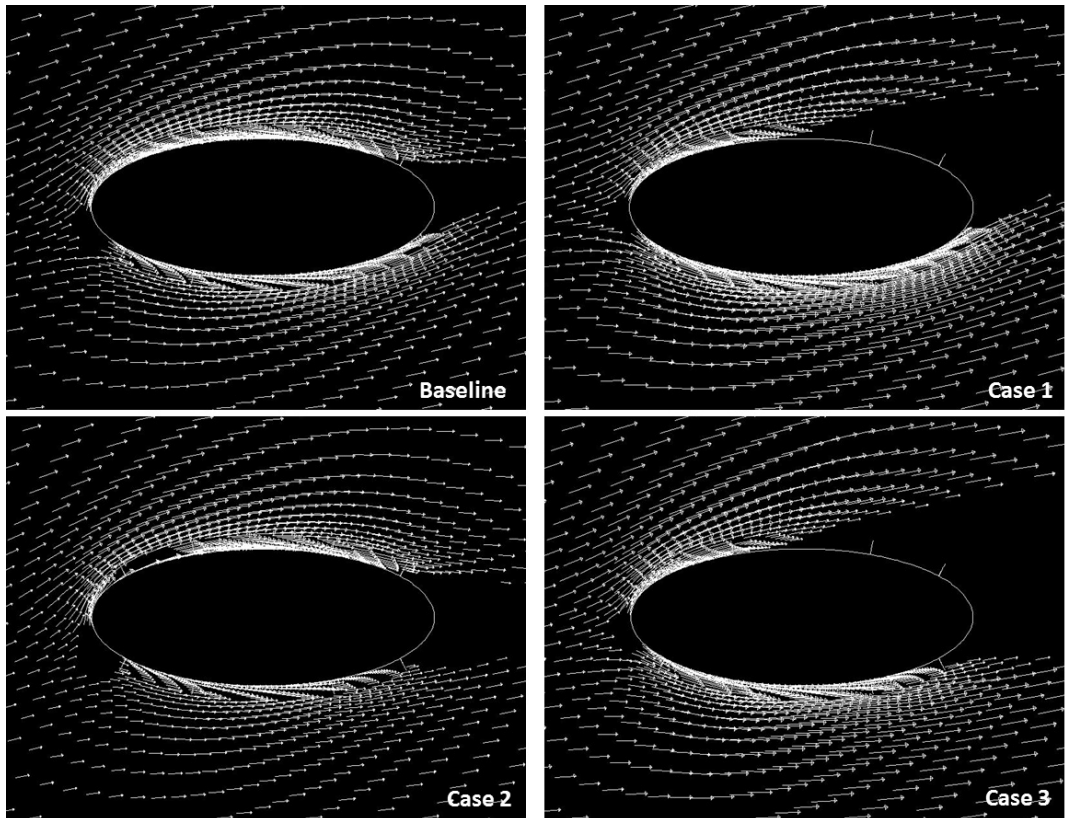
Figure 33: Velocity vectors for elliptical cross-section building
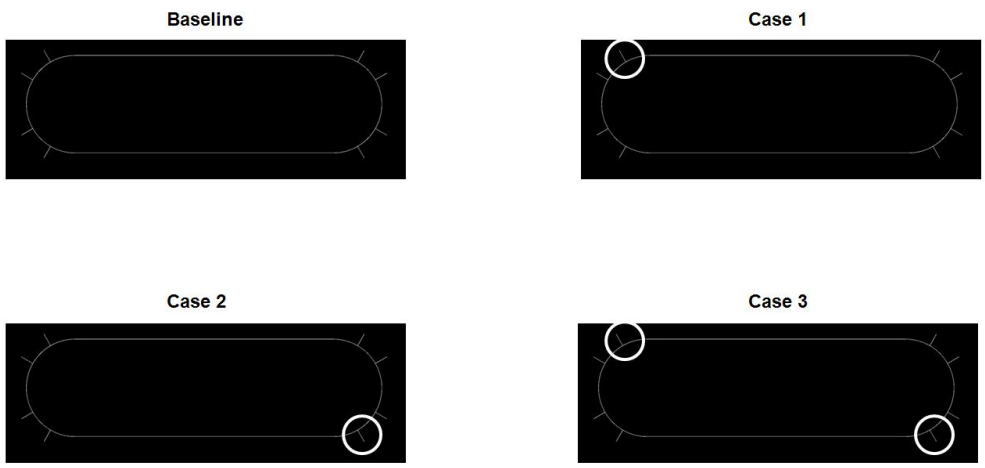
Figure 34: Case description for rectangular cross-section building

circled locations. First, unsteady simulations are performed for the cases described. The purpose is to investigate whether vortex shedding is a significant factor for a building of this cross-section at the given wind incidence angle.
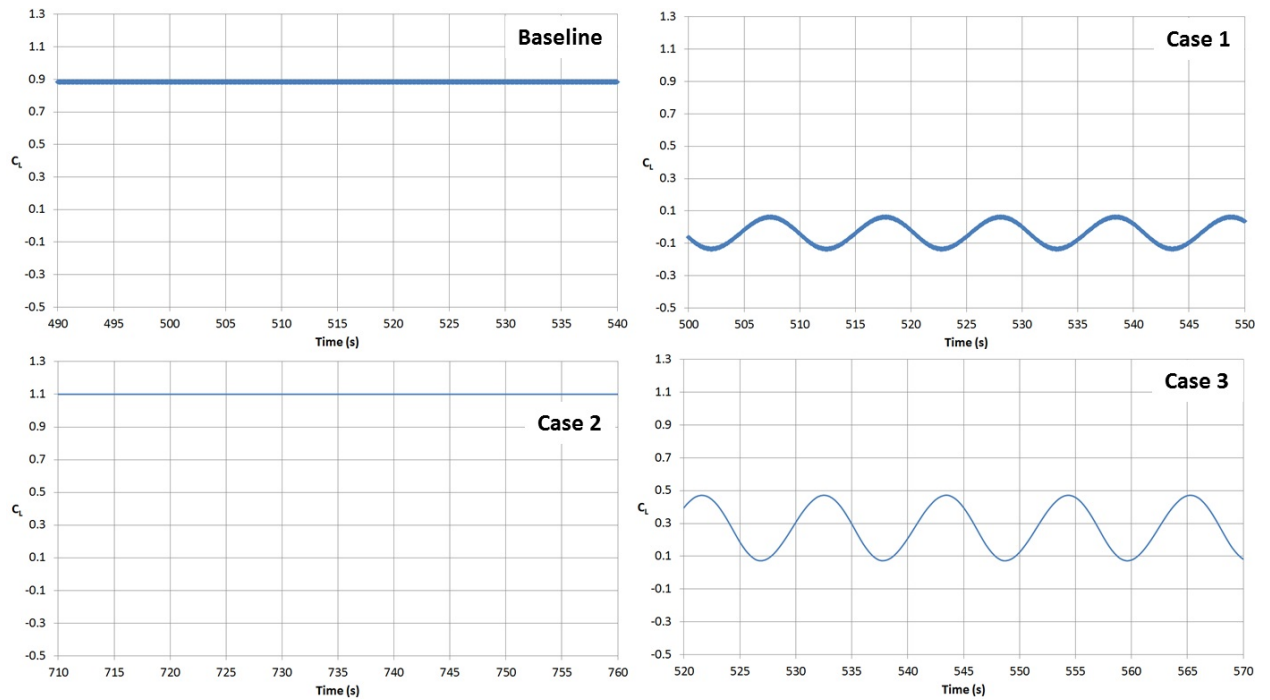
Figure 35: Variation of lift coefficient with time for rectangular building cases

Figure 35 displays the variation of the lift coefficient with time for the cases under consideration. It is observed that vortex shedding is not observed for the baseline case and case 2, whereas the fluctuations in the lift coefficient for cases 1 and 3 indicate that vortex shedding is present in these scenarios.

In order to further investigate the impact of the vortex shedding on the envelope pressure distribution, the results for case 3 are studied further. Four points along the vortex shedding cycle are selected, as shown in Figure 36, and the pressure coefficient distributions at these points are compared.
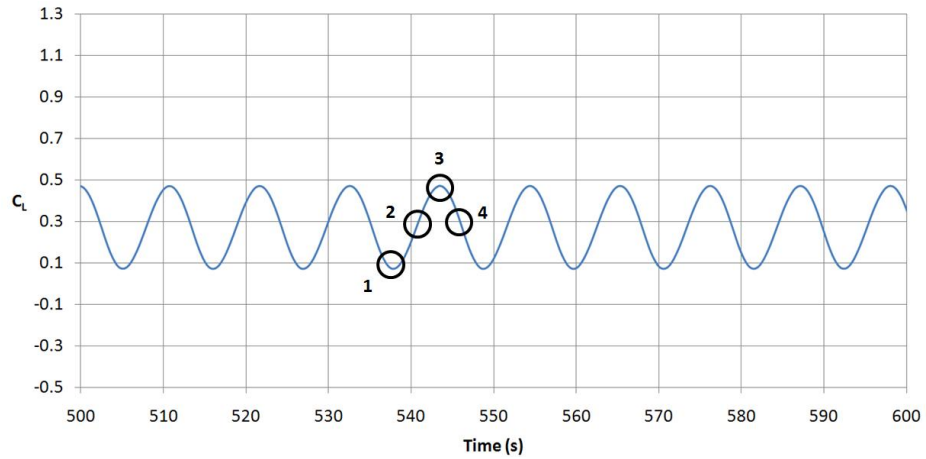
Figure 36: Points selected for pressure coefficient comparison for rectangular building (case 3)
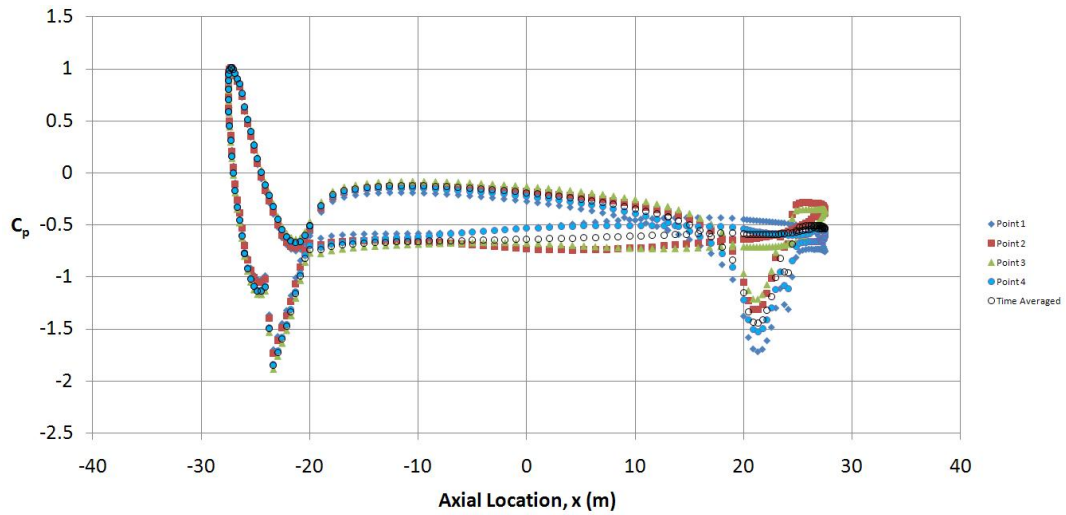
Figure 37: Comparison of pressure coefficient comparison at selected points for rectangular building (case 3)

Figure 37 shows the pressure coefficient distributions at the four selected times. It is seen that vortex shedding has more of an impact for this building cross-section as compared to the elliptical building. There is a relatively large variation observed in the pressure distribution near the trailing edge of the building at different times, on account of the vortex shedding. However, the period of the fluctuation quite small (around 10 s) and the

time-averaged distribution is quite similar to the steady-state solution. Therefore, it is reasonable to perform steady-state CFD simulations for the scenarios being considered for this building cross-section.

Figure 38 displays the pressure coefficient distribution over the building envelope for the cases under consideration. It is observed that the resistance device location shown in case 1 has a significant impact on the magnitude of the pressure loading on the building envelope. For case 1, the difference in static pressures between the upper and lower surfaces of the building is reduced by a large amount as compared to the baseline case.
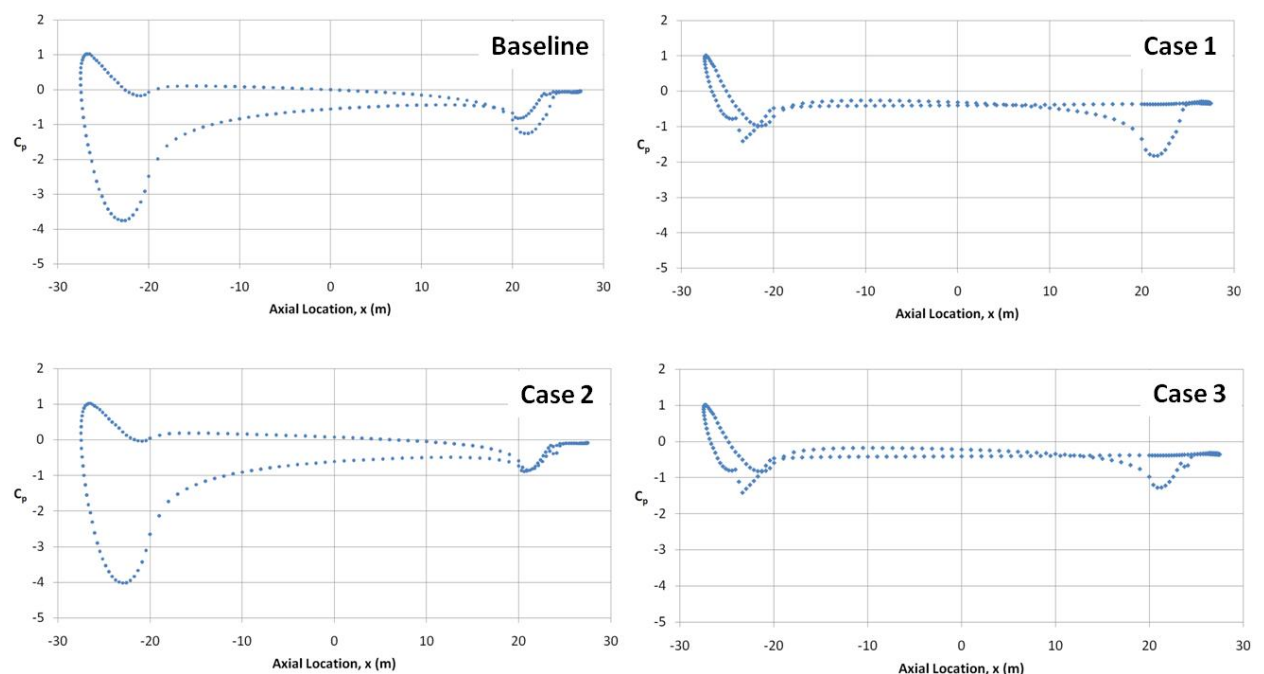
Figure 38: Pressure coefficient distribution for rectangular building cases

This means that the amount of ventilation airflow provided will be reduced significantly for case 1 as compared to the baseline scenario, without having to change the sizes of the ventilation openings to the ambient. In addition, it seen in a later section that the distribution pattern of the airflow exchange also changes considerably on activation of this

resistance device. However, the resistance device location shown in case 2 does not have a significant impact on the overall pressure distribution when employed by itself. However, when used in conjunction with the resistance device located on the suction surface (i.e., Case 3), this resistance device has the effect of increasing the pressure loading near the trailing edge of the building. The cases shown are the device configurations which have the largest impact on the building envelope pressure distribution. Resistance devices located near the stagnation point (i.e., near the leading edge of the pressure surface) were found to have a negligible impact on the pressure distribution.
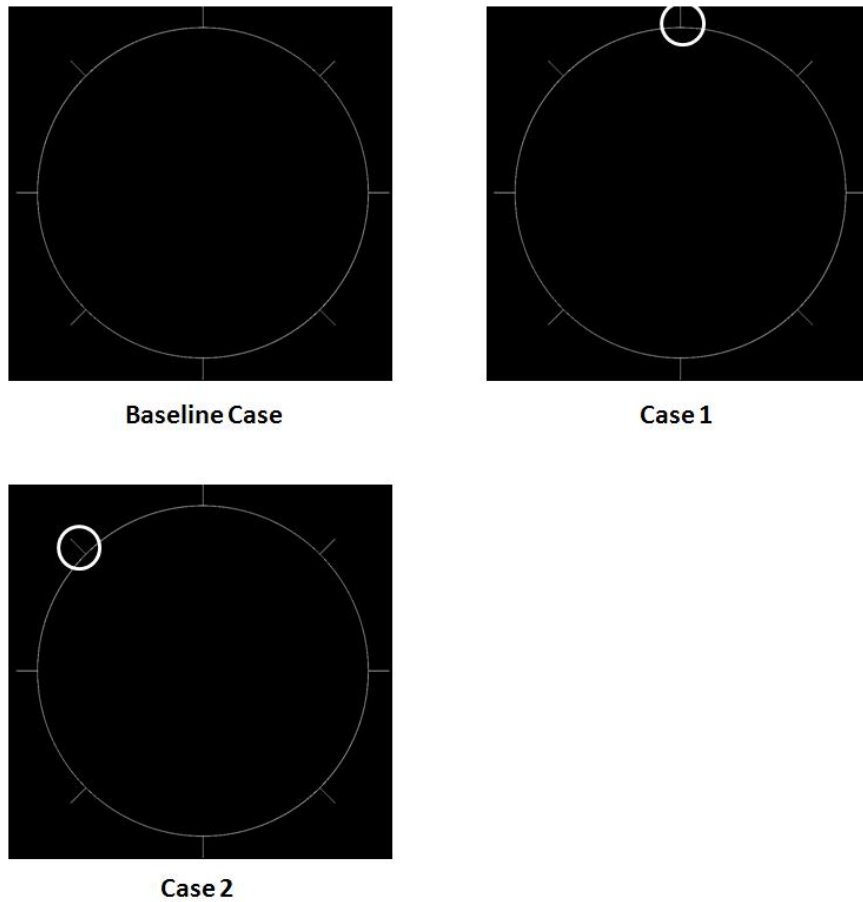
Figure 39: Case description for circular building cases

Next, the circular cross-section shown in Figure 14 (a) is investigated. Here, three cases are considered, namely, the baseline case with no resistances activated, and cases 1 and 2, with the resistance device placed at the circled locations in Figure 39. In this problem, the wind is aligned with the horizontal. Flow separation is expected over the rear half of the cross-section, and therefore, any resistance devices located in this region will not be effective. The three cases considered here therefore cover all possible resistance device configurations regardless of the prevailing wind direction. As seen previously, vortex shedding is a significant factor affecting the pressure distribution over the envelope, and therefore, unsteady CFD simulations are performed.
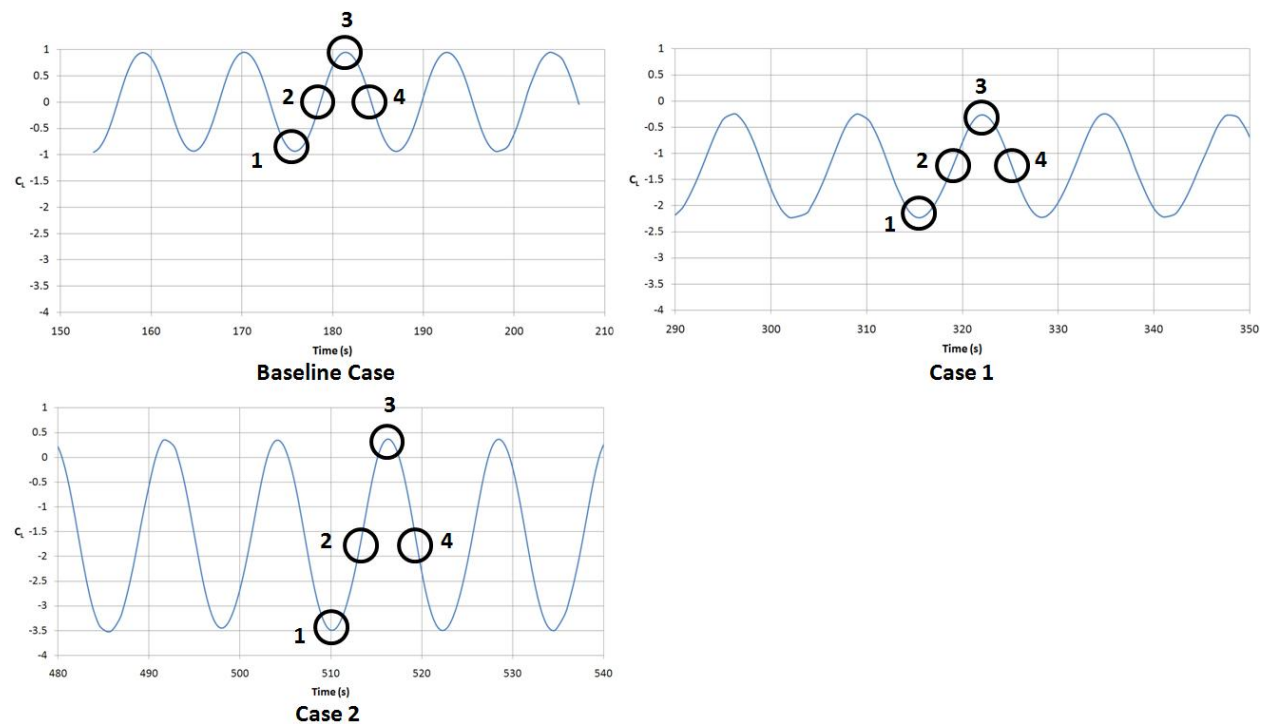
Figure 40: Variation of lift coefficient for circular building

The vortex shedding for all the cases can be seen in the variation of the lift coefficient with time in Figure 40. The pressure distributions at the four points indicated in the vortex

shedding cycle are compared for each case. It can be seen that the unsteadiness associated with the vortex shedding has a large impact on the pressure distribution around the building perimeter. Another factor to note is that the vortex shedding time period is of the order of 10 s. This is much shorter than the time scales over which ventilation requirements change.
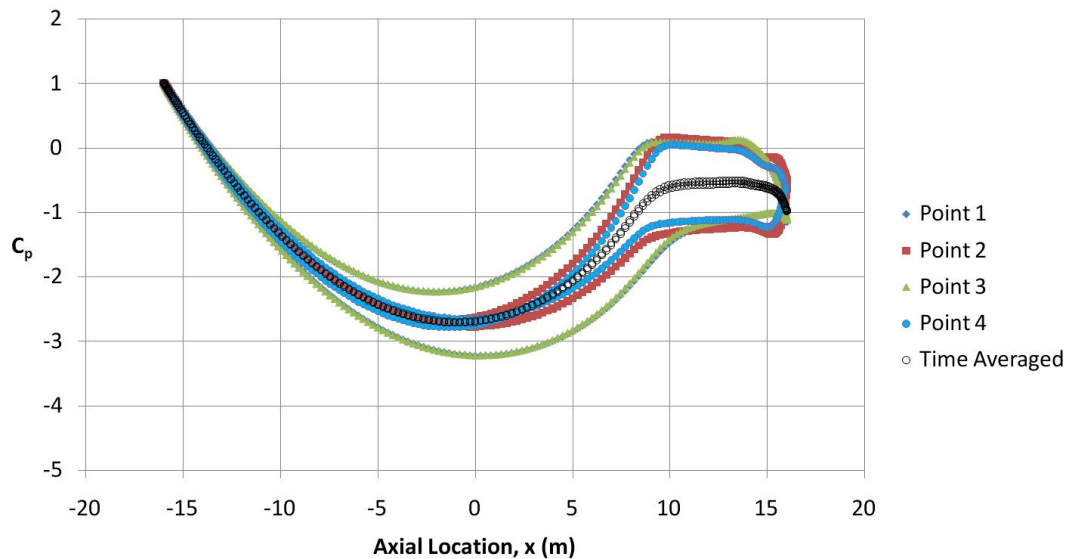
Figure 41: Variation of envelope pressure coefficient distribution for circular building (baseline case)

Figures 41, 42 and 43 display the variation of the pressure distribution at four points in the vortex shedding cycle for the baseline case, case 1 and case 2 respectively. It is observed that vortex shedding still has a large impact on the overall pressure distribution. Significant differences are observed between the pressure distributions at different points along the vortex shedding cycle for both cases. Note that the pressure loading does increase upstream of the mid-chord location for cases 1 and 2 as compared to the baseline. This may be useful as it can allow for greater intake/exhaust of airflow in this region of the building. Finally, we note that the time-averaged pressure loading for the baseline case is
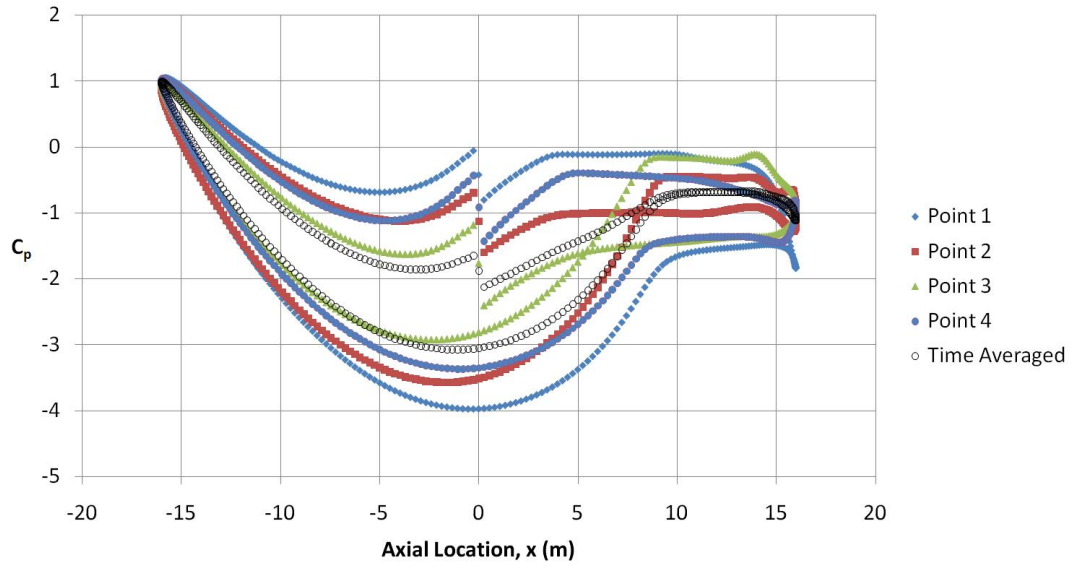
Figure 42: Variation of envelope pressure coefficient distribution for circular building (case 1)
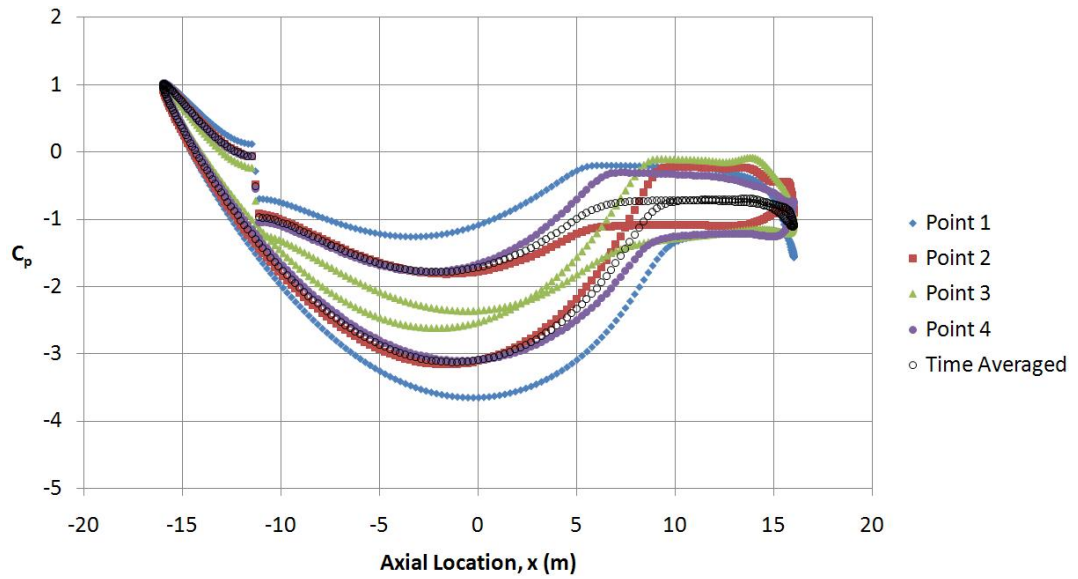
Figure 43: Variation of envelope pressure coefficient distribution for circular building (case 2)

zero, as expected.

3.4.2 Effect of resistance device pressure drop coefficient

Now, we continue with studying the elliptical cross-section building. In the next part of the study, the effect of changing the magnitude of the flow resistance, as characterized by K, is presented.
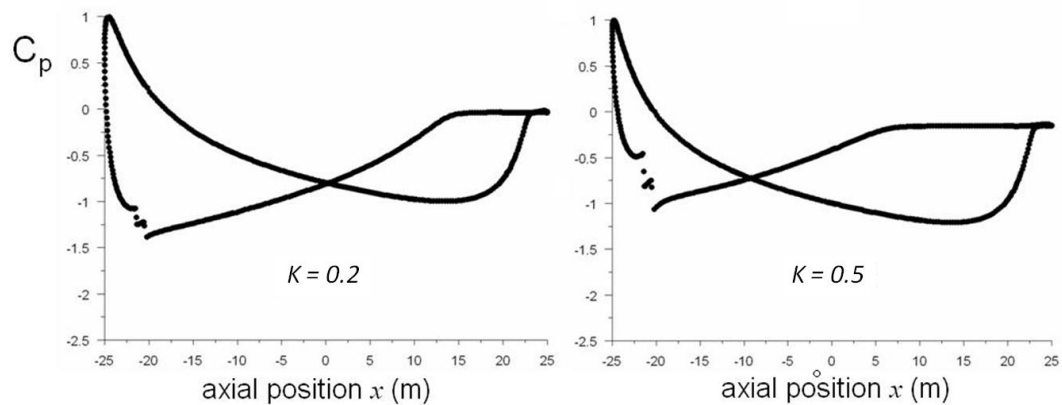
Figure 44: Effect of varying pressure drop coefficient for Case 1

Figure 44 shows the pressure distributions for Case 1 (device U10 activated) at K = 0.2 and K = 0.5. Inspection of this figure along with Figure 30 clearly shows the effects of varying the flow resistance magnitude on the crossover point. Originally at x/L = 0.65 when the U10 device is off (baseline case in Figure 30), the crossover point moves upstream to x/L = 0.5 at K = 0.2 (Figure 44), then to x/L = 0.32 at K = 0.5 (Figure 44), and finally to x/L = 0.25 when K = 0.9 (Case 1 in Figure 30). Hence, it can be seen from these results that changing the flow-resistance value is another effective way of manipulating the pressure distribution along the building envelope. These results suggest that, by properly deploying four stationary devices with variable flow-resistance (e.g. shutter window type), one can achieve the same effects as deploying two movable devices with variable flow-resistance. This may prove to be a more economical design with respect to both

capital and operational costs.

Figure 45: Example of spoiler deployment on aircraft
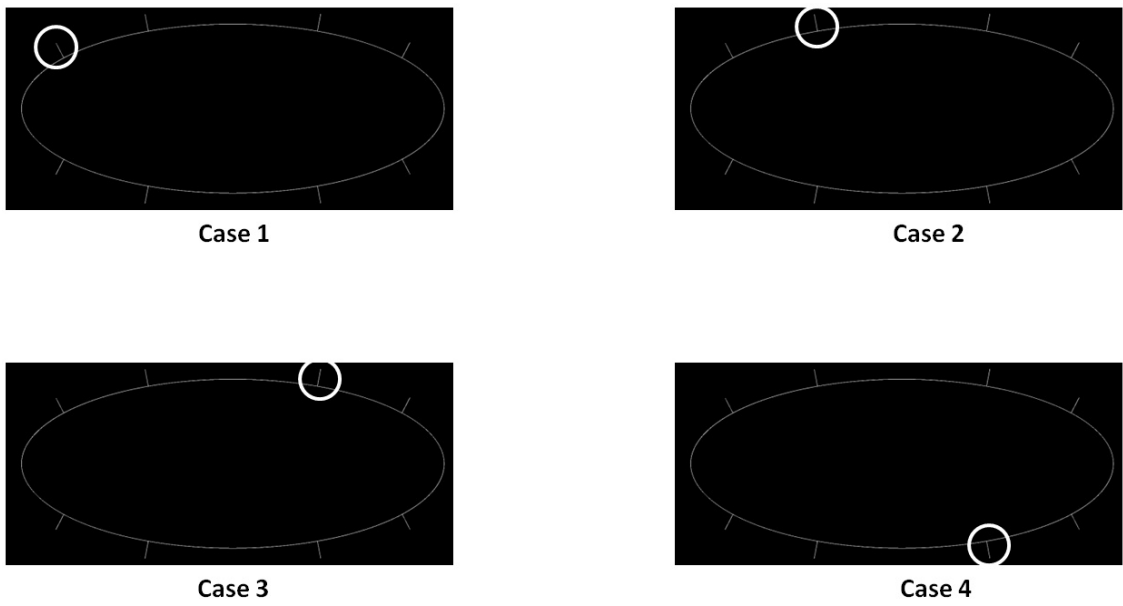
Figure 46: Location of flaps on elliptical cross-section building

Next, a special case of the resistance device concept where the coefficient approaches

infinity is considered. This can be used to model a scenario where a solid surface projects from the building envelope, similar to the deployment of spoilers on an aircraft. An illustration of this concept is shown in Figure 45. The resistance device locations for this scenario are shown in Figure 46. Two device sizes are investigated; in one scenario, the resistance devices are 2 m in length (4% of the chord), whereas in the second scenario, the devices are 4 m long (8% of the chord). The pressure distributions around the envelope resulting from these configurations are compared to those obtained for the baseline scenario. Again, in all the scenarios considered, the angle of incidence of the wind is 10°.
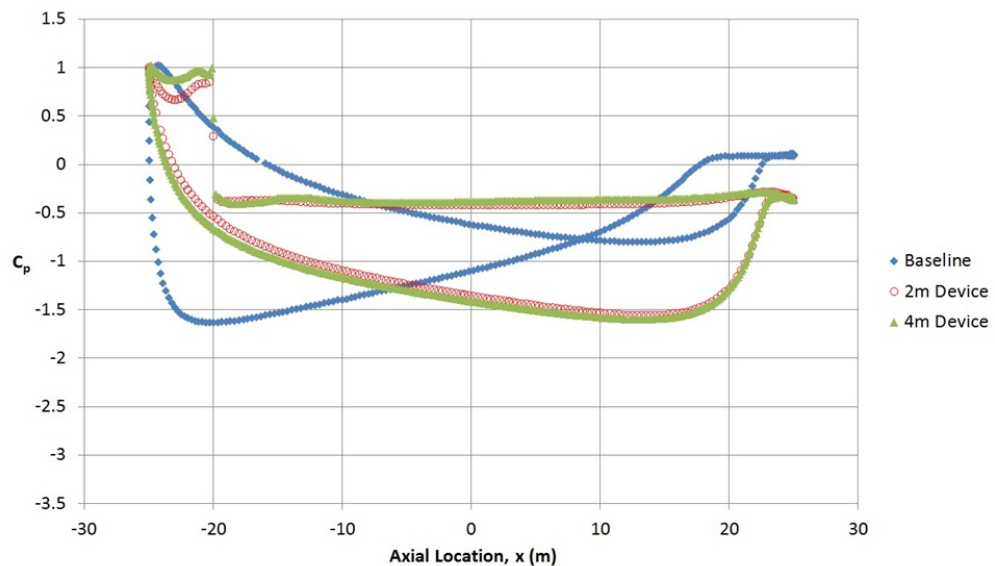
Figure 47: Pressure coefficient distribution for elliptical building with flaps (case 1)

Figure 47 shows the distribution of pressure coefficient around the building perimeter for case 1 predicted by steady-state CFD simulations. It can be seen that introducing the resistance device in this location has a dramatic impact on the envelope pressure distribution. The high pressure and low pressure surfaces are reversed as compared to the baseline case. The suction (or low pressure) surface in the baseline scenario becomes the

high pressure surface in this case. As one surface of the building is at a higher pressure than the other surface over the entire length of the building, this can be utilized for the purpose of cross-ventilation of the building. This also means that the airflow exchange directions may be reversed as compared to the baseline case by introducing a high coefficient resistance device in this location. However, going from a 2 m long flap to a 4 m long flap does not have as significant an impact as introducing the 2 m flap.
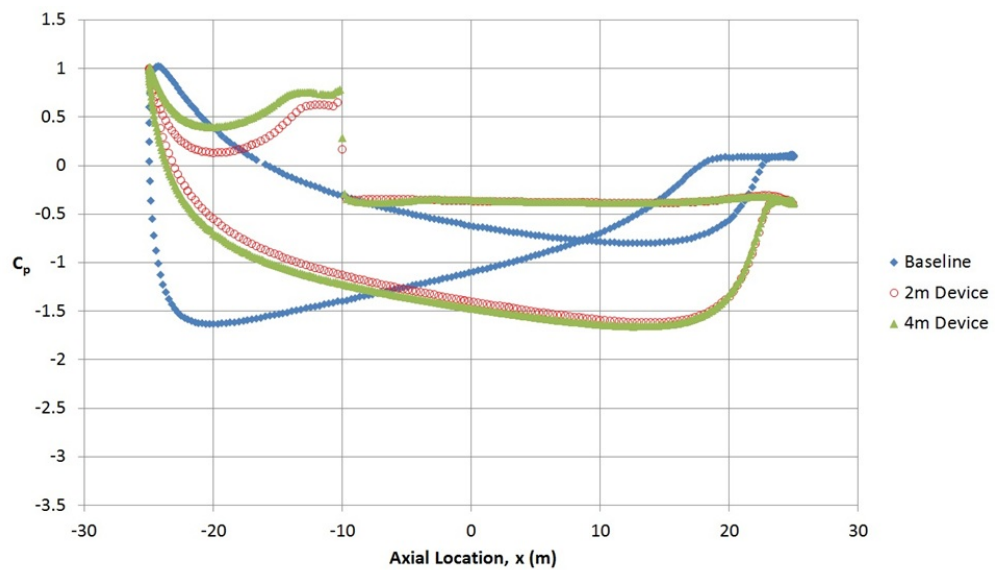
Figure 48: Pressure coefficient distribution for elliptical building with flaps (case 2)

Figure 48 shows the distribution of pressure coefficient around the building perimeter for case 2. Again, introducing the flap has a dramatic impact on the pressure loading around the building. The effect is very similar to case 1, in that the suction and pressure surfaces are reversed as compared to the baseline. Again, there is negligible difference between the pressure distributions obtained using a 2 m resistance device and a 4 m resistance device.

Figure 49 displays the pressure coefficient distribution for case 3. We again notice that the
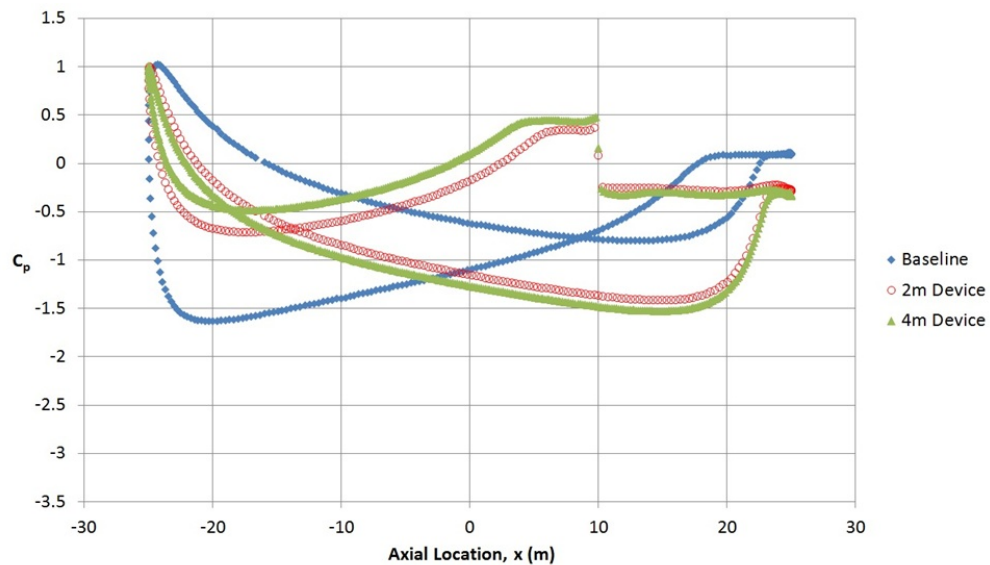
Figure 49: Pressure coefficient distribution for elliptical building with flaps (case 3)

shape of the pressure distribution is radically altered by introducing a high coefficient resistance device. In particular, the location of the "crossover" point is shifted from around 10 m in the baseline case, to around -15 m for the case with the 2 m device, and to about -20 m for the 4 m device. This indicates that it may be possible to reverse the airflow exchange direction over a large section of the building cross-section.

Finally, Figure 50 illustrates the pressure coefficient distribution case 4. The resistance device in this location also has a significant impact on the building envelope pressure distribution. The magnitude of the loading on the building is increased dramatically, up to a maximum of about four wind dynamic pressures near the leading edge. Therefore, this configuration may be used in low wind speed conditions for increasing the amount of ventilation airflow by magnifying the driving wind pressure differential across the two sides of the envelope.
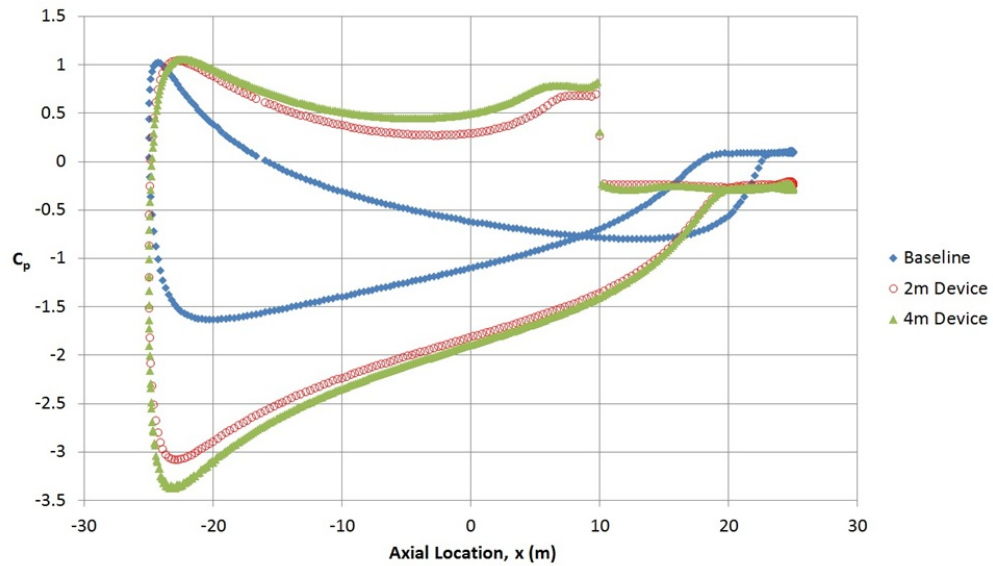
Figure 50: Pressure coefficient distribution for elliptical building with flaps (case 4)

3.4.3   Effect of wind incidence angle

Next, the effect of changing wind direction is investigated. To this end, the angle-of-attack is varied from 5^0 to 20^0 with an increment of 5^0. Figure 51 shows the pressure distributions for Case 1 (device U10 activated) at the various angle-of-attacks. It can be seen from these results that the change in the static pressure on the building envelope due to the variation in angle-of-attack is weaker than the effect of flow-resistance activation discussed earlier. Specifically, although the overall magnitude does vary, the overall shape is unchanged.

It is interesting to observe that, using the U10 device alone, the pressure distribution of the combination ($\alpha = 20°$, K = 0.9) shown in Figure 51 is similar to the combination ($\alpha = 10°$, K = 0.5) shown in Figure 44. In particular, both have the crossover point located at around x/L = 0.3, and the overall pressure loading magnitude is also about the same. In practice, this implies that if the wind shifts from $\alpha = 20^0$ to $\alpha = 10^0$, the same cross
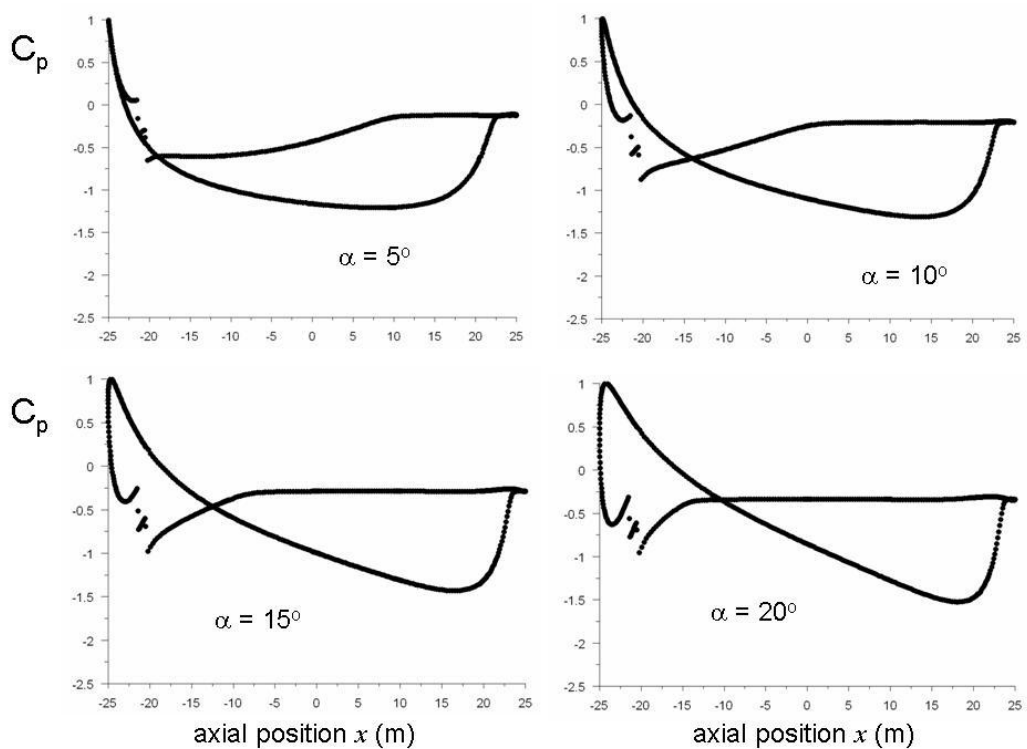
Figure 51: Effect of wind incidence angle for Case 1

ventilation setup (i.e. intake/exhaust distribution) can be preserved if one changes the flow-resistance value of the U10 device from K = 0.9 to K = 0.5, along with some adjustments of the size of the openings between indoor and outdoor to maintain the same local flow rate. This suggests that, since each flow-resistance device has two degrees of freedom (position and flow-resistance magnitude), and combining with the ability to adjust the size of the openings between indoor and outdoor, control algorithms may be developed to obtain arbitrary localized ventilation requirements under any wind conditions.

Based on these results, it is observed that the resistance device concept is effective when the body is not bluff, and when streamline curvature is present. Flow separation on account of a bluff body makes it difficult to control pressure distribution using this

concept. The resistance device is effective in regions of high velocity as the pressure drop as given by Equation (25) is larger. The mechanism of manipulating the pressure distribution via the curvature of the building geometry can be explained as follows. The pressure gradient normal to a streamline is given by Equation (26),

$$\frac{\partial p}{\partial n} = \frac{\rho V^2}{R} \tag{26}$$

where n is the direction normal to the building envelope surface, and R is the local radius of curvature of the building envelope surface. Since the pressure at infinity is equal to the free stream pressure, then, according to Equation (26), the pressure near the body can be changed if the local velocity can be manipulated. As an example, at a given location, the local velocity will be different if a resistance device is placed upstream. However, as streamline curvature decreases (i.e., as $R \to \infty$), Equation 26 states that the normal pressure gradient approaches zero, and therefore, there is no change in the static pressure. This mechanism is illustrated in Figure 52, which displays the streamlines around the 15% thick ellipse discussed previously, with and without a jet flap.

No jet flap   **With jet flap (C$_\mu$ = 0.24)**
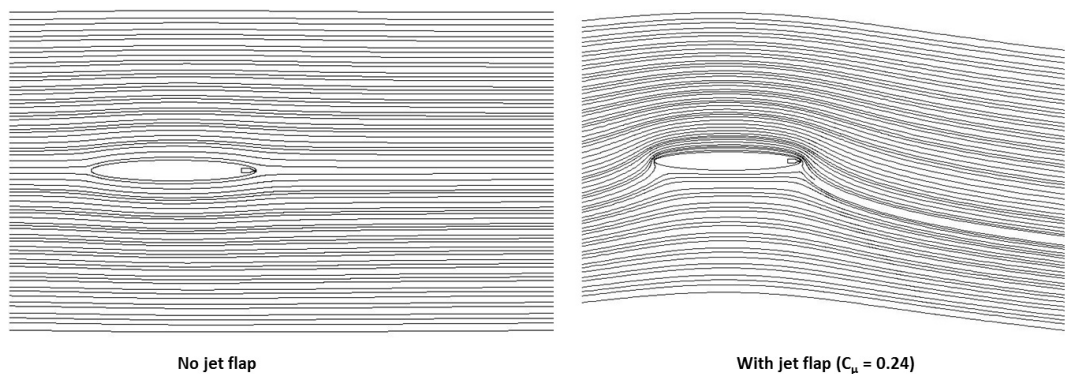
Figure 52: Effect of streamline curvature

The streamline pattern in the case without a jet flap is symmetrical, and the stagnation

point is located at the leading edge of the ellipse. In the case with a jet flap, it is seen that the location of the stagnation point moves to the lower surface of the ellipse. Consequently, we observe a significant change in the flow pattern around the ellipse. The streamline curvature near the lower surface of the ellipse indicates that the pressure is higher near the ellipse as compared to the free-stream value, as described by Equation 26. Similarly, for the upper surface, Equation 26 dictates that the pressure is lower near the ellipse as compared to the free-stream pressure. Consequently, the surface pressure distribution is significantly altered as compared to the case with no jet flap, and a net pressure difference is generated across the two surfaces of the ellipse.

3.5   3-D CFD Study

The 2-D CFD study described above demonstrates the potential for manipulation of building envelope wind pressure distribution by using the flow resistance device method. In particular, it is seen that the elliptical cross-section building is well suited for application of this technique. It is then necessary to study the effectiveness of this method when applied to a full-scale building.

In this section, a 3-D CFD study of a full-scale building is described, in which the effect of the resistance device concept is evaluated. To this end, an elliptical cross-section building with the same cross-sectional dimensions as discussed previously is considered. The building under consideration is 130 m tall. For the full scale building, the computational grid is developed by extruding a 2-D mesh in the vertical direction and specifying the required number of grid points in this direction. However, the grid requirements for studying the flow around a full scale 3-D building are quite significant. For example,
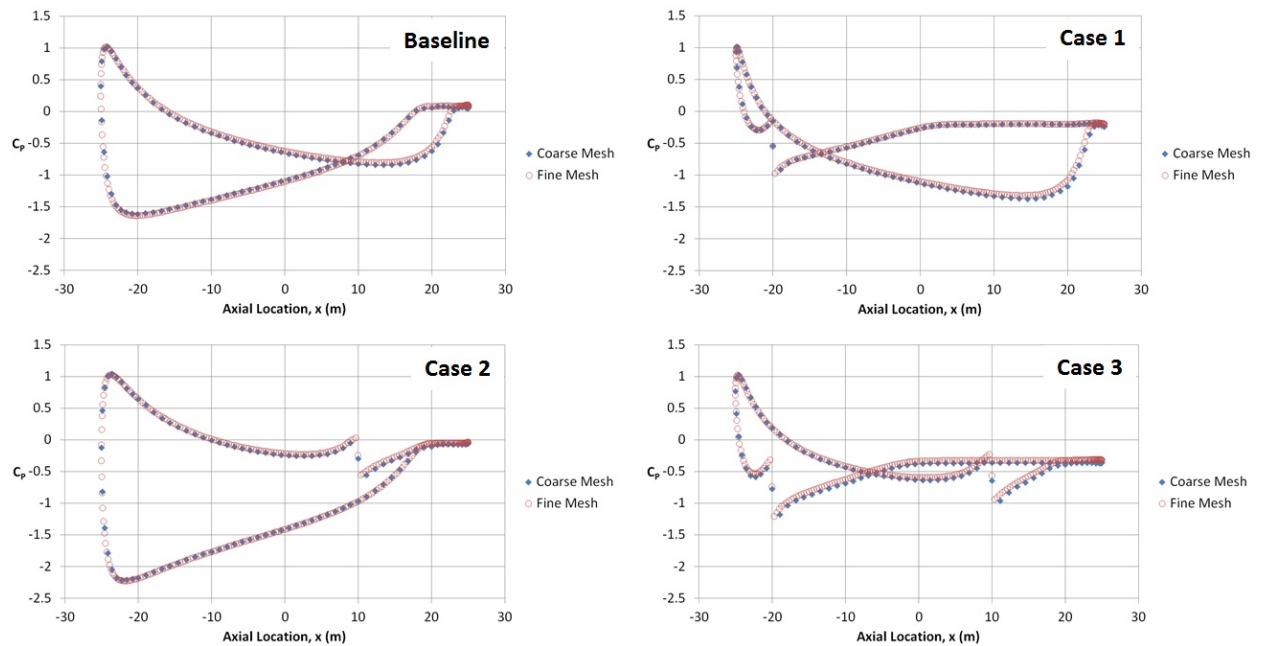
Figure 53: Comparison of pressure coefficient results obtained using fine and coarse meshes

extruding the mesh previously developed during the 2-D study ($\sim$ 50,000 cells) and using a cell for every meter in the vertical direction necessitates the use of a grid with about 6.75 million cells to model the entire building. In addition, the far field boundary has to be 2-3 times the height of the building away from the roof for numerical convergence. Hence, it is apparent that the computational requirements are very steep when attempting to model a full-scale building. It is therefore necessary to reduce the computational demands given the resources available. The 2-D study was conducted using a very fine mesh which used enhanced wall treatment for the turbulence model chosen ($y^+ < 1$). For the 3-D study, the computational resources available rule out the use of a very fine mesh. Therefore, we seek to use a coarse mesh and standard wall functions for the turbulence model ($30 < y^+ < 300$) to model the flow around the elliptical high-rise building.

The coarse 2-D mesh developed for this purpose has approximately 4,500 cells, as

compared to around 50,000 cells in the fine mesh used previously. It is first necessary to ensure that this coarse mesh can reproduce the results obtained using the fine grid accurately. Figure 53 shows the comparison of the results obtained using both the fine and the coarse grid for the cases studied previously. There is very good agreement between the results obtained with coarse mesh and those obtained using the fine mesh. Therefore, the coarse mesh is chosen as the starting point from which the computational grid for the 3-D building is generated.

(a)   (b)

(c)
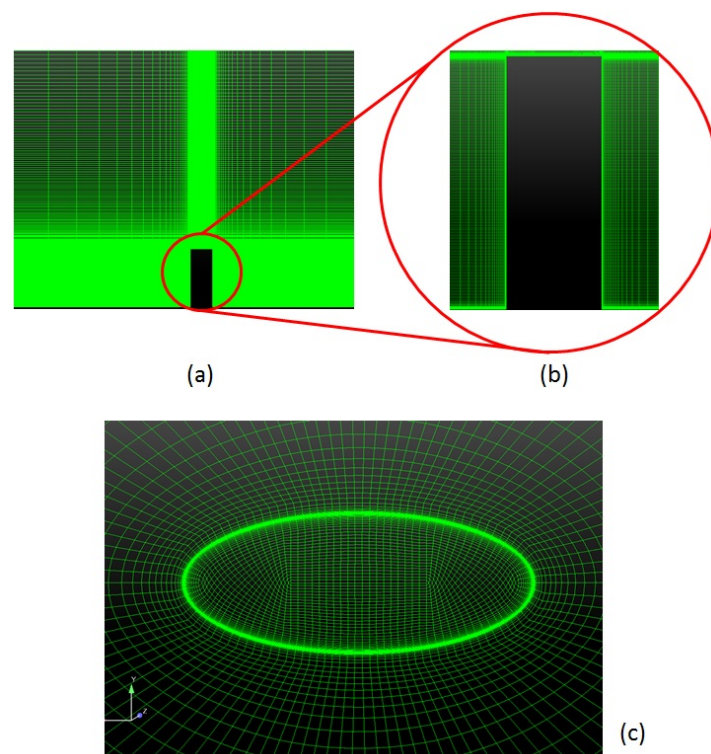
Figure 54: Mesh used for 3-D calculations (a) Elevation (b) Elevation close up (c) Plan

The 3-D grid is extruded from the 2-D grid by using an average cell spacing of 0.3 m over almost the entire height of the building, excepting the region near the ground and the roof, where this spacing is reduced significantly in order to ensure y^+ values that are in the

appropriate range. The mesh generated contains approximately 2.5 million cells. Various cross-sections of the 3-D mesh generated are shown in Figure 54.

The airflow near the earth's surface is slowed down on account of the presence of obstacles such as trees, buildings etc. This leads to the formation of an atmospheric boundary layer (ABL), where the wind speed increases from a value of zero at the surface to the free-stream speed, over a distance, which is called the ABL thickness. This distance is mainly a function of the terrain over which the wind blows, with small values associated with open terrain, and large values observed where large obstacles are present, such as city centers with many tall buildings. According to the ASHRAE Handbook of Fundamentals, the ABL velocity profile may be modeled by an equation of the form,

$$U_H = U_{met} \left(\frac{\delta_{met}}{H_{met}} \right)^{a_{met}} \left(\frac{H}{\delta} \right)^a \tag{27}$$

where U_H is the wind speed at a height H meters above the ground. δ_{met} is the typical ABL thickness for the terrain in which the meteorological station is location, while a_{met} is an exponent used to model the ABL velocity profile for the same terrain. δ and a are the corresponding values for the terrain of interest for which the ABL profile is created. U_{met} is the wind speed measured by the meteorological station at a distance H_{met} (in m) above the ground. The standard value for H_{met} is 10 m, and meteorological stations are usually located in flat, open terrain, where typical values of δ_{met} and a_{met} are 210 m and 0.1 respectively. The ASHRAE Handbook provides typical values for δ and a for a variety of terrain conditions. By knowing the type of terrain, and the measured wind speed (U_{met}), it is then possible to obtain the ABL profile (i.e., obtain U_H as a function of H).

Typical velocity profiles for open terrain and a city center are shown in Figure 55. These
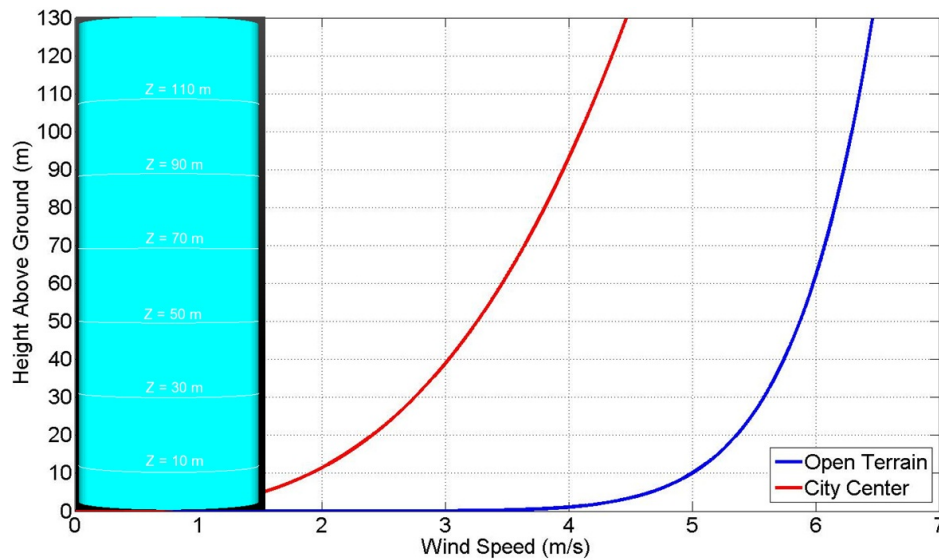
Figure 55: ABL velocity profiles for two types of terrain

profiles were created using a measured wind speed (U_{met}) of 5 m/s at 10 m (H_{met}) from the ground. We see that for the open terrain, there exists a very high velocity gradient close to the ground where most of the velocity change occurs. The ABL thickness for the city center is quite large (the ASHRAE Handbook recommends a typical value of 460 m) compared to that over open terrain, therefore, the velocity gradient near the ground is not as steep. Here, at a height of 10 m, the wind speed in the city center profile is less than the meteorological wind speed (U_{met}), as it is assumed that the meteorological station is located in open terrain. The velocity profile shown above for the open terrain will be used for all the 3-D CFD simulations performed in this section. One of the issues of interest to us is the effect the presence of the ABL has on the pressure distribution on the building surface, and how it impacts the performance of the resistance devices.

The wind angle of incidence for all the scenarios considered in this section is 10°. First, we consider the baseline scenario, with no resistance devices activated. The contours of static

pressure for this case are shown in Figure 56. The direction of flow in these plots is from the left to the right of both figures. Apart from the regions near the two ends of the building, the static pressure distribution is relatively two dimensional between 30 m and 110 m (i.e., contour does not change a lot with respect to height). Near the ground, we see large gradients in the vertical (z) direction, especially on the suction surface.
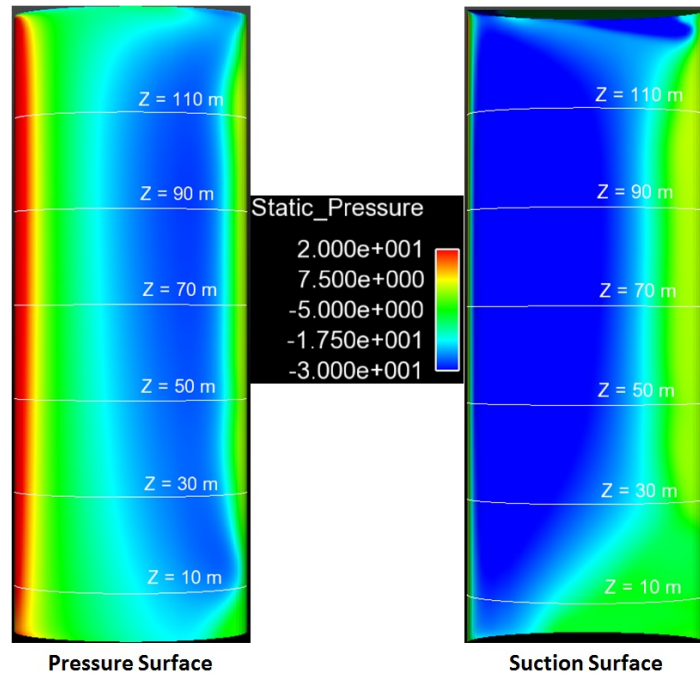
Figure 56: Static pressure contours (in Pa) for baseline scenario

Figure 57 displays the x-component vorticity contours on two planes that are normal to the building's major axis. The large velocity gradient near the ground (see Figure 55) causes the formation of regions of high streamwise vorticity ("horseshoe" vortices) close to the ground. These can be seen in Figure 57 (a) as regions of x-vorticity of opposite sense on the two sides of the building. These induce velocity in the vertical direction, as can be seen in Figure 58.

These regions of vertical velocity are present till around 30 m from the ground, and are
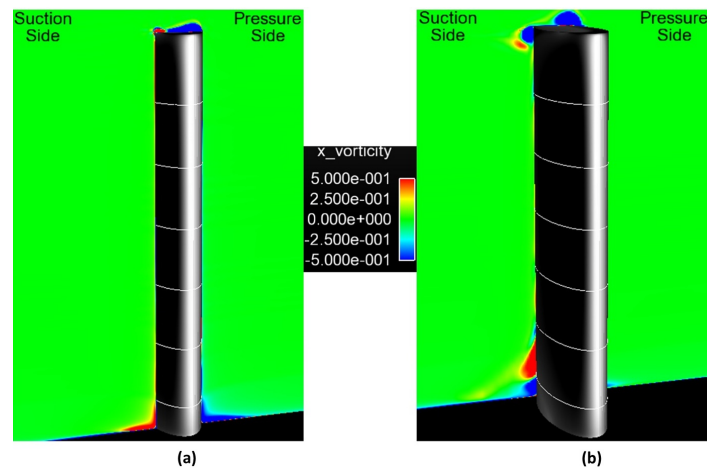
Figure 57: x-**vorticity contours (in 1/s) for baseline scenario :   a) 10 m downstream of leading edge b) 45 m downstream of leading edge**

responsible for the three dimensionality in static pressure observed on the building surface in this region. Above around 30 m, the vertical velocities are very small, and therefore, from this point onwards, the static pressure distribution exhibits negligible gradient in the z-direction. Such horseshoe vortices are encountered at the intersection of a solid surface and an object, whenever an object is immersed in a flow with free-stream velocity gradient. Based on these results, we see that the CFD simulation is able to qualitatively capture the effects of the presence of the horseshoe vortices. Near the roof of the building, large regions of vertical velocity are again encountered. This can be attributed to the formation of tip vortices, similar to those found near the wing tips, where air from the high pressure side flows around the tip of the wing towards the low pressure side. We note that this affects the pressure distribution till about a height of 110 m, or about 20 m away from the roof of the building.

Figure 59 compares the static pressure distribution around the building perimeter at five heights along the building. The locations at $z = 10$ m and at $z = 120$ m are chosen to
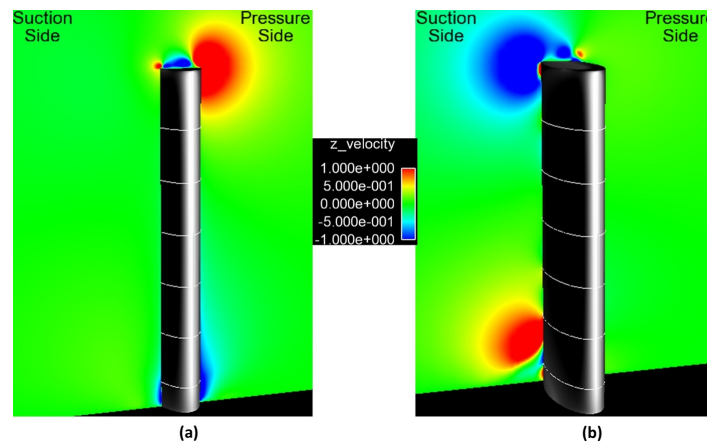
Figure 58: Vertical velocity contours (in m/s) for baseline scenario : a) 10 m downstream of leading edge b) 45 m downstream of leading edge

represent the regions influenced by the presence of the ground and end effects, respectively. The remaining three locations represent the central region of the building. The pressure distribution at the 10 m level is quite different as compared to those at the other heights. In particular, the location of the "crossover" point is approximately at $x = $ -2 m as compared to around $x = 6$ m at $z = 65$ m. At $z = 120$ m, a reduction in the magnitude of the pressure loading is observed as compared to $z = 90$ m. This is caused by the end effects, where air flows over the top of the building from the high pressure side to the low pressure side, thus providing a "relieving" effect. In the central region, the pressure distribution is seen to be relatively two dimensional. The value of the peak positive and negative pressures increases as the height increases. This is on account of the presence of the ABL, due to which free-stream velocity increases along the height of the building.

Next, for the purpose of investigating the effect of resistance devices, the building is first divided into two blocks of equal height. Each block has two resistances located at the U10 and L70 locations (refer Figure 25) which extend through its entire height, i.e., each resistance spans half the height of the building. All 4 resistance devices can be controlled
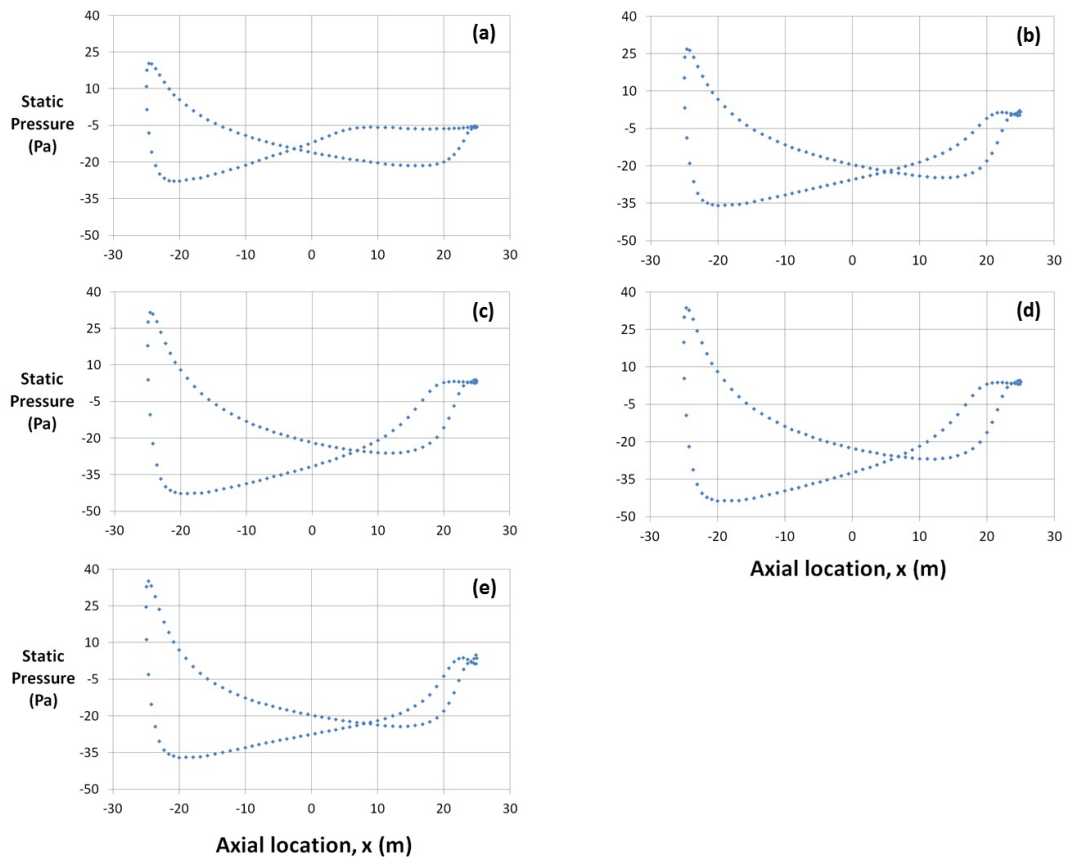
Figure 59: Comparison of static pressure for baseline scenario at : (a) $z = 10$ m (b) $z = 30$ m (c) $z = 65$ m (d) $z = 90$ m (e) $z = 120$ m

independently (i.e., turned on/off). We seek then seek to explore the extent to which it is possible to have independent control over the pressure distribution over each of the two blocks of the building. Achieving independent control may allow us to control the direction of airflow exchange (as well as the amount of airflow) in the zones within each block independently. These issues will be examined in the following chapter.

Figure 60 illustrates the location of the resistance device for the first configuration considered. Here, the resistance device located on the suction surface (U10 location) extends throughout the entire height of the building, and there is no resistance device on

the pressure surface. Note that for this scenario, the resistance pressure drop coefficient is 0.5.
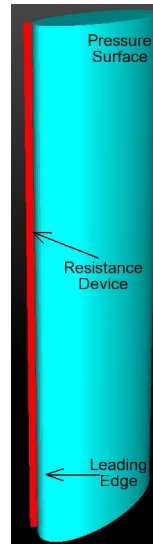
Figure 60: Resistance device locations : configuration 1

Figure 61 displays the contours of static pressure on the pressure surface for this configuration. On this surface, for configuration 1, we see that the static pressure distribution is two-dimensional over almost the entire height of the building. Vertical gradients are observed near the two ends of the building, however, these are restricted to about a distance of 10 m from either end. Apart from these regions, the pressure distribution in the vertical direction is negligible. The magnitude of peak suction (i.e., low pressure) is lower for configuration 1 as compared to that for the baseline. Also, in configuration 1, the region of low pressure extends over a larger portion of this surface as compared to the baseline.

The corresponding static pressure contours on the suction surface for this configuration are displayed in Figure 62. Again, the pressure distribution is observed to be two-dimensional over a significant portion of the building height. On this surface, vertical gradients are
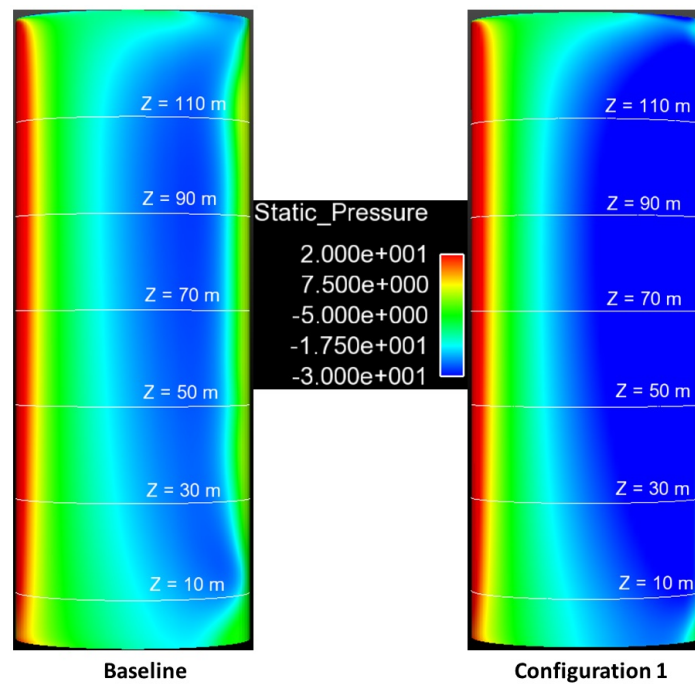
Figure 61: Contours of static pressure on pressure surface (in Pa) : configuration 1

observed up to a distance of about 30 m from the ground, and also about 10 m away from the roof of the building. The pressure distribution in between these regions does not vary significantly with height. On this surface, the region of low pressure observed is smaller in area for configuration 1 in comparison with the baseline scenario.

In the next configuration considered, a resistance located on the pressure surface (L70 location) extends throughout the height of the building, while there is no resistance device present on the suction surface. This configuration is shown in Figure 63. Again, for this scenario, the resistance device pressure drop coefficient is 0.5.

The static pressure contours on the pressure surface for configuration 2 are displayed in Figure 64. As was observed in configuration 1, the pressure distribution resulting from this
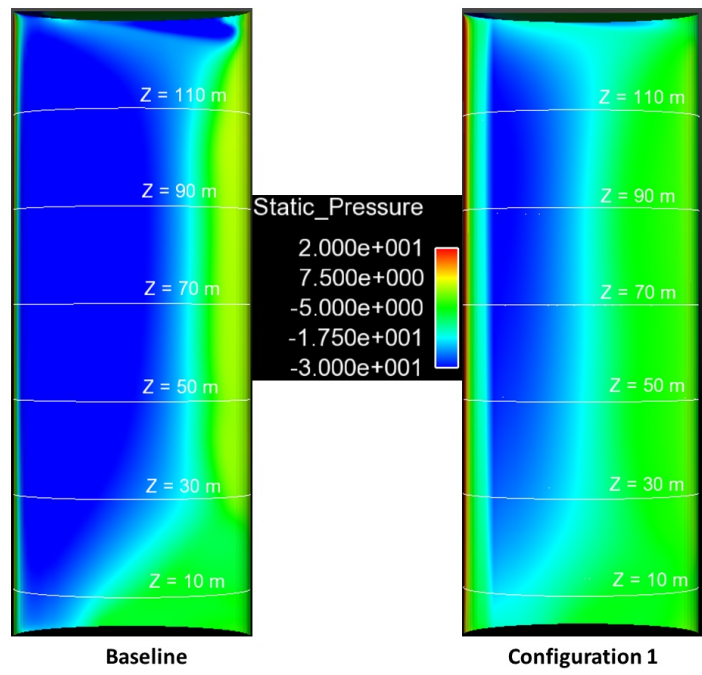
Figure 62: Contours of static pressure on suction surface (in Pa) : configuration 1
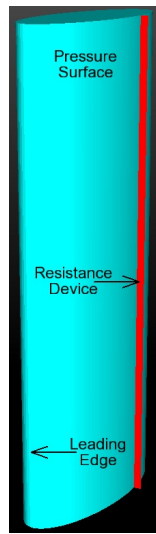
Figure 63: Resistance device locations : configuration 2

resistance configuration exhibits negligible vertical gradients over most of the building

height. Vertical gradients are observed over a small portion near the trailing edge of the

surface up to about 30 m from the ground, and around 5 m from the roof.
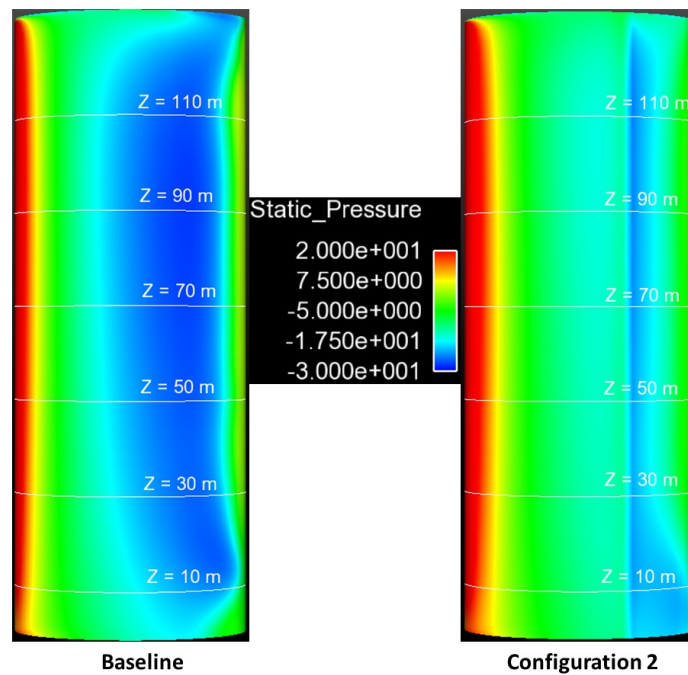
Figure 64: Contours of static pressure on pressure surface (in Pa) : configuration 2

The static pressure contours on the suction surface for configuration 2 are shown in Figure 65. The region of low pressure is slightly larger in area for configuration 2 as compared to the baseline. Aside from this, the pressure distributions for the two scenarios are quite similar. A steep vertical gradient is observed in the pressure distribution up to a height of 30 m, however, aside from this region, the pressure distribution is relatively two-dimensional. Looking at the results for configurations 1 and 2, it can be concluded that utilizing continuous resistance devices that extend over the entire height of the building, it is possible to achieve a mostly two-dimensional pressure distribution over the building surface, except for the regions near the two ends of the building.

Figure 66 displays the locations of the resistance devices for configuration 3. In this
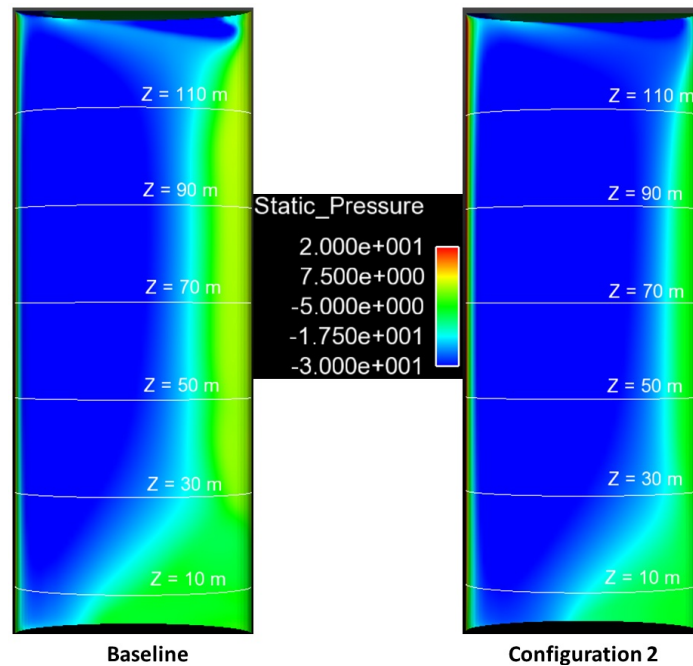
Figure 65: Contours of static pressure on suction surface (in Pa) : configuration 2

scenario, a resistance device is located throughout the entire height of the building on the suction surface (U10 location), and on the pressure surface, a resistance device is present in the L70 location on the upper half of the building. For this resistance device configuration, as well as all the subsequent configurations considered, the pressure drop coefficient is 0.9.

For this configuration, the static pressure contours on the pressure surface of the building envelope are shown in Figure 67. It is seen that the pressure distribution on this surface is quite different compared to the baseline scenario. The pressure distribution for the upper and lower halves differ markedly on account of the change in the resistance device configuration on this surface. In contrast, the pressure contours are relatively two-dimensional for the baseline scenario as discussed previously. In configuration 3, the pressure distribution is relatively two dimensional in the region from around 20 m to 50 m,
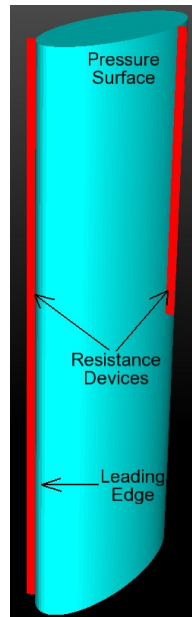
Figure 66: Resistance device locations : configuration 3

and again from around 70 m to 120 m. As in the baseline scenario, we observe the influence of the both the ground and the end effects at the two ends of the building. The vertical gradients observed from 50 m to 70 m are a result of the change in the resistance device configuration that occurs in this region (at 65 m).

Figure 68 shows the static pressure contours on the suction surface for this configuration. Again, the pressure distribution differs markedly from that observed in the baseline case. The large region of low pressure seen in the baseline scenario reduces significantly on account of the presence of the resistance device on this surface. In contrast with the pressure surface, the resistance device on this surface extends throughout the height of the building for this scenario. Hence, the pressure distribution is relatively two dimensional on this surface. Figure 69 shows the distribution of static pressure at the five locations along the building height selected for the baseline scenario.

Figure 67: Contours of static pressure on pressure surface(in Pa) : configuration 3
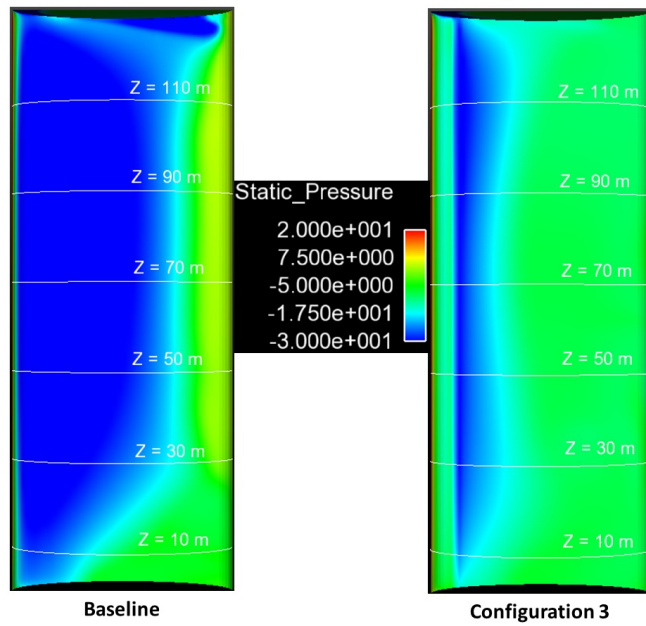
**Figure 68: Contours of static pressure on suction surface (in Pa) : configuration 3**
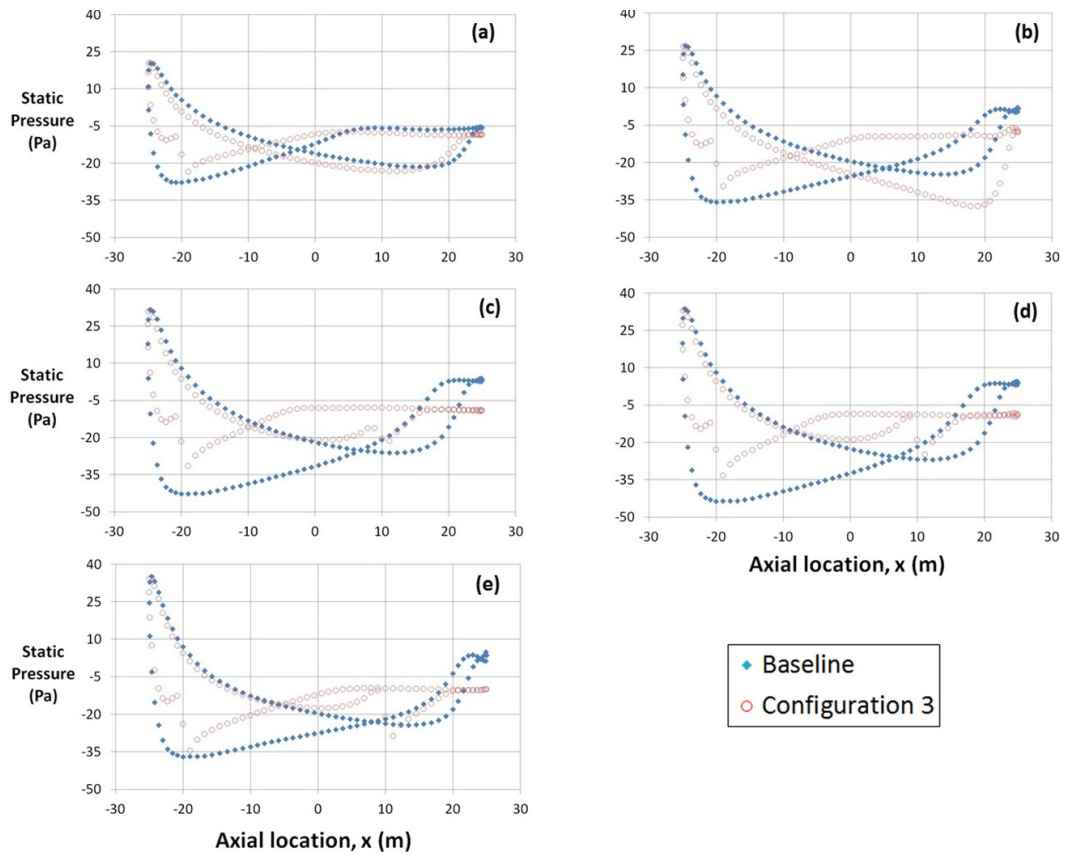
Figure 69: Comparison of static pressure for configuration 3 at : (a) $z = 10$ m (b) $z = 30$ m (c) $z = 65$ m (d) $z = 90$ m (e) $z = 120$ m

In this case, two locations ($z = 10$ m and $z = 30$ m) represent the pressure distributions resulting from the resistance device configuration in the lower half of the building, two locations ($z = 90$ m and $z = 120$ m) represent the pressure distributions resulting from the resistance device configuration in the upper half of the building, and the fifth location ($z = 65$ m) is chosen to represent the region where the resistance device configuration transitions from the lower half to the upper half. It is readily apparent that the presence of the resistance devices in both halves of the building allow us to modify the building envelope pressure distribution quite significantly as compared to the baseline scenario. At $z = 10$ m, the pressure profiles for configuration 3 and the baseline case are similar. At all

other heights, the pressure profiles are quite different, both in terms of the location of the "crossover" point, as well as the magnitude of the loading imposed on the building envelope. Comparing the pressure profiles at $z = 30$ m and $z = 90$ m, the main difference between the pressure distributions between the upper and lower halves of the building is a reduction in the magnitude of the pressure loading downstream of the mid-chord ($x = 0$ m) location for the upper half of the building.

The next resistance device configuration considered is shown in Figure 70. In this configuration, a resistance device is located over the entire height of the building on the pressure surface (L70 location), and a device in the U10 location is located on the upper half of the building (from 0 m to 65 m).
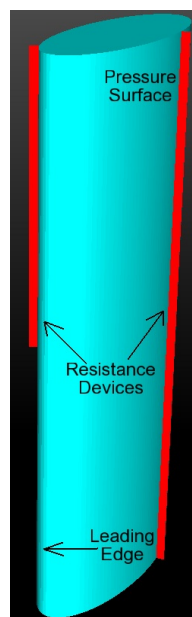
Figure 70: Resistance device locations : configuration 4

The static pressure contours on the pressure surface for this case are shown in Figure 71. As seen previously, the pressure distribution is quite different from that observed for the baseline scenario. The region of low pressure observed throughout the building on this

surface in the baseline case is greatly reduced in area. As the resistance device on this surface extends throughout the entire height of the building, there is not a lot of difference between the pressure distributions for the upper and the lower halves of the building, i.e., the pressure distribution is relatively two dimensional.
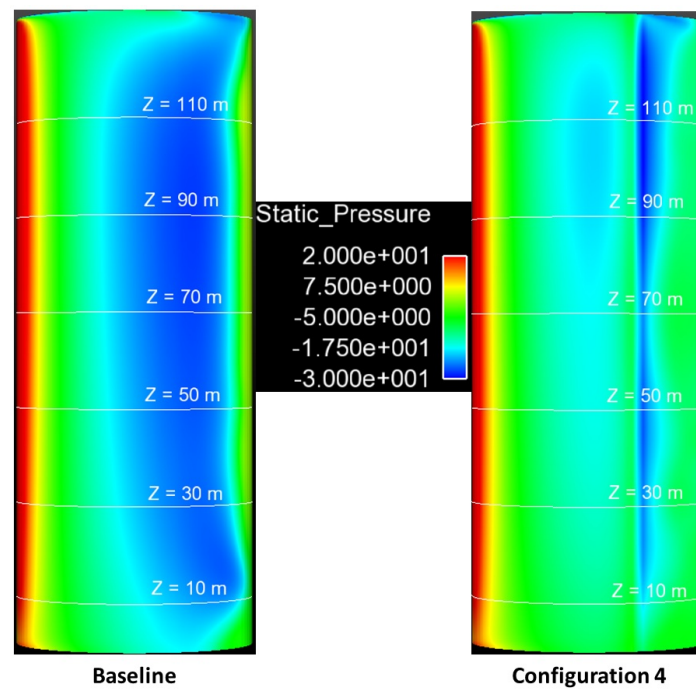
Figure 71: Contours of static pressure on pressure surface(in Pa) : configuration 4

The corresponding contours on the suction surface are displayed in Figure 72. On the suction surface, large vertical gradients are observed till about a height of around 65 m (mid-height). From 0 m to 30 m, the vertical pressure gradients can be attributed to the same mechanism explained in the baseline scenario. From 30 m to 65 m, the pressure distribution on this surface is affected by the resistance device located on this surface in the upper half of the building, and therefore, vertical gradients are present.

Figure 73 shows the pressure distribution at different heights along the building. At $z = 10$
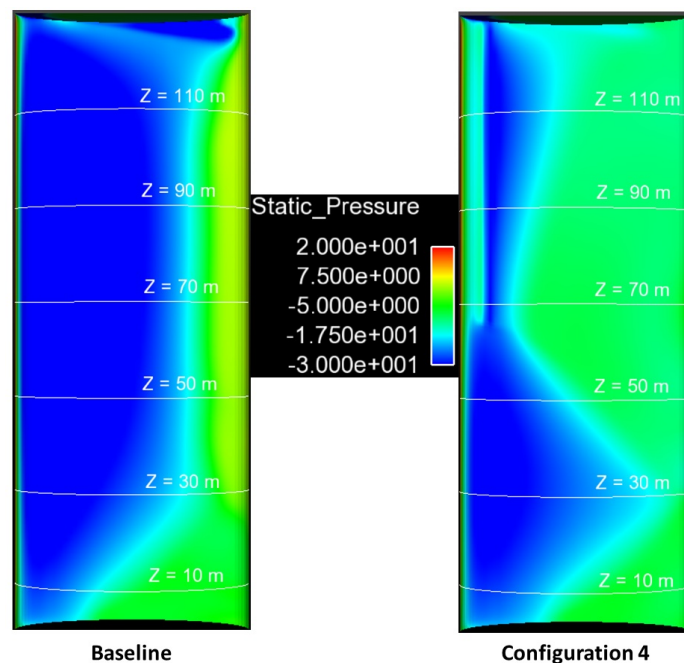
Figure 72: Contours of static pressure on suction surface(in Pa) : configuration 4

m, it is seen that the magnitude of the pressure loading (i.e., pressure difference between upper and lower surfaces) is close to zero downstream of $x = 0$ m except for the region in the immediate vicinity of the resistance device. At $z = 30$ m, the magnitude of loading downstream of $x = 0$ m increases marginally as compared to the previous location ($z = 10$ m). In both cases, the pressure distributions upstream of $x = 0$ are quite similar to the respective baseline pressure distributions. At $z = 65$ m and $z = 90$ m, the pressure distributions are quite similar. At $z = 120$ m, the location of the "crossover" point is shifted downstream as compared to $z = 90$ m. We also observe a decrease in the magnitude of the pressure loading downstream of the crossover point.

The next resistance device configuration is displayed in Figure 74. In contrast with the preceding configurations, in this scenario, only a single resistance device is used in each half

Figure 73: Comparison of static pressure for configuration 4 at : (a) $z = 10$ m (b) $z = 30$ m (c) $z = 65$ m (d) $z = 90$ m (e) $z = 120$ m

of the building. Here, a resistance device is located in the L70 position throughout the upper half of the building, and a device is located in the U10 position in the lower half of the building.

Figure 75 displays the contours of static pressure on the pressure surface of the building envelope for this configuration. The upper and lower halves of the building exhibit different pressure distribution for this scenario. Looking at the lower half of this surface, it is seen that vertical gradient near the middle of the building extends to about 50 m. In other words, the resistance device in the L70 location affects the pressure distribution to about
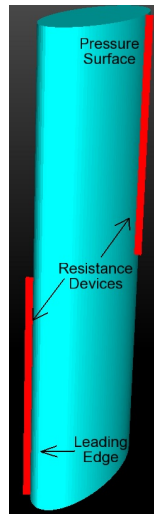
Figure 74: Resistance device locations : configuration 5

15 m away from its location vertically (from 65 m to 50 m).
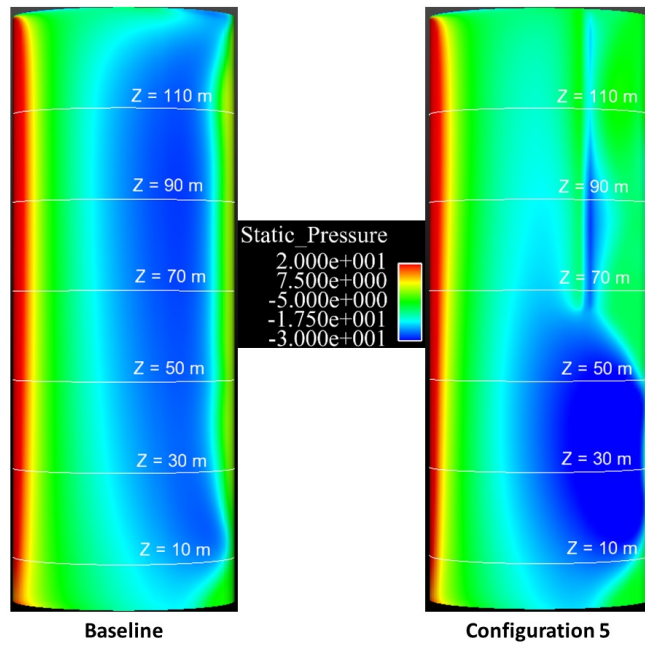
Figure 75: Contours of static pressure on pressure surface(in Pa) : configuration 5

The static pressure contours on the suction surface for configuration 5 are shown in Figure

98
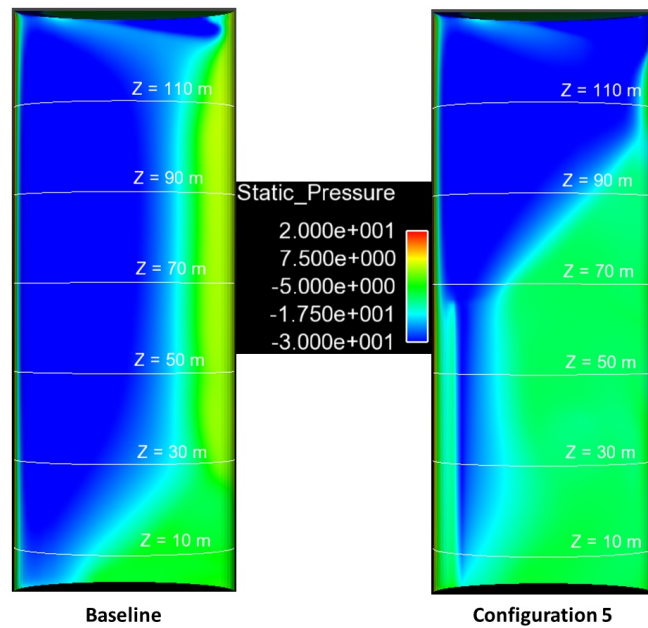
Figure 76: Contours of static pressure on suction surface(in Pa) : configuration 5

76. Again, the pressure distribution for the upper and lower halves are quite different. In particular, the region of low pressure that extends over a large portion of the upper half of the pressure surface is reduced in size over the lower half of the building. The pressure distribution on the lower half of the suction surface is similar to that seen in configuration 2, as in this region, the resistance device is the same in both cases. In contrast to the L70 location, the resistance device in the U10 location can affect the pressure distribution up to around 30 m away in the vertical direction. This can be seen from the fact that the vertical gradients seen on the suction surface extend from 65 m (where the resistance device configuration changes) to about 95 m.

Figure 77 compares the pressure distributions at five heights along the building. It can be seen that at $z = 10$ m, the crossover point is shifted upstream as compared to the baseline, however, for a large portion of the building cross-section, the pressure distribution is quite

similar to the baseline scenario.
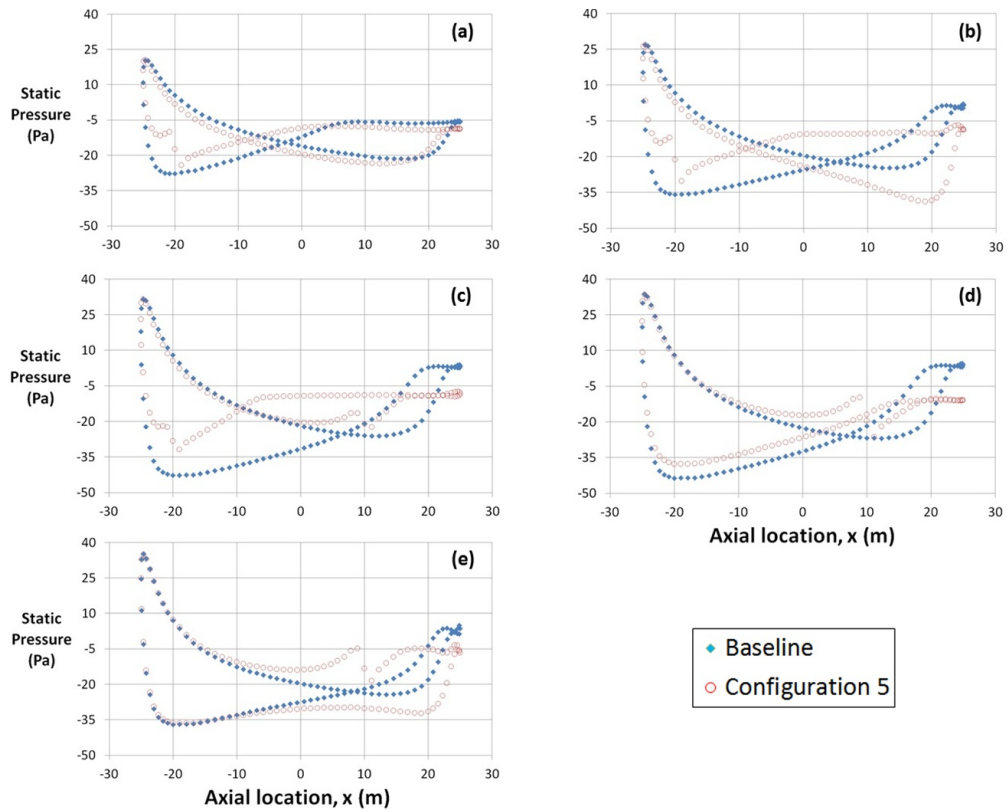
Figure 77: Comparison of static pressure for configuration 5 at : (a) $z = 10$ m (b) $z = 30$ m (c) $z = 65$ m (d) $z = 90$ m (e) $z = 120$ m

In addition, the pressure distributions over the upper and lower halves of the building are very different. The crossover point observed upstream of $x = 0$ m in the lower half of the building disappears in the upper half of the building. Also, at $z = 120$ m, we observe a significant increase in the pressure loading in the downstream section of the building. At this height, one surface of the building is at a higher pressure as compared to the other throughout the entire length of the building.

In the next configuration considered, the resistance device locations are reversed as compared to configuration 5. A resistance device is located in the U10 position in the

upper half of the building, and in the L70 position in the lower half of the building, as shown in Figure 78.
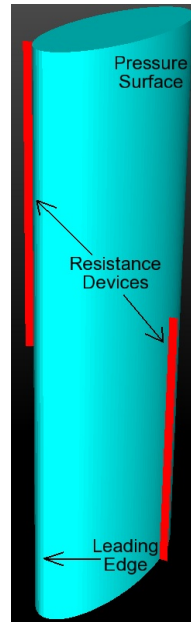
Figure 78: Resistance device locations : configuration 6

The pressure contours on the pressure surface for configuration 6 are displayed in Figure 79. The trends observed here are similar to those seen in configuration 5. For instance, the region of low pressure present in the upper half of the surface disappears in the lower half due to the presence of the resistance device in this region on the lower half. This is similar to the upper half of the pressure surface in configuration 5.

Figure 80 displays the static pressure contours on the suction surface for configuration 6. These contours are quite similar to those observed on the suction surface for configuration 4. Over the upper half of the surface, the pressure distribution remains relatively constant on account of the presence of the resistance device in this half. Over the lower half, we see the effect of the presence of the ground (leading to the gradient from 0 m to 30 m), and the
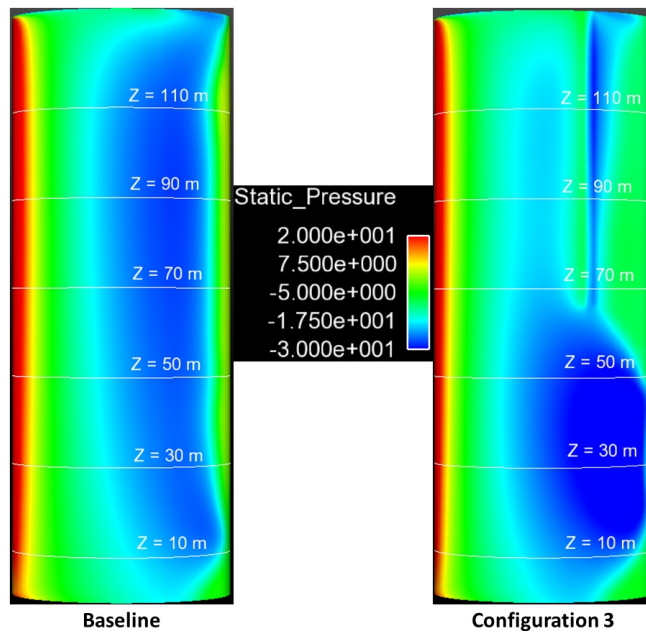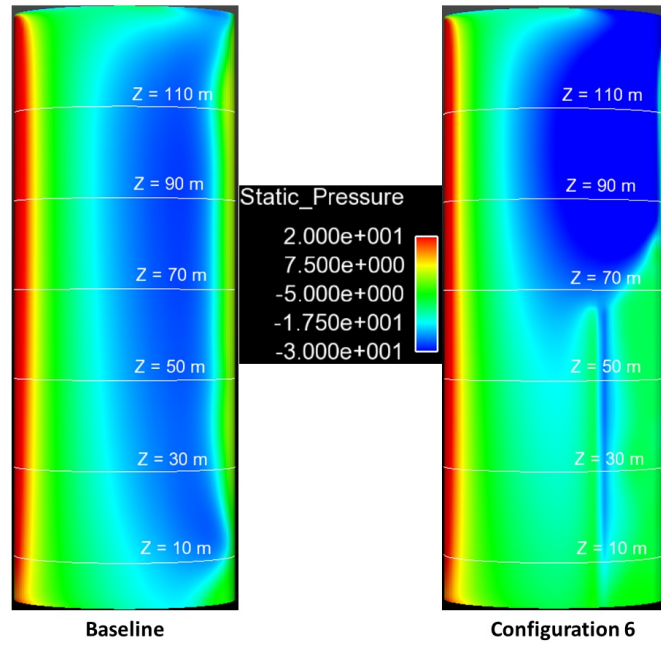
Figure 79: Contours of static pressure on pressure surface(in Pa) : configuration 6
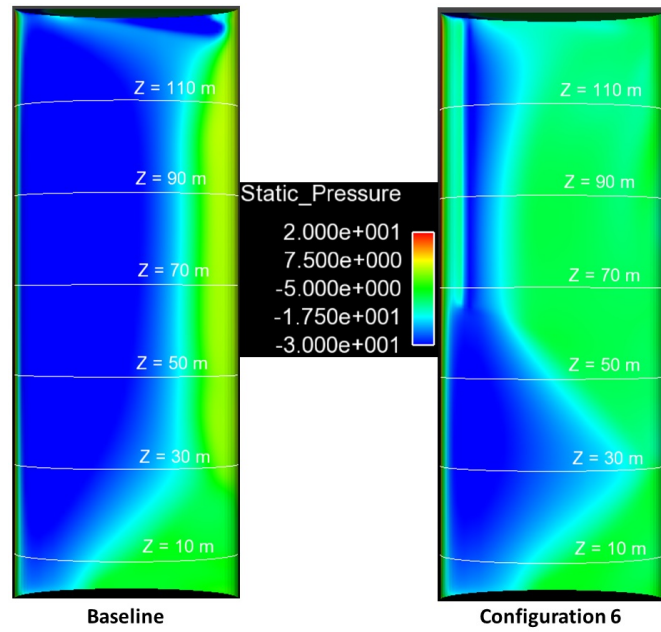
**Figure 80:** Contours of static pressure on suction surface(in Pa) : configuration 6

effect of the resistance device on the upper half (causing the gradient from 30 m to 65 m).

Figure 81 compares the pressure distributions at five heights along the building. The pressure distributions over the upper and lower halves are quite different, as was the case in configuration 5. In the lower half of the building, we observe small magnitudes of pressure loading downstream of the mid-chord location ($z = 10$ m & $z = 30$ m) . As we move upwards along the building, we notice a transition where the loading on the downstream section gradually increases ($z = 65$ m), and finally, in the upper half of the building ($z = 90$ m & $z = 120$ m), we observe relatively large pressure loadings present. Another interesting point is that in the upper half of the building, the location of the crossover point is shifted by around 20 m ($\sim 40\%$ chord) as compared to the baseline scenario.

On the basis of these results, it can be seen that it is possible to have very different pressure distributions for the upper and lower halves of the building by utilizing continuous banks of resistance devices. Away from the ends of the building, and the regions where there is a change in the device configuration, the pressure distributions approach those obtained from the 2-D CFD simulations. Resistance devices located in the U10 position affect the pressure distribution up to around 30 m away in the vertical direction, whereas devices in the L70 position only affect the distribution up to about 15 m away. The steep velocity gradient near the ground and the end effects present near the top of the building cause the pressure distribution in this region to diverge from what is expected on the basis of the 2-D results.

The next question is to determine the minimum number of resistance devices that are needed in order to achieve the level of control demonstrated in the above results. Instead of utilizing continuous banks of devices, we now employ discrete devices and seek to determine the vertical spacing between them such that we can maintain the level of
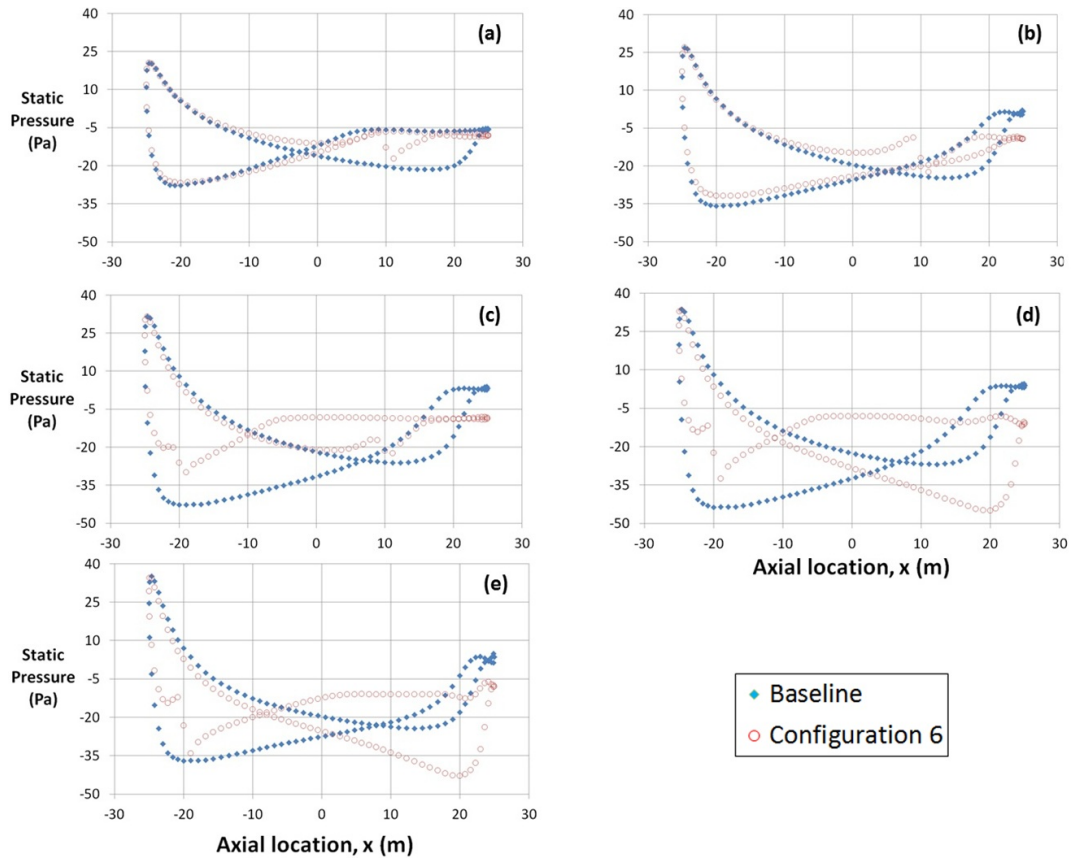
Figure 81: Comparison of static pressure for configuration 6 at : (a) $z = 10$ m (b) $z = 30$ m (c) $z = 65$ m (d) $z = 90$ m (e) $z = 120$ m

pressure control obtained using the continuous banks of devices.

For this purpose, we consider a scenario where the resistance locations are the same as in configuration 6, but with discrete devices instead of continuous devices. Figure 82 shows the resistance device locations for configuration 7. In this scenario, each resistance device is 3 m high, and the resistance devices are separated by a gap of 9 m.

Figure 83 shows the distribution of static pressure on the pressure surface for configurations 6 and 7. There are some gradients in the z-directions that can be observed downstream of the resistance devices in the discrete case that are not present in the
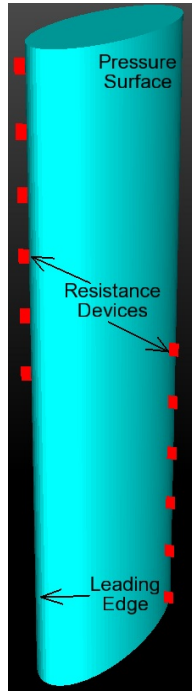
Figure 82: Resistance device locations : configuration 7
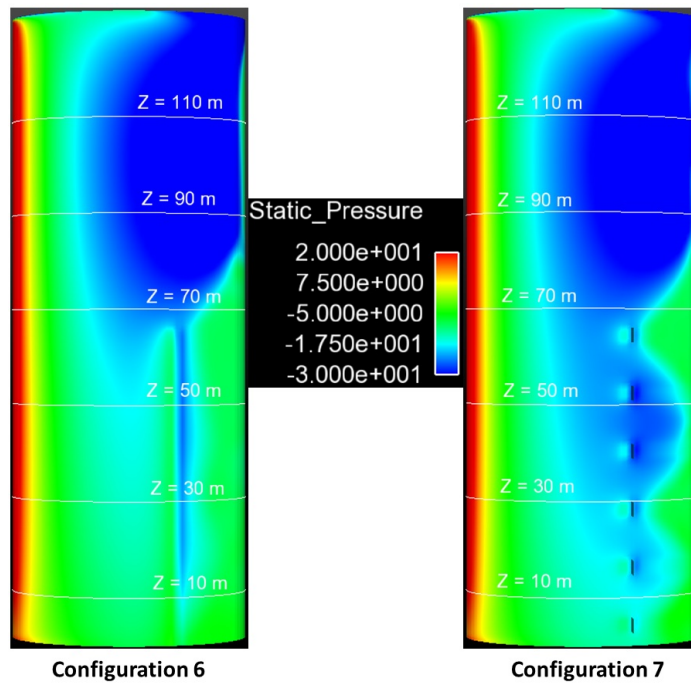
Figure 83: Comparison of static pressure contours : pressure surface
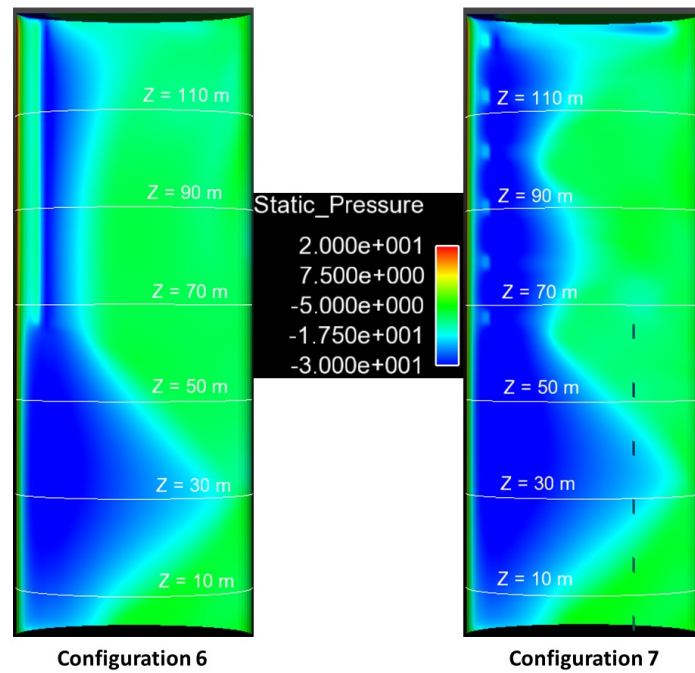
Figure 84: Comparison of static pressure contours : suction surface

continuous case, but on the whole, the pressure distributions are quite similar.

The corresponding pressure contours on the suction surface are shown in Figure 84. Again, there are some vertical gradients present downstream of the resistance devices in the discrete case, however, the pressure distributions for the discrete and continuous cases are similar in nature.

Figure 85 compares the pressure distributions at five heights along the building for these two configurations. It is readily seen that the pressure plots at all the heights considered are similar. Minor deviations from the configuration 6 pressure distribution are observed, particularly at $z = 10$ m, and $z = 90$ m. On the whole, the discrete resistance device case produces results that are very similar to those obtained using continuous resistance devices.
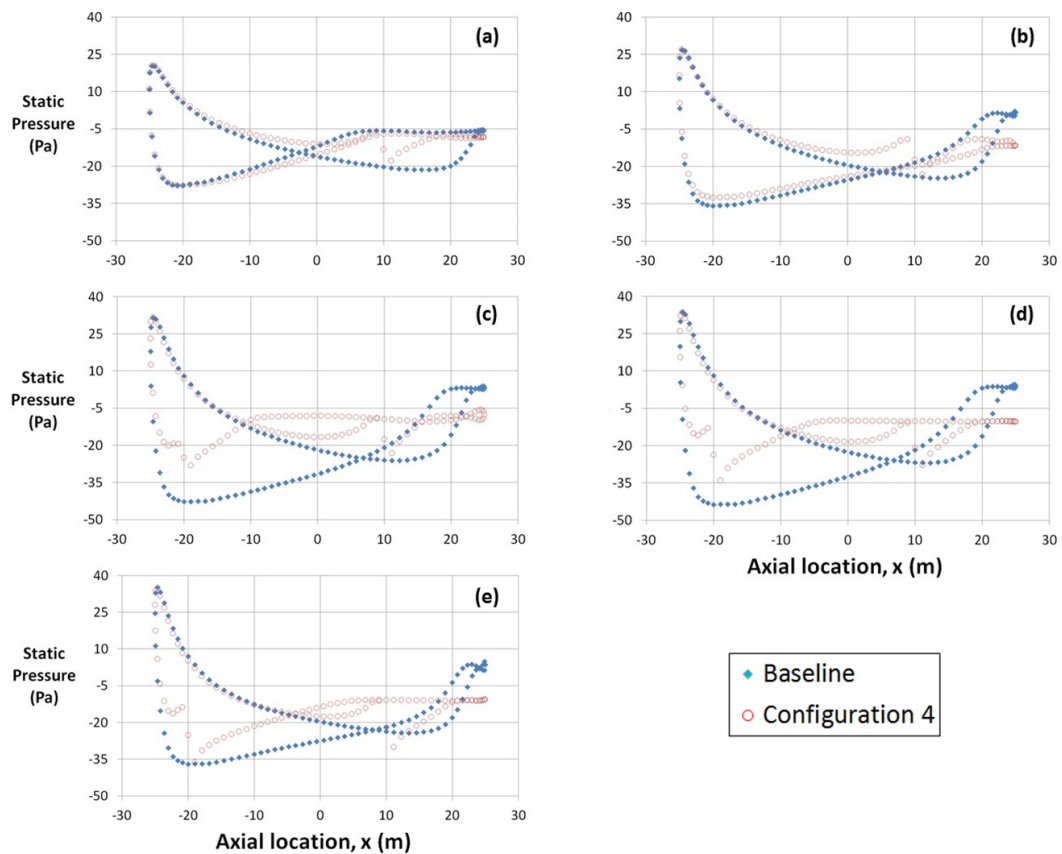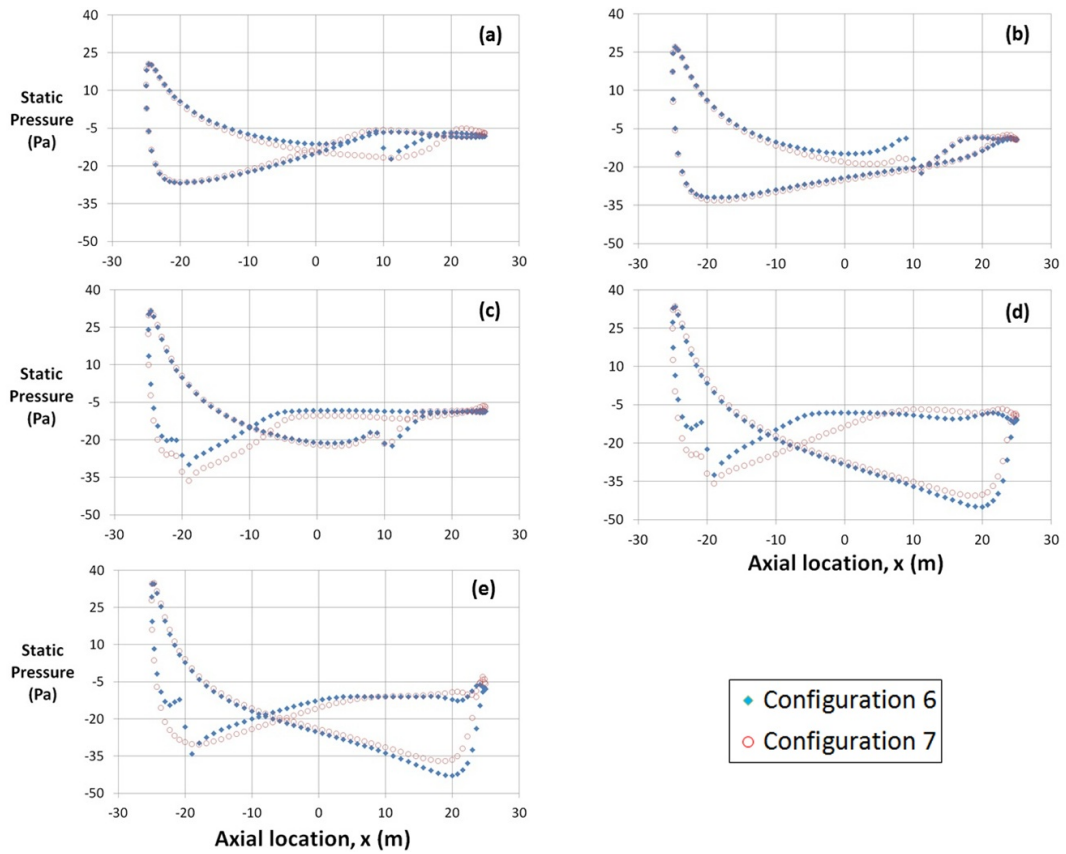
Figure 85: Comparison of static pressure for configurations 6 and 7 at : (a) $z = 10$ m (b) $z = 30$ m (c) $z = 65$ m (d) $z = 90$ m (e) $z = 120$ m

Utilizing continuous banks of resistance devices provides the maximum possible control over building envelope pressure distribution. However, it may be the case that this configuration is financially expensive to implement. On the basis of these results, it may be sufficient to employ resistance devices spaced 9 m apart as opposed to continuous devices, and this may be a more viable solution. Finer control may be achieved using discrete devices by reducing the vertical spacing between them.

4   Control of natural ventilation

4.1   Need for control

One of the main challenges encountered during implementation of natural ventilation is the unpredictability of the driving forces involved. Both diurnal and seasonal variations are observed in ambient wind and temperature. On account of varying wind and temperature, there may be scenarios where the driving forces are insufficient to meet the ventilation requirements. Conversely, there may also be situations where the driving forces are much stronger than necessary, and may lead to occupant discomfort on account of factors such as draft. In addition, in natural ventilation, there is the factor of communication between zones, which is usually not present in conventionally ventilated systems. This means that improving the ventilation provided in one zone may actually lead to a decrease in the quality of ventilation provided to another zone on account of the airflow exchange that takes place between zones in natural ventilation. Therefore, in order to ensure that adequate ventilation is provided to all the zones of a building, it is necessary to have a centralized decision-making process. Hence, in order to account for changing ambient weather condition, changing ventilation demands and the communication between zones, it is necessary to develop a suitable control strategy for the application of natural ventilation.

4.2   Control framework

In this section, the use of the resistance device concept to control natural ventilation is discussed. It needs to be emphasized that the use of the word "control" in this section does

not imply formal application of classical control techniques. Rather, this work should be interpreted as an exploratory investigation of how the resistance device concept can be applied in a useful manner for the purpose of manipulating the airflow distribution in a naturally ventilated building, depending upon the prevailing ventilation requirements. In this study, the aim is to automatically control the airflows in the building by changing the openings of ventilation ports and the location of external resistance devices. In real life applications, the decisions of a controller developed for this purpose would be based on measurements of the contaminant distribution in various zones, the pressure distribution around the building envelope, and the indoor environment conditions in various zones and the ambient. Due to a number of dynamically changing factors such as wind speed and direction, and occupancy distribution, optimization and intelligent control algorithms are needed to achieve the ventilation objectives.

In this work, a methodology based on model-predictive control is adopted, which may be interpreted as a series of optimization problems. Furthermore, a quasi-steady state approach is implemented in which it is assumed that at each time step, the conditions are at steady state. A fully dynamic approach that accounts for transient effects is beyond the scope of this work. Finally, due to the coupling between zones, ventilation ports, and pressure distribution, a local or decentralized control strategy cannot be used and hence a centralized controller that simultaneously processes all this information is needed.

The method developed uses information relating to the pressure distribution around the building and the contaminant distribution inside the building to determine the optimal configuration of external resistance devices and ventilation port openings. To determine optimal configurations of resistance devices and port openings, model-based optimization is
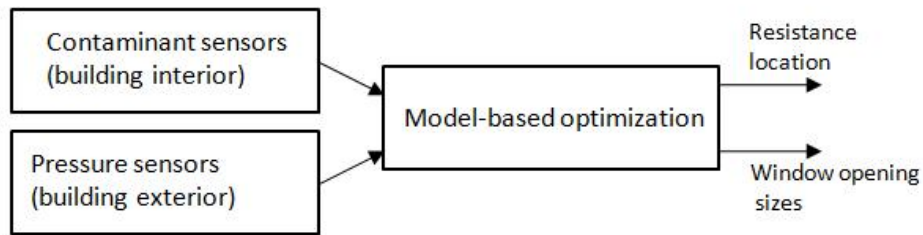
Figure 86: Block diagram representation of the components of the control scheme

used. Figure 86 summarizes the sensors and actuators needed for the centralized controller.

For implementation of the control logic, model-based optimization is used, and thus the capability to model both the interior and exterior of the building and perform iterative numerical optimization is needed. For this purpose, the following three components are integrated:

a) Building exterior: CFD simulations using a commercially available software package is used to determine the pressure distribution around the building exterior due to the wind, building geometry, and resistance location. Note that a full set of CFD simulations are only required in the development stage. However, CFD simulations of a full-scale building are not practical for control purposes on account of the significant amount of time required for such cases. Therefore, in the final implementation, pressure sensors inside and outside the building will replace or reduce the need for CFD simulations.

b) Building interior: CONTAM, a multi-zone modeling software package developed by National Institute of Standards and Technology (NIST) is used to determine the effect of the external pressure distribution on IAQ for a set of given ventilation port openings [32]. In practice, it is difficult to obtain real-time information about

parameters such as airflow rates in the interior of the building. In this work, it is assumed that the results obtained from CONTAMW are reasonable estimates of the conditions present in the building interior.

c) Optimization: Optimization and control algorithms in MATLAB that iteratively use the above-mentioned CONTAM and CFD simulations to determine the optimal configuration of the degrees of freedom to meet the changing needs for fresh air in individual zones.

In this research, the multi-zone modeling software package CONTAMW is used to simulate the airflow and contaminant distribution in the interior of a building. This software enforces the conservation of mass in well-mixed (i.e., spatial homogenous temperature, contaminant concentrations etc.) zones. Airflow paths (e.g., windows, doors) are modeled using power-law of quadratic relationships between the imposed pressure difference across the path and the flow rate through them. The airflow rate from zone j to zone i is a function of the pressure difference across the flow path $P_j - P_i$ (i.e., $F_{ji} = f(P_j - P_i)$). Then, conservation of mass dictates that,

$$\sum_j F_{ji} = 0 \tag{28}$$

If there are multiple zones present in a building, then, the steady-state airflow analysis requires the simultaneous solution of the above equation. The equation used to model the airflow across a path is usually nonlinear. Therefore, we require a method for the solution of simultaneous, nonlinear, algebraic equations. For this purpose, the Newton-Raphson method is used, which solves this problem by the iteratively solving a system of linear equations. In this method, a new estimate of the vector of zone pressure $P*$ is computed

from the current estimate P according to,

$$P* = P - C \tag{29}$$

where the correction vector C is computed according to the matrix relationship,

$$[J]C = B \tag{30}$$

where B is a column vector with each element described by,

$$B_i = \sum_j F_{ji} \tag{31}$$

and $[J]$ is the Jacobian matrix defined by,

$$J_{ij} = \sum_i \frac{\partial F_{ji}}{\partial P_j} \tag{32}$$

In the above equations, F_{ji} and $\frac{\partial F_{ji}}{\partial P_j}$ are evaluated using the current pressure estimate P. The CONTAMW solver contains subroutines for each airflow element which compute the mass flow rates and derivative values for a given pressure difference. The workings of this software package is described in greater detail in the CONTAMW user manual [32].

Demetriou & Khalifa have developed a method that can be used to couple components b) and c), referred to here as the CONTAM-MATLAB Bridge [64]. The CONTAM-MATLAB Bridge is implemented in MATLAB and uses a TCP/IP connection with Java commands to pass information between the two software packages. This is used to run all simulations using MATLAB while calling CONTAM from within MATLAB when needed.

Traditional model predictive control algorithms use model equations to predict the effect of choosing a control action and these predictions along with past control values are used to minimize an objective function. Here, a numerical version of model-predictive control is implemented, in which we use simulations models described in components a) and b) to determine the effect of candidate control actions. The objective functions chosen for optimization are discussed in a later section.

To deal with the complexity of integrating three software packages and the large computation load of CFD simulations, the simplifying assumption that steady-state calculations provide a reasonable approximation of the interaction between the pressure distribution around the building exterior and the airflow paths in the building is made. This may be the case when the response of the building environment to control actions is much faster than the rate of change of weather conditions, occupancy patterns etc. Thus, dynamic simulations are treated as quasi steady-state simulations. Moreover, it is assumed that the ventilation ports do not change the pressure distribution around the building exterior, which is justified since the ventilation ports are small (0.05 m^2) relative to the area of the building façade. For example, the elliptical building discussed in this work has a circumference of approximately 120 m. Assuming a floor height of 3 m, this means that the area of the façade per floor is 360 m^2. Given ten such ventilation ports floor, this means that the total area of the ports is 0.5 m^2, which is about 0.1 % of the façade area per floor. For reference, with the chosen opening size, it is possible to maintain airflow rates on the order of 1 ACH for a wind speed of 9 m/s. Figure 87 represents the numerical implementation of the centralized controller logic. The red block and arrows in the figure represent off-line calculations, while blue arrows represent real-time communications.
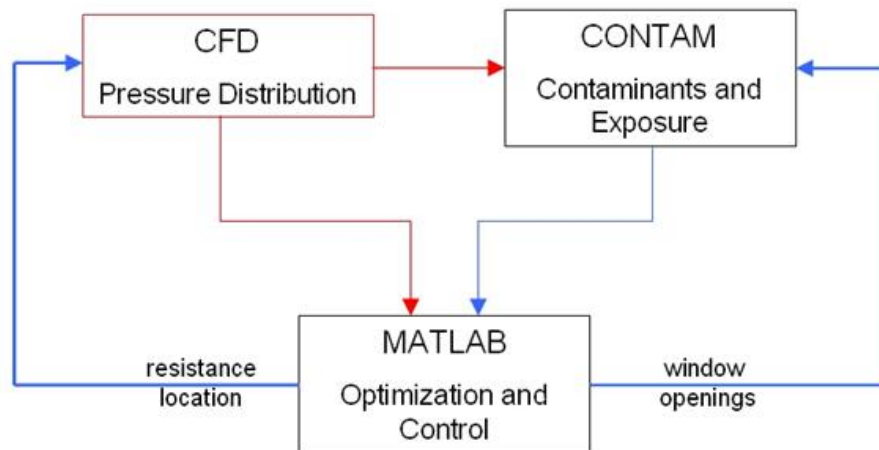
Figure 87: Schematic representing the coupling of the different software packages

The control algorithms and the interaction of the three software packages can be thus be summarized as follows. At each time step, the optimization algorithms in MATLAB tests the effect of varying the ventilation port openings and the resistance locations, by looking up external pressure distributions from off-line CFD simulations and interior contaminant concentrations from steady-state CONTAM simulations. Furthermore, MATLAB evaluates the effect of these configurations and chooses the optimal configuration based on minimizing a user-chosen objective function. The candidate configurations are chosen by MATLAB using standard gradient-based updates. It should be noted that the quasi-steady assumption is made for the purposes of these analyses (i.e., the problem is not dynamic).

4.3 Equivalent fresh air

Before discussing the exploratory work done related to control of natural ventilation, it is first necessary to discuss the fact that in naturally ventilated buildings, it is not always possible to have a direct supply of outdoor air to each zone. The supply air to a zone may

have passed through several zones and in this process may have become partially or fully polluted. To assess whether this polluted air satisfies ventilation requirements for the zone, the notion of ASHRAE-equivalent airflow is introduced. This development of ASHRAE-equivalent airflow is based on the assumption that the CO_2 concentration in a zone is an indicator of the indoor air quality in that zone, with a higher concentration corresponding to poorer air quality. This is based on the fact that CO_2 concentration is a surrogate measure for people and their related emissions. This does not take into account emissions from stationary surfaces and objects (e.g., carpet, furniture etc.). However, a similar procedure may be followed in order to obtain corresponding metrics based on these other pollutant sources. The airflow rate recommended under such circumstances would then be based on the component of ASHRAE 62 (2004) guidelines that depends on the floor area of the building. This concept of ASHRAE-equivalent airflow is also applicable to a mechanically ventilated building with significant airflows between zones.

As an example, consider a zone with a CO_2 source of generation rate R [mass/time] ventilated by N inflows Q_n (n = 1,2,...,N) [volume/time], with corresponding CO_2 concentrations C_n [mass/volume] as shown in Figure 88(a). This represents the general case of a zone receiving air from a combination of adjacent zones and the ambient. Let C* represent the effective concentration of the total inflow air, that is, the concentration of the total inflow if all N inflows were fully mixed and combined into a single supply. Therefore, considering the mass conservation of CO_2, the following is obtained,

$$C^* = \frac{\sum_{n=1}^{N} Q_n C_n}{Q_{SUP}}, \tag{33}$$
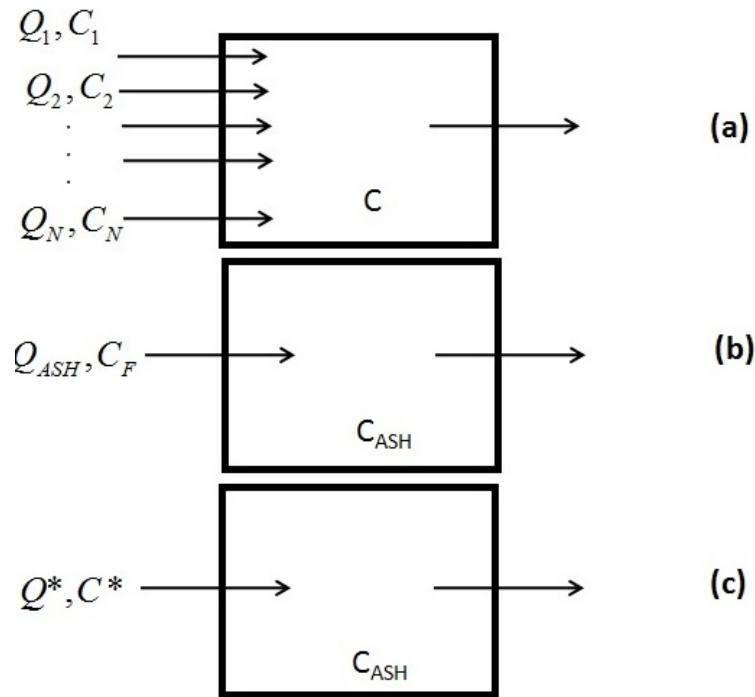
Figure 88: The zone under consideration ventilated by (a) n different inflows (b) ASHRAE-recommended airflow (c) ASHRAE-equivalent airflow

where

$$Q_{SUP} = \sum_{n=1}^{N} Q_n \tag{34}$$

is the total airflow entering the zone.

To determine the ASHRAE-equivalent airflow for this zone, the amount of air required at concentration C* to match the IAQ achieved by following ASHRAE guidelines is computed. Let Q_{ASH} be the ASHRAE-recommended (Standard 62) outdoor air supply rate (at CO_2 concentration C_F) for the zone under consideration as shown in Figure 88(b), and C_{ASH} be the corresponding steady-state CO_2 concentration in that zone,

$$C_{ASH} = \frac{R}{Q_{ASH}} + C_F. \tag{35}$$

C_{ASH} is chosen to be the reference CO_2 concentration for quantifying the quality of the total incoming airflow. When the outdoor air CO_2 concentration C_F is taken to be 400 ppm, for a zone ventilated according to ASHRAE Standard 62 (considering only occupancy), C_{ASH} is 1008 ppm. Next, let Q^* be the amount of airflow needed at the actual incoming CO_2 concentration C^* to obtain a steady-state CO_2 concentration of C_{ASH} in the zone, as shown in Figure 88(c). Then, it follows that

$$\frac{R}{Q^*} + C^* = C_{ASH}. \tag{36}$$

Next, it follows from Equations(12) and (13) that,

$$R = Q_{ASH}(C_{ASH} - C_F) = Q^*(C_{ASH} - C^*), \tag{37}$$

and hence

$$Q^* = \frac{Q_{ASH}(C_{ASH} - C_F)}{C_{ASH} - C^*}. \tag{38}$$

Physically, Q^* is the airflow needed at concentration C^* to achieve a steady-state concentration of C_{ASH} in the zone, and thus, is equivalent to the ASHRAE-recommended airflow rate.

Finally, dividing Equation (11) by Equation (15) and using Equations (10) and (11), we get

$$\frac{Q_{SUP}}{Q^*} = \frac{\sum_{n=1}^{N} Q_n(C_{ASH} - C_n)}{Q_{ASH}(C_{ASH} - C_F)}. \tag{39}$$

Since Q^* represents the total air inflow required at CO_2 concentration C^* to meet ASHRAE recommendations, the non-dimensional ratio Q_{SUP}/Q^* helps determine whether

the zone is being under-ventilated or over-ventilated relative to ASHRAE guidelines. For the remainder of this work, the non-dimensional ratio Q_{SUP}/Q^* is referred to as the ASHRAE-equivalent airflow ratio and $(Q_{SUP}/Q^*)Q_{ASH}$ as the ASHRAE-equivalent airflow.

When the ratio Q_{SUP}/Q^* is equal to 1, the steady-state CO_2 concentration in the zone under consideration is exactly the same as the steady-state CO_2 concentration obtained by mechanically ventilating the zone according to ASHRAE 62. Therefore, the amount of air at C^* is exactly equal to that needed to satisfy ASHRAE requirements.

When Q_{SUP}/Q^* is greater than 1, the IAQ in the zone is better than that achieved following ASHRAE Standard 62. Furthermore, since in this case the zone is over-ventilated, it is possible to exactly meet ASHRAE standards by reducing Q_{SUP}, or equivalently, proportionally reducing all air inflows Q_n.

When Q_{SUP}/Q^* is less than 1, the IAQ in the zone is worse than that achieved by ASHRAE Standard 62, and therefore, the room is under-ventilated. There are three possible scenarios in this case. If Q_{SUP}/Q^* is between 0 and 1, the effective concentration C^* of the inflow air is less than the reference concentration C_{ASH}, and therefore, it is possible to satisfy ASHRAE guidelines by proportionally increasing the amount of all inflows Q_n. If Q_{SUP}/Q^* is equal to zero, then, the effective concentration of the inflow air is equal to C_{ASH}, and if the ratio is negative, the effective concentration of the incoming air is greater than C_{ASH}. Therefore, any source of contaminant present in the zone will lead to worse IAQ as compared to that corresponding to the ASHRAE recommended ventilation rate. It follows that when the ASHRAE-equivalent airflow ratio Q_{SUP}/Q^* is less than or equal to zero, it is not possible to meet the ASHRAE guidelines by increasing Q_{SUP} or proportionally increasing the amount of all inflows Q_n.

To illustrate the above development of ASHRAE-equivalent airflow, a simple scenario shown in Figure 89 is considered, in which five zones are connected in series. The zones are of equal volumes and there is a single airflow path connecting any two adjacent zones. A supply for ventilation airflow is located in the first zone (zone 1), and a return is located in the last zone (zone 5). This example is representative of both a mechanical ventilation system with significant airflows between zones, and a natural ventilation system with an air inflow in the first zone and an air outflow in the last zone.
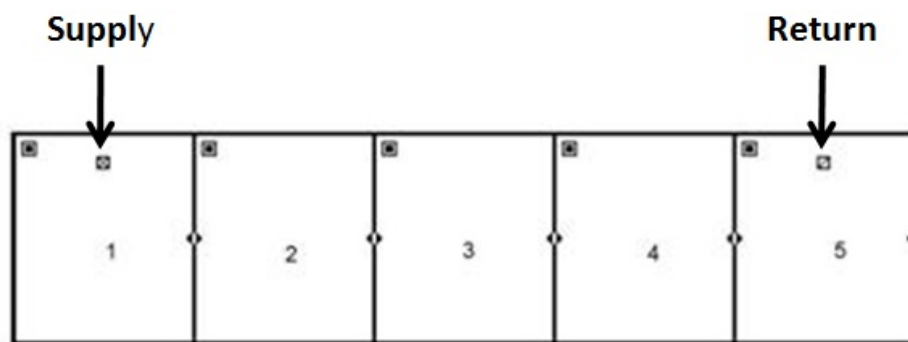
Figure 89: Zones connected in series

Various configurations of supply airflow rate and occupancy distribution are considered, and the values obtained for the ASHRAE-equivalent airflow ratios in each case are noted. First, consider a configuration with a uniform occupant distribution of 3 occupants in each zone, and the supply flow rate in zone 1 is enough to meet the ASHRAE 62 guidelines for all 15 occupants in all zones, that is, the supply airflow is 15 times the ASHRAE recommended airflow rate per person.

Figure 90 shows the ratio of Q_{SUP}/Q^* for each zone for this case. It is observed that zone 1 receives 5 times as much air as required at the supply concentration (equal to the fresh air concentration for this zone), whereas zone 5 receives exactly the required amount of air at the supply air concentration (equal to the concentration of zone 4).
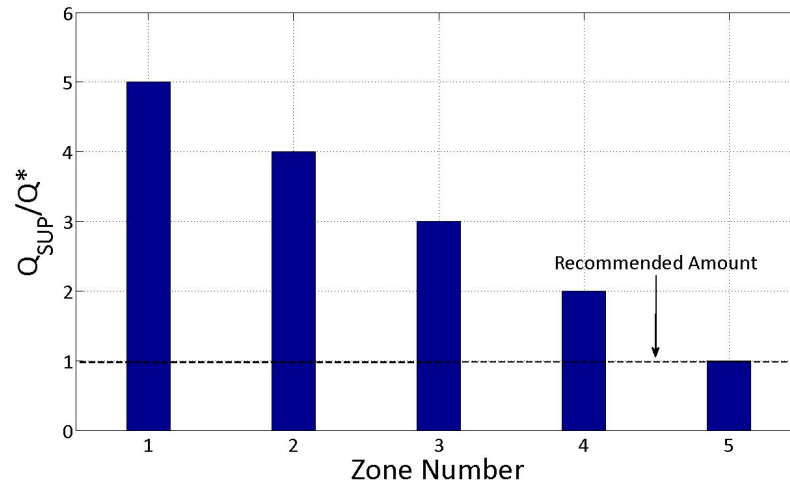
Figure 90: $Q_{SUP}/Q^*$for all five zones with uniform occupancy and supply airflow in zone 1 equal to total ASHRAE-recommended airflow for all five zones

It is to be noted that the IAQ in the first four zones are better than IAQ achieved by ventilating each individual zone according to ASHRAE recommendations. An interesting observation from this example is that with respect to CO_2 concentration level, following this ventilation strategy provides better air quality than the conventional method of having individual supply/exhaust in each room to meet the ASHRAE 62 guidelines. However, the disadvantages of this ventilation strategy include potential thermal and draft discomfort and higher chance of airborne disease transmission.

Next, a configuration with the same occupant distribution as before is considered, with the supply flow rate equal to the ASHRAE recommended airflow for one zone. Figure 91 shows that zone 1 receives exactly the amount of air required to satisfy ASHRAE requirements, which is in agreement with the setup. Zone 2 receives no fresh air, as the supply air is at the reference concentration C_{ASH}.

Therefore, the presence of CO_2 source in Zone 2 would result in an IAQ level lower than
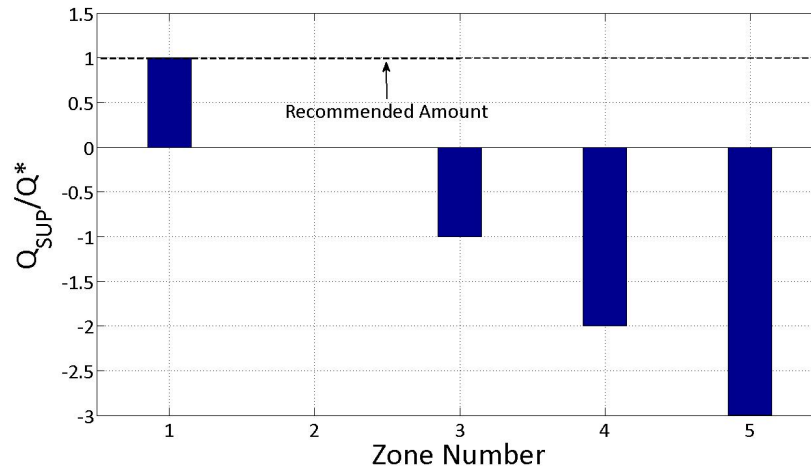
Figure 91: Q_{SUP}/Q^* for all five zones with uniform occupancy and supply airflow in zone 1 equal to ASHRAE-recommended airflow for one zone

that required by ASHRAE 62 guidelines. From zone 3 onwards, the supply airflow is at a concentration greater than C_{ASH}, therefore, it is impossible to meet the IAQ corresponding to the reference concentration. The negative ratios for these zones indicate that additional "cleaner" air (e.g. ambient air) must be supplied to these zones to achieve the reference steady-state concentration.

For a zone with a non-positive ratio of Q_{SUP}/Q^*, the quantity $Q_{ASH}($ $Q_{SUP}/Q^*-1)$ indicates the amount of excess airflow required at ambient concentration C_F in order to satisfy ASHRAE guidelines. To illustrate this point, consider the same setup as that associated with Figure 4, where zone 1 is supplied with enough air to meet requirements for one zone. In this case, zone 5 has a Q_{SUP}/Q^* ratio of -3 associated with it. Now, in addition to the air entering zone 5 from zone 4, if zone 5 is supplied with excess fresh air with the flow rate calculated on the basis of the negative ratio associated with that zone. The excess airflow supply in zone 5 is equal to four times the ASHRAE-recommended rate for that zone, and is only added to zone 5. Figure 92 shows that under these conditions, zone 5 receives the

required amount of airflow in order to satisfy ASHRAE recommendations.
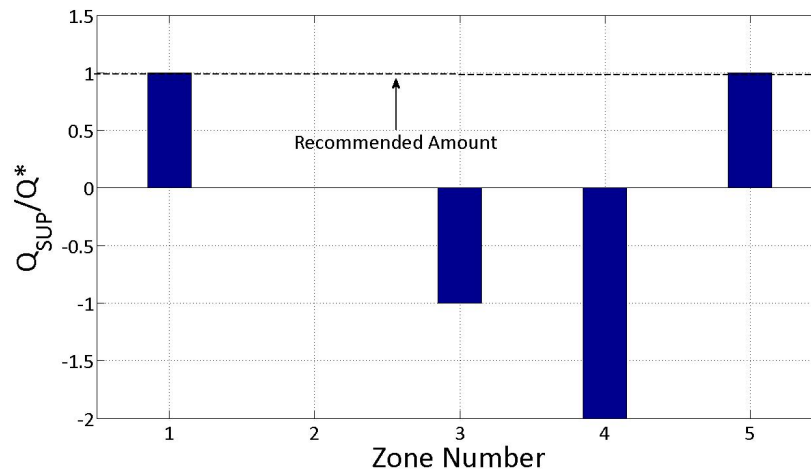
Figure 92: Q_{SUP}/Q^*, uniform occupancy, adequate supply for one zone in zone 1, excess fresh air supply in zone 5

Finally, two cases of non-uniform occupant distribution are studied. In both cases, the total number of occupants is the same as before. In the first case, the number of occupants in each zone increases from 1 (in zone 1) to 5 (in zone 5) in steps of one, while, in the second case, the number of occupants decreases from 5 (in zone 1) to 1 (in zone 5), also in steps of one. Figures 93(a) and (b) show the ASHRAE-equivalent airflows for these two cases respectively.

From Figure 93(a), it is seen that zone 1 is supplied with 15 times its recommended amount. As the total supply rate is based on the requirements of the total number of occupants (15), and in this case, zone 1 has one occupant, the ASHRAE-equivalent airflow ratio for this zone is correct. A similar reasoning applies to the results shown in Figure 93(b); it is noted that zone 1 is supplied with 3 times its recommended amount. As the total supply rate is based on the requirements of the total number of occupants (15), and zone 1 has five occupants in this case, the ASHRAE-equivalent airflow for this zone is
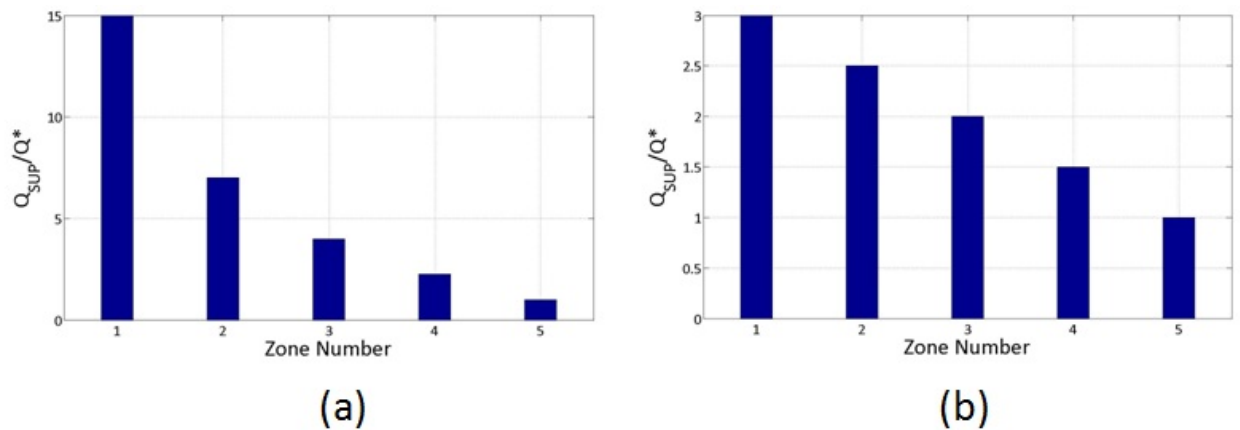
Figure 93: ASHRAE-equivalent airflow ratios for (a) Non-uniform occupant distribution 1 (b) Non-uniform occupant distribution 2

observed to be correct. Finally, given the rationale behind calculating the supply airflow rate, it is expected that the IAQ requirements for all zones are satisfied. In both cases, it is seen that zone 5 is supplied with exactly the right amount of air required, and all other zones are supplied with excess air.

4.4 Effect of resistance devices on airflow distribution

In this section, the changes in the amount of airflow induced, as well the distribution pattern of the airflow when the resistance device concept is applied to rectangular, circular and elliptical cross-section buildings are studied. For this purpose, a simple floor plan shown in Figure 94 is created using CONTAM to model the interior of the buildings under consideration. The floor plan consists of eight inter-connected zones, with a central passage. This floor plan is chosen of a typical architectural floor plan, as shown in Figure 95. All the zones on the periphery have an opening to the ambient. The total floor area of the model is 785 m^2, which corresponds to the areas of the building cross-sections. The

height of a floor is taken to be 3 m. The openings to the ambient are 0.05 m^2 in area and the opening between zones are 2 m^2 in area. Therefore, these openings are not conventional windows, which may not be suitable for application in high-rise buildings on account of the high wind speeds likely to be encountered, as well as for reasons of safety.
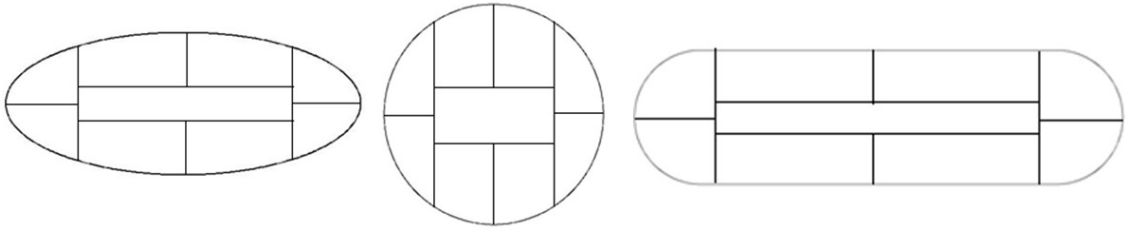
Figure 94: Floor plan chosen for buildings under consideration

Instead, they are meant to represent small ventilation ports as illustrated in Figure 96, which shows a proposed design for the implementation of the resistance device concept (using VAWT's) for an elliptical cross-section building by Pelken [65]. Figure 96 (a) shows the implementation of small ventilation ports in the Uptown Tower located in Munich, Germany, while Figure 96 (b) illustrates a proposed implementation of this concept along with VAWT's in an elliptical cross-section building. Note that the floor plan shown is a schematic representation of the interior zones and may be used for all the building cross-sections considered.
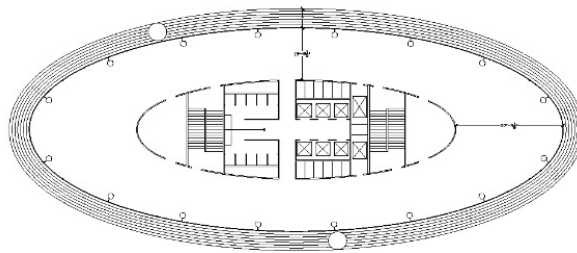
Figure 95: Typical architectural office plan with a central core arrangement

First, the airflows induced for the rectangular cross-section building with rounded edges are
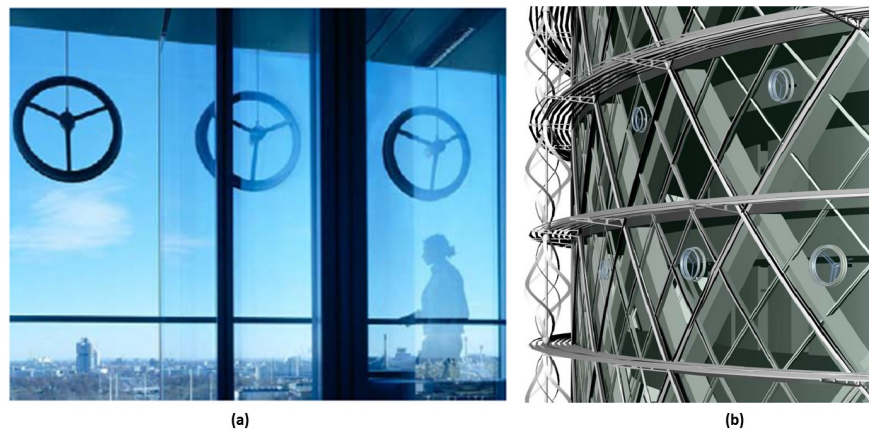
Figure 96: Illustration of ventilation ports on building façade

studied, both for the cases with a resistance device activated, and without a resistance device. For all the cases considered here, the static pressure at specified locations is taken from the CFD results and input into the CONTAM model as the static pressure acting at the locations where the openings to the ambient are located in each peripheral zone. For the rectangular building, the cases under consideration are illustrated in Figure 34 and the relevant CFD data is obtained from Figure 38.

Comparing Figures 97 and 98, it is seen that the total amount of intake airflow is reduced by more by more than half in the case 1 resistance device configuration. In particular, zones 1, 2, 6 and 7 see a large reduction in the amount of air exchange with the ambient.

Looking at Figure 38, it is observed that the effect of the resistance device configuration for case 1 is to reduce the magnitude of the static pressure loading on the building. Therefore, it is expected that there will be a large reduction in the amount of airflow exchange induced in case 1 as compared to the baseline scenario. Under high wind conditions that may be experienced at the upper floors of tall buildings, it may be useful to have the capability to reduce the amount of airflow induced, as the high airflow rates likely to be

Total Air Intake = 1.159 m³/s
(Equivalent to 1.77 ACH)

0.334 m³/s   0.117 m³/s

0.539 m³/s   0.107 m³/s

1   2   3   4

5   6   7   8

0.200 m³/s   0.179 m³/s

0.493 m³/s   0.350 m³/s
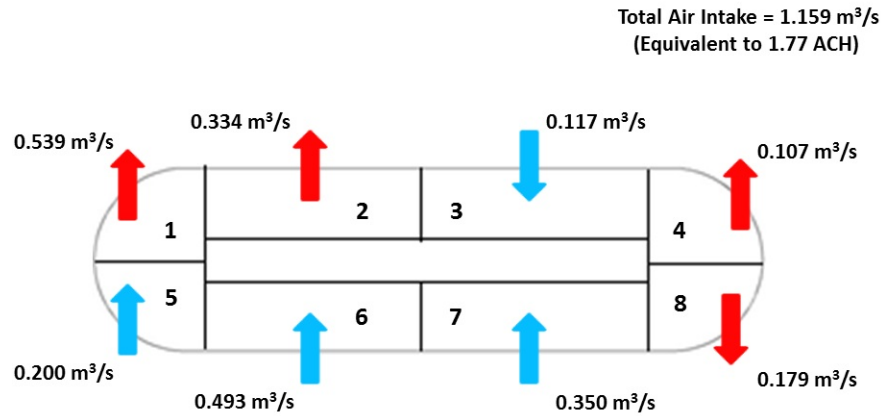
Figure 97: Airflow pattern for rectangular building (baseline case)

Total Air Intake = 0.564 m³/s
(Equivalent to 0.86 ACH)

0.073 m³/s   0.147 m³/s

0.031 m³/s   0.081 m³/s

1   2   3   4

5   6   7   8

0.126 m³/s   0.346 m³/s

0.263 m³/s   0.061 m³/s
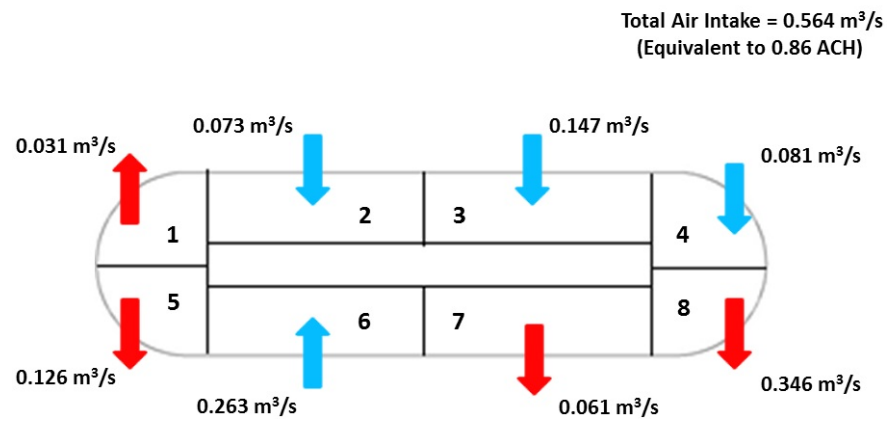
Figure 98: Airflow pattern for rectangular building (case 1)

experienced under such conditions may lead to undesirable draft and thermal comfort issues. In addition, reduction in the envelope pressure loading may also be beneficial from a structural point of view.

It is also observed that the distribution pattern of the airflow changes when the resistance device is activated. The direction of the airflow exchange is reversed in zones 2, 4, 5 and 7 in the case 1 configuration as compared to the baseline scenario. This provides us with a method to control the distribution of the airflow depending on the prevailing ventilation

Total Air Intake = 1.170 m³/s
(Equivalent to 1.78 ACH)
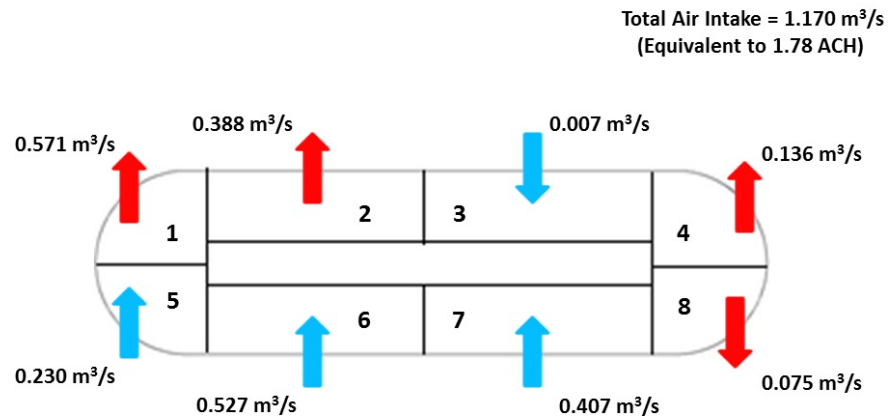
Figure 99: Airflow pattern for rectangular building (case 2)

requirements. For instance, it may be the case that zone 2 has large occupancy at a certain time of the day. Therefore, it is beneficial to directly supply this zone with fresh air from the ambient instead of relying on partially polluted air from other zones to provide the required airflow. In this case, it is then useful to utilize the case 1 resistance device configuration as this reverses the airflow exchange pattern for zone 2 as compared to the baseline scenario.

The resistance device configuration shown in case 2 is not effective in manipulating the airflow distribution pattern. Comparing Figures 97 and 99, it is noticed that the airflow exchange pattern is not changed, and in addition, the amount of airflow exchange with the ambient is not altered significantly. This is because the pressure distribution around the building envelope does not change appreciably for this configuration as compared to the baseline scenario. The resistance device in this case is located in a region where the velocity is not significantly higher than the free-stream velocity, and hence, the device is not very effective in manipulating the wind pressure distribution.

However, when combined with the resistance device on the suction surface (case 3), this

device can be useful in controlling the distribution of the airflow within the building interior, as seen in Figure 100. This is because when the resistance device on the suction surface is activated, the resistance device on the pressure surface is then located in a region of high velocity relative to the free-stream, and hence, is more effective at manipulating the envelope pressure distribution.
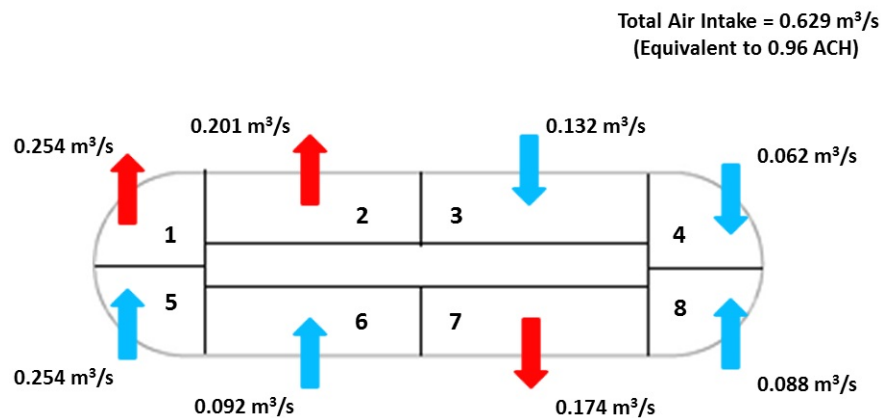
Figure 100: Airflow pattern for rectangular building (case 3)

Next, the effect of the resistance device when applied to a circular building is studied. For this problem, the same interior floor plan layout as considered for the rectangular building is used to model the layout of the circular building. Figures 41 and 42 demonstrate that the pressure distribution around the circular building envelope is unsteady on account of vortex shedding. Therefore, for this problem, the time-averaged pressure distribution around the envelope is computed for each case, and this pressure data is then input into CONTAM. Figure 101 shows the time-averaged airflow distribution pattern for the baseline case for the circular building. On comparing it with Figure 102, which shows the distribution pattern for Case 1, it is seen that the resistance device has the effect of reversing the direction of airflow exchange in zones 2 and 3. The amount of airflow exchange for zone 4, 6, 7 and 8 also changes significantly, however, the total amount of
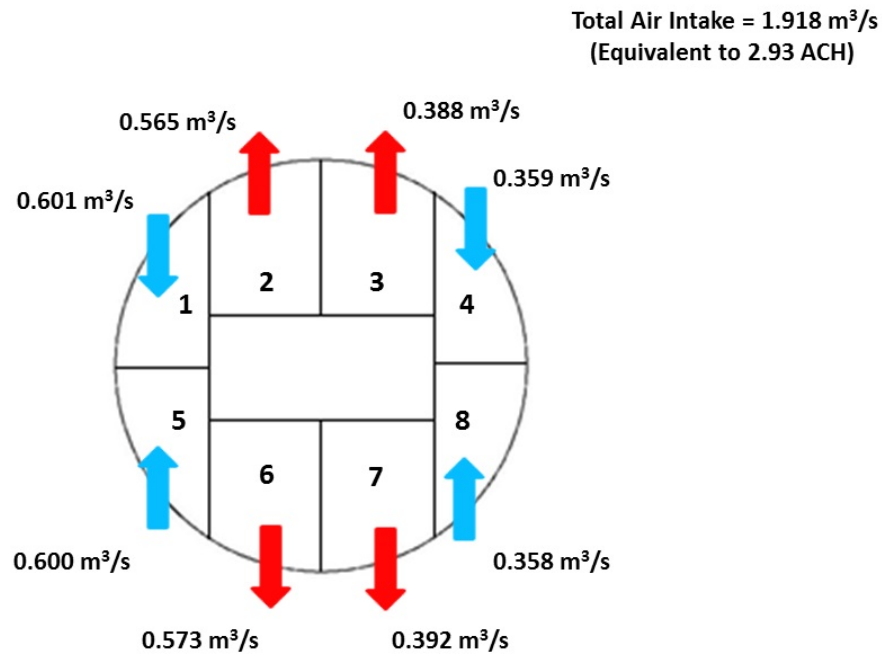
Figure 101: Airflow pattern for circular building (baseline case : time averaged)

airflow exchange with the ambient does not change appreciably.

Next, the variation in the induced airflows for the elliptical building on application of the resistance device concept is considered. Comparing Figures 103 and 104, we observe that the total amount of airflow intake remains similar. However, the distribution of the airflow with the interior changes dramatically. Zone 1 is located in the peak suction, zone 4 is located in the separated region, and zone 5 is located in the stagnation region. Therefore, it is difficult to control the direction of air exchange for these two zones. However, we see that apart from these zones and zone 6, we are able to reverse the direction of airflow in all the other zones by using the case 1 resistance device configuration. In addition, the amount of air exchange for these zones also changes appreciably.

Looking at the results for the case 2 configuration (Figure 105), we notice a large increase

Total Air Intake = 2.146 m³/s
(Equivalent to 3.28 ACH)
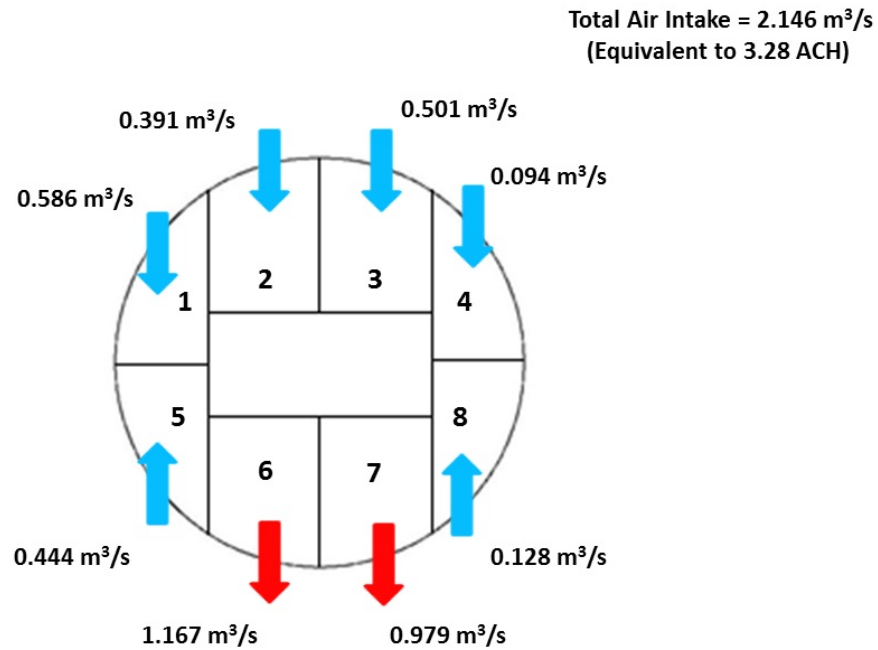
Figure 102: Airflow pattern for circular building (case 1 : time averaged)

Total Air Intake = 1.075 m³/s
(Equivalent to 1.64 ACH)
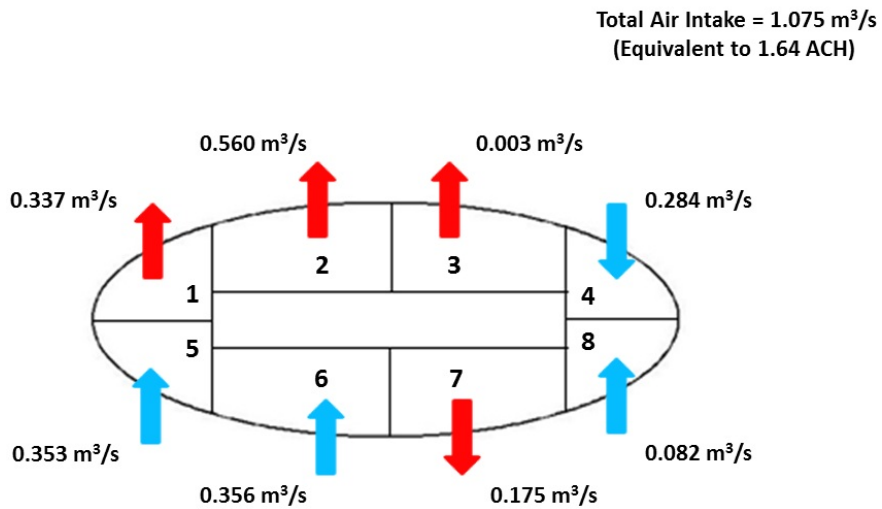
Figure 103: Airflow pattern for elliptical building (baseline case)

in the total amount of air intake with the ambient as compared to the baseline case.
Though the direction of air exchange with the ambient is reversed only for zone 7, the total
amount of air intake increases from 1.07 m³/s to 1.63 m³/s. In addition, the total amount

Total Air Intake = 1.010 m³/s
(Equivalent to 1.54 ACH)
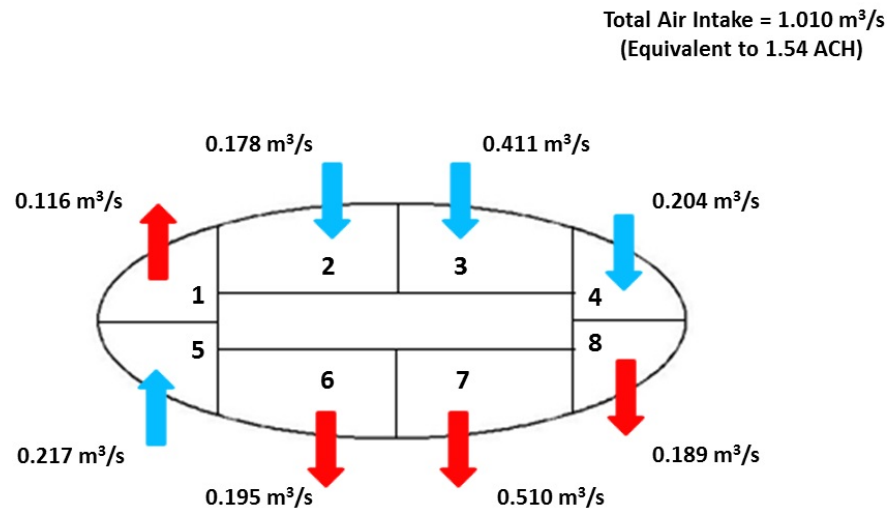
Figure 104: Airflow pattern for elliptical building (case 1)

Total Air Intake = 1.634 m³/s
(Equivalent to 2.49 ACH)
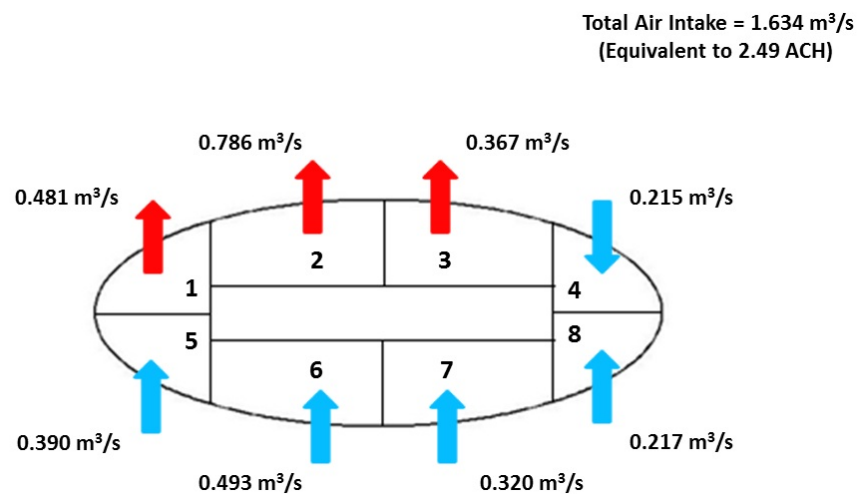
Figure 105: Airflow pattern for elliptical building (case 2)

of air exhausted from zone 3 increases dramatically. Therefore, this configuration may be useful in situations where a particular floor needs to be supplied with larger amounts of airflow. It may be also be considered in scenarios where zone 3 is heavily polluted, and therefore, it is desirable to ensure that the amount of airflow from zone 3 to the other zones is to be minimized.

Total Air Intake = 0.629 m³/s
(Equivalent to 0.96 ACH)

0.201 m³/s

0.132 m³/s

0.254 m³/s

0.062 m³/s

2

3

1

4

5

8

6

7

0.254 m³/s

0.088 m³/s

0.092 m³/s

0.174 m³/s
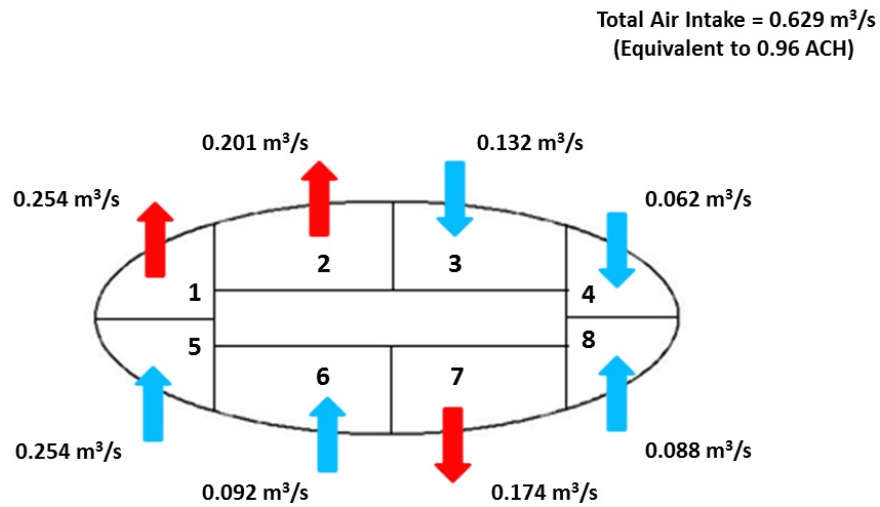
Figure 106: Airflow pattern for elliptical building (case 3)

Next, considering the results for the case 3 resistance device configuration (Figure 106), it is seen the total amount of intake is greatly reduced. This is because for this particular configuration has the effect of reducing the pressure loading on the building, leading to reduced pressure differences driving the airflow exchange. Therefore, this may be suitable for upper floors of a high-rise building where wind speeds are high, and consequently, so is the pressure loading on the building. Under such conditions, the total amount of airflow intake may be much higher than necessary, leading to thermal comfort and draft problems. Therefore, it may be useful to reduce the amount of airflow intake by decreasing the magnitude of the pressure loading.

The results presented above indicate that it is possible to control both airflow exchange direction, as well as the magnitude of airflow exchange by controlling only the pressure distribution around the building. Different resistance device configurations allow for varying airflow exchange directions, as well as varying control over the amount of airflow intake/exhaust. In particular, for the elliptical building, it is possible to manipulate the

direction of airflow exchange for several zones on the periphery of the building

cross-section. However, these results are only applicable for scenarios where the wind

incidence angle is 10° with respect to the major axis of the ellipse. In practice, the wind
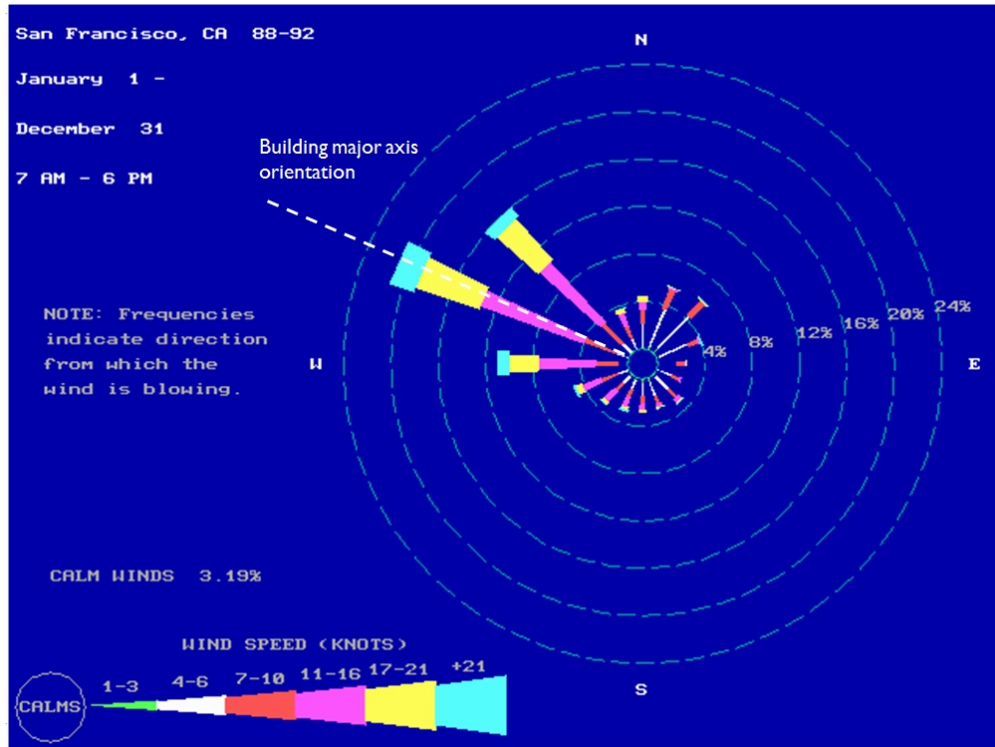
Figure 107: Wind rose for San Francisco

speed and direction are not constant, and vary all year round. It is then of interest to

explore how the proposed concept performs under such changing conditions. The variation

in wind characteristics can be represented by a plot called a wind rose. An example of a

wind rose is shown in Figure 107, which is for the city of San Francisco. It is a type of

histogram in which both wind speed as well as direction are represented graphically. The

color of the bars in the wind rose represent the wind speed, whereas the direction in which

they point represents the direction from which the wind blows. The concentric rings

represent the percent of the time period, during which the wind blows from a given speed,

at a given direction. The wind rose shown is created using data obtained over a period of 4 years. To illustrate how the wind rose is interpreted, consider the horizontal bar pointing left (towards the west). The yellow segment of the bar spans about half the distance between two rings (2 % of the total time). According to the color key, yellow corresponds to wind speeds in the range of 17 knots to 21 knots (19 mph to 24 mph). This means that the wind blows from the west between speeds of 17 knots and 21 knots for 2 % of the year. The rest of the segments are interpreted in this fashion.

Now, utilizing this wind data for San Francisco, we pick an orientation for the elliptical building considered, and assess how well the resistance device concept performs. The primary goals are to determine whether it is possible to control the direction of airflow exchange within the zones of the building, and to determine the extent to which the amount of airflow exchange can be controlled. Specifically, the goal is to determine the amount of time over the course of a year during which an airflow rate equivalent to 1 ACH can be maintained for the opening size assumed previously. For this purpose, 2-D CFD simulations are conducted for wind incidence angles of up to 45º. The pressure data is taken from these simulations, and input into CONTAM as before to assess the performance of the resistance device concept.

The orientation chosen for the major axis of the ellipse is shown in Figure 107. It can be seen that for a large percentage of the year, the incident wind is at a maximum incidence angle of around 25º with respect to the major axis. This orientation is chosen because we are interested in studying buildings that cannot rely on cross-ventilation, as the resistance device concept works best under such circumstances. For instance, such a situation may present itself in practice when the plot of land on which a building is situated is oriented

such that it is aligned with the predominant wind direction. For large angles of incidence, the flow pattern is expected to resemble cross-ventilation configurations, in which case, supplying large amounts of airflow becomes a trivial matter. Also, it is not possible to control indoor airflow direction in case of an implementation of cross-ventilation. First, a

	Zone 1	Zone 2	Zone 3	Zone 4	Zone 5	Zone 6	Zone 7	Zone 8
Baseline	-	-	-	+	+	+	-	+
Case 1	+	+	+	+	+	-	-	-
Case 2	-	-	-	+	+	+	+	+
Case 3	-	-	+	+	+	+	-	+

Airflow direction **cannot** be reversed for this zone

Airflow direction **can** be reversed for this zone

Can change airflow direction for 6 zones
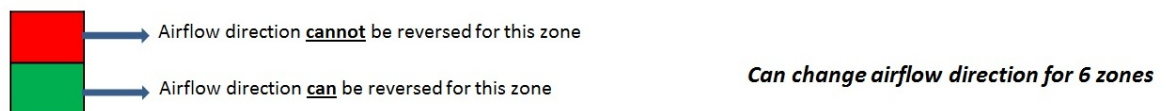
Figure 108: Airflow directions for each zone : 10° angle of incidence

summary of the results for the 10° angle of incidence case is presented. Figure 108 displays the direction of airflow exchange for all the zones on the periphery of the building cross-section for various resistance device configurations as well as the baseline scenario. A positive sign indicates inflow from the ambient into a particular zone, and a negative sign indicates that air is exhausted from a zone to the surroundings. The results indicate that it is possible to control the direction of airflow exchange with the ambient for 6 out of a total of 8 zones that are present on the external periphery of the building. It is not possible to control the airflow exchange direction for zone 4 as it is present in the region where the flow is separated, and for zone 5, as it is in the vicinity of the stagnation point. However, for all the remaining zones, depending upon the resistance device configuration employed, it possible to have either inflow of air from the ambient, or to have air exhausted to the ambient. Next, we consider the case where the angle of incidence of the wind is at 20° with respect to the major axis of the ellipse. Figure 109 displays the airflow exchange directions

	Zone 1	Zone 2	Zone 3	Zone 4	Zone 5	Zone 6	Zone 7	Zone 8
Baseline	-	-	+	+	+	+	-	-
Case 1	-	+	+	+	+	+	-	-
Case 2	-	-	+	+	+	+	+	+
Case 3	-	-	-	-	+	+	-	-

Airflow direction **cannot** be reversed for this zone

Airflow direction **can** be reversed for this zone

Can change airflow direction for 5 zones
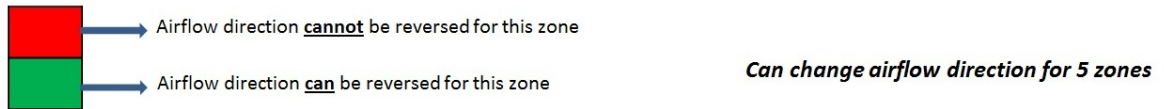
Figure 109: Airflow directions for each zone : 20° angle of incidence

for this scenario. For this case, we see that is possible to exert control over the airflow direction for 5 out 8 zones. Again, zone 5 is located near the stagnation point, therefore, it is not possible to change the airflow direction for this zone. Zone 1 is located near the region of peak negative pressure, therefore, air is always exhausted from this zone to the ambient. Also, none of the resistance device configurations tested are able to reverse the airflow exchange direction for zone 6.

In the next scenario, the angle of incidence of the free-stream wind is 30° to the major axis of the ellipse. Figure 110 shows the airflow exchange directions for this incidence angle. Here, it is observed it is only possible to control airflow directions three zones out of eight. Employing cases 1, 2 and 3, we are able to reverse the direction of airflow exchange in one zone for each case as compared to the baseline. In other words, it is not possible to reverse the direction of airflow for more than one zone at a time as compared to the baseline.

Finally, we consider the case with a wind incidence angle of 45°. The airflow directions for this case are displayed in Figure 111. Here, we see that it is no longer possible to exert any level of control over the direction of airflow exchange for any of the zones in the building.

	Zone 1	Zone 2	Zone 3	Zone 4	Zone 5	Zone 6	Zone 7	Zone 8
Baseline	-	-	+	+	+	+	-	-
Case 1	-	-	-	+	+	+	-	-
Case 2	-	-	+	+	+	+	+	-
Case 3	-	-	-	-	+	+	-	-

Airflow direction **cannot** be changed for this zone

Airflow direction **can** be changed for this zone

Can change airflow direction for 3 zones
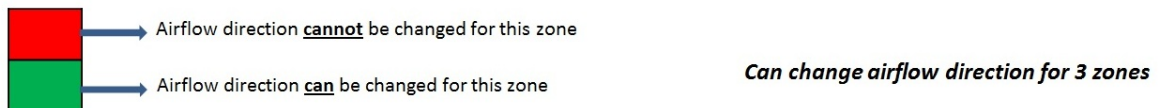
Figure 110: Airflow directions for each zone : 30° angle of incidence

The airflow directions indicated reveal that at this angle of incidence a cross-ventilation pattern is established in the building. Zones 5, 6 and 7 are all present on the high pressure surface of the building, and therefore, air enters through these zones and exits through the remaining zones which are all present on the low pressure surface of the building (except zone 8).

	Zone 1	Zone 2	Zone 3	Zone 4	Zone 5	Zone 6	Zone 7	Zone 8
Baseline	-	-	-	-	+	+	+	-
Case 1	-	-	-	-	+	+	+	-
Case 2	-	-	-	-	+	+	+	-
Case 3	-	-	-	-	+	+	+	-

Airflow direction **cannot** be changed for this zone

Airflow direction **can** be changed for this zone

Can change airflow direction for 0 zones
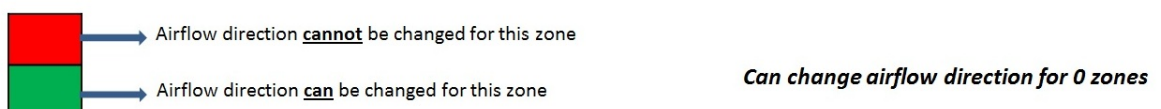
Figure 111: Airflow directions for each zone : 45° angle of incidence

From the above results, we see that it is possible to control airflow exchange direction in interior zones within a certain range of angle of incidence. The number of zones that we are able to exert control over ranges from 6 in the case of 10° angle of incidence to none in the case of 45° angle of incidence. As the angle of incidence increases, flow separation becomes

increasingly prominent leading to the loss of our ability to manipulate airflow direction. However, until about 30º angle incidence, it is still possible to reverse the airflow exchange direction in a number of zones, solely by moving the location of the resistance devices.

The other goal mentioned at the outset was to determine the conditions under which it would be possible to supply airflow equivalent to at least 1 ACH. In conventional mechanical ventilation systems, the supply airflow rate is typically equivalent to 5 ACH, out of which 1 ACH is composed of fresh (outside) airflow. It is with this factor in mind that the target flow rate is set to 1 ACH. However, it should be noted that the amount of airflow intake in a naturally ventilated depends on external weather conditions. During the heating season, when external temperatures are low, the amount of air intake will typically be small, in order to minimize the amount of energy spent in conditioning this supply airflow. However, in the cooling season, it may be useful to increase the amount of supply airflow to well above 1 ACH depending upon the amount of cooling required.

Table 2 shows the variation of ACH with both wind incidence angle as well as resistance device location for a wind speed of 5 m/s (11 mph). Refer Table 1 for the corresponding resistance device locations. The opening area is equal to 0.05 m². At this wind speed, the amount of airflow exchanged with the surroundings exceeds 1 ACH for most resistance device configurations and wind incidence angles. The general trend observed is that as the angle of incidence increases, the amount of airflow exchange also rises correspondingly. As discussed previously, this is because as the incidence angle increases, the conditions resemble a cross-ventilation pattern, where the driving pressure differential across the building envelope is relatively large. At this wind speed, some configurations allow for air exchange rates less than 1 ACH. However, under such circumstances, selecting an

appropriate resistance device location may allow us to supply the required amount of airflow. For example, selecting the resistance device location corresponding to case 2 for the 10º angle of incidence case allows us to meet the specified requirements. Below 5 m/s, it is difficult to supply an airflow rate equivalent to 1 ACH for the given opening size. Under such conditions, the opening sizes need to be increased in order to fulfill the ventilation requirements. Table 3 shows the airflow rates as a function of resistance device

	Baseline	Case 1	Case 2	Case 3
10º	0.76	0.69	1.16	0.41
20º	1.16	0.75	1.14	0.47
30º	1.21	0.77	1.10	0.82
45º	1.02	0.98	1.17	1.44

Table 2: Variation of ACH with wind incidence angle for wind speed of 5 m/s

configuration and wind incidence angle for a wind speed of 9 m/s ($\sim$ 20 mph). In this case, we see that the pressure differences created across the building envelope are large enough to supply the required amount of airflow in most cases. In fact, the amount of airflow in most cases is much larger than 1 ACH. In such a situation, it may be required to reduce the amount of airflow entering the building (e.g., in the heating season). Then, it may make sense to a resistance device configuration that brings the amount of airflow closes to 1 ACH (e.g., case 3 for the 20º angle of incidence). Based on these results, it is apparent

	Baseline	Case 1	Case 2	Case 3
10º	1.64	1.54	2.49	0.96
20º	2.50	1.62	2.46	1.02
30º	2.61	1.67	2.36	1.76
45º	2.20	1.60	2.51	3.11

Table 3: Variation of ACH with wind incidence angle for wind speed of 9 m/s

that the resistance device concept is effective up to angles of incidence of about 30º with

respect to the major axis. Above this angle of incidence, resistance devices do not affect the pressure distribution around the building perimeter as much on account of flow separation. Based on the wind rose for San Francisco, it can be seen that for the chosen building orientation, the wind is always within this limiting angle of incidence for a large percentage of time ($\sim 50\%$ of the year). In addition, on account of the symmetry of the elliptical cross-section, the concept is still effective under conditions where the wind direction is reversed. Therefore, even for the portions of the year when the wind blows from the south-east, this concept will work effectively, albeit with the airflow exchange directions reversed. The wind rose for San Francisco indicates that the wind speed is above 5 m/s for over 60% of the year. Therefore, under such conditions, 1 ACH can easily be supplied for a large portion of the year.

4.5   Application to a full-scale building

Based on the results presented thus far, we have seen that it is possible to manipulate both airflow exchange direction as well as the amount of airflow by controlling the building envelope pressure distribution by utilizing various combinations of resistance device locations. Now, we seek to extend this study by utilizing the results obtained from the 3-D CFD study of the full scale, elliptical cross-section building. Our primary objective is to determine the extent to which the airflow exchange directions can be altered as compared to the baseline scenario. In addition, we also seek to ascertain the extent to which airflow directions can be reversed for a given zone location at different heights along the building. For this purpose, we assume that the building layout is such that each floor in the building has the same floor plan, as shown in Figure 112. The floor height is taken be 3 m. For each

resistance device investigated, the pressure distribution data for each floor is extracted and input into CONTAMW in order to obtain the resulting airflow distribution in the interior of the building.
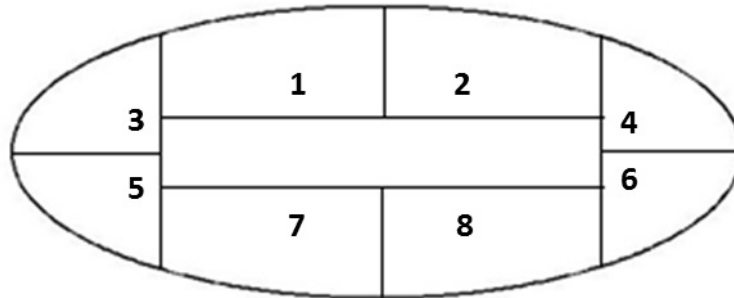
Figure 112: Floor plan layout for full scale, elliptical building

Figure 113 shows the variation in airflow direction along the height of the building for configuration 3 (refer Figure 66) for three zones. The x-axis denotes airflow exchange rate. Positive values indicate that air is exhausted to the ambient, whereas negative values indicated inflow into a given zone from the ambient. The vertical axis represents the height along the building.

It is readily apparent that the airflow exchange characteristics for these zones vary markedly for configuration 3 as compared to the baseline. Air enters zone 3 throughout the height of the building for configuration 3, whereas in the baseline, for the majority of the height of the building, air is exhausted to the ambient from this zone. For zone 6, air is exhausted to the ambient for the baseline scenario over a large portion of the building's height. For configuration 3 however, we see that there are regions where flow is exhausted to the ambient, and regions where flow enters this zone from the ambient. The changes in airflow direction near the heights of 5 m and 125 m can be attributed to the effect of the ground and the roof the building respectively. The transition near 60 m occurs because of
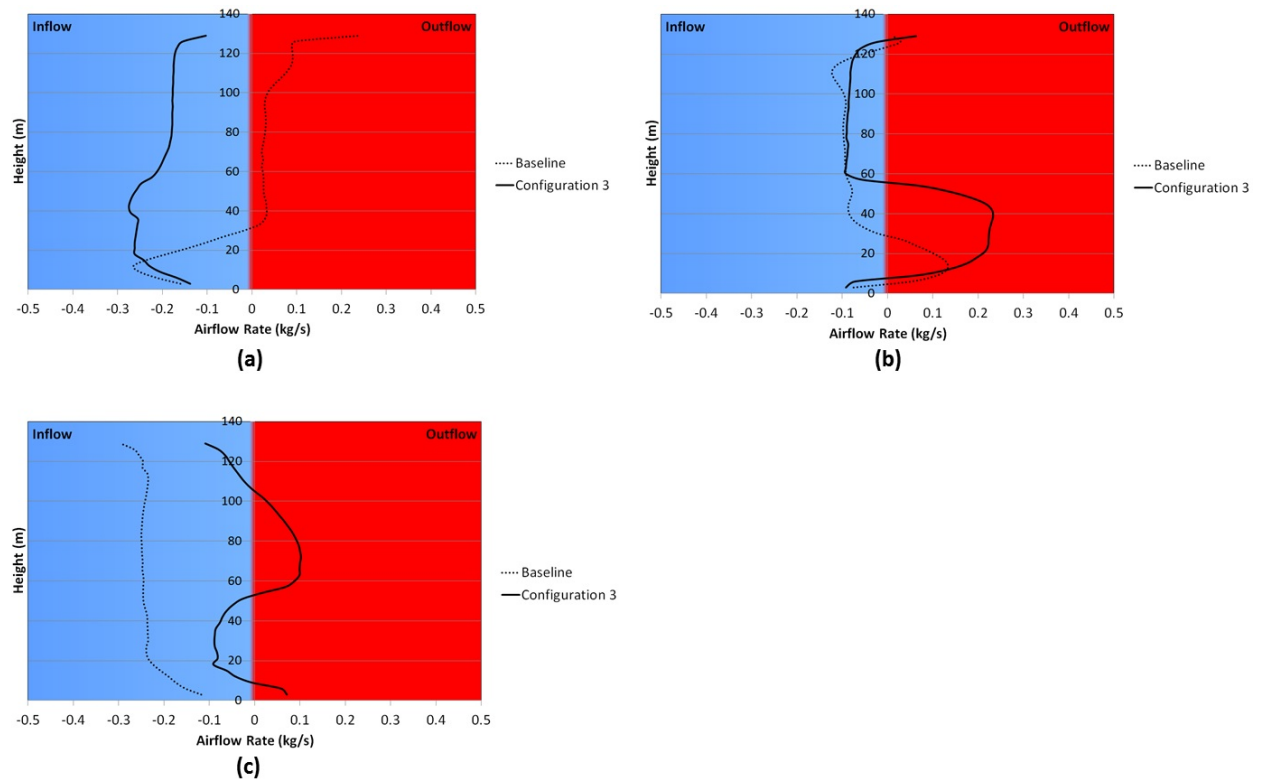
Figure 113: Variation of airflow direction with height for select zones (configuration 3) : (a) Zone 3 (b) Zone 8 (c) Zone 6

the change in the resistance device configuration that occurs in this region (at 65 m). Similarly, for zone 6, we again see that airflow direction changes over the height of the building for configuration 1, whereas for the baseline case, air enters this zone throughout the entire height of the building.

Figure 114 displays the airflow exchange directions for four zones for configuration 4. Looking at zones 2 and 6, we see that airflow direction is reversed as compared to the baseline in the region where the resistance device configuration changes (near the mid-height of the building). For these zones, we also notice a dramatic difference in the amount of airflow exchange with the ambient over large portions of the building height as
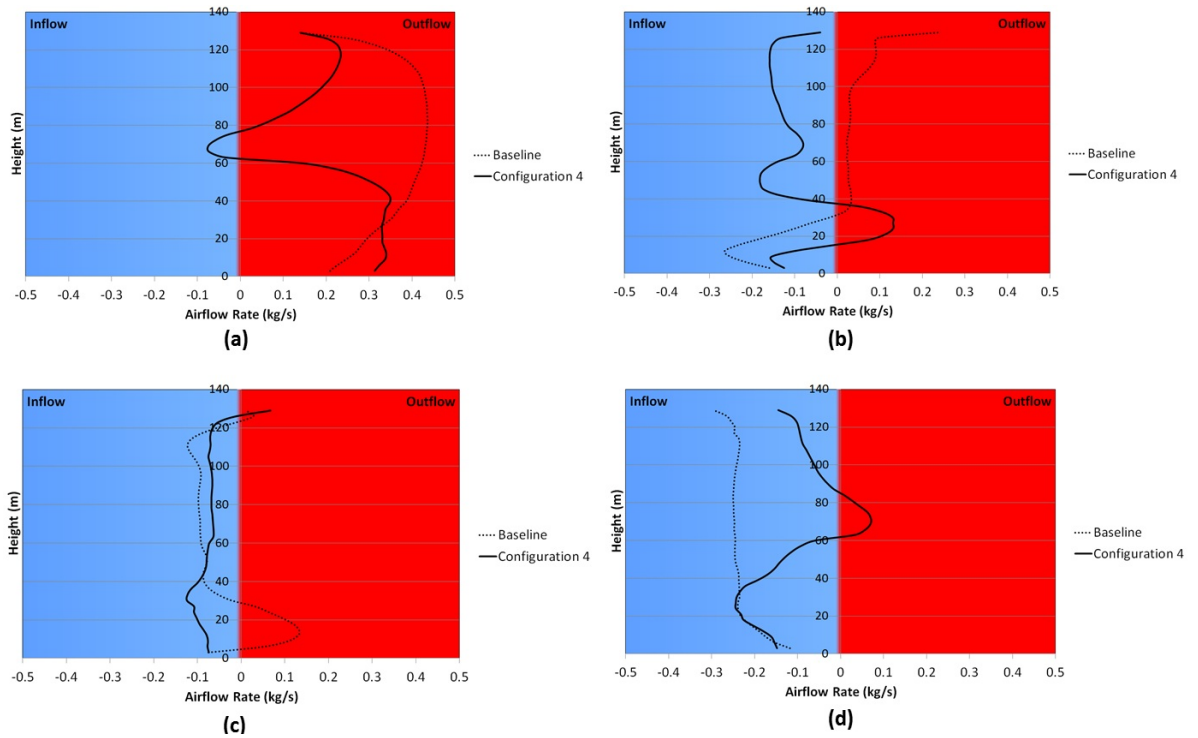
Figure 114: **Variation of airflow direction with height for select zones (configuration 4) : (a) Zone 2 (b) Zone 3 (c) Zone 8 (d) Zone 6**

compared to the baseline case. For zone 3, the airflow directions are reversed as compared to the baseline from about 40 m upwards.

For configuration 5, the airflow exchange direction for four zones are shown in Figure 115. For all the zones shown, we see significant variation in the direction of the airflow exchange with the height of the building. For the baseline scenario, the airflow direction remains fixed, except near the ends of the building, where we observe some variation.

In the baseline case, for zone 3, air is exhausted to the ambient from about 30 m to 90 m, whereas air enters zone 3 in this region for configuration 3. We again see a reversal in airflow direction near mid-height for the zone 8, which is absent in the baseline scenario.
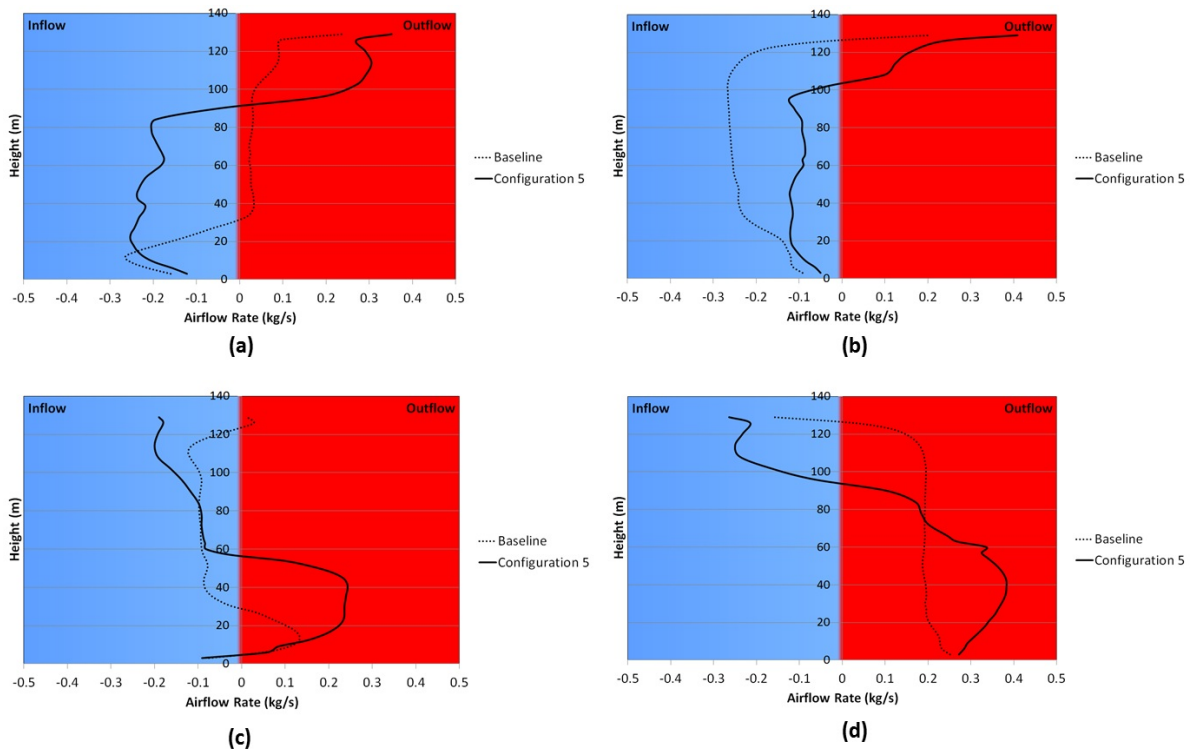
Figure 115: **Variation of airflow direction with height for select zones (configuration 5) : (a) Zone 3 (b) Zone 4 (c) Zone 8 (d) Zone 7**

For zones 4 and 7, The reversal in airflow direction occurs 20 - 30 m lower along the height of the building for configuration 5 as compared to the baseline scenario.

Figure 116 indicates the airflow exchange directions resulting from configuration 6 for four zones. As observed in the previous cases, noticeable differences are present between the baseline scenario and configuration 6. For all the zones, we observe reversals in airflow directions along the height of the building for configuration 6.

The plots for zones 6 and 8 again indicate that the change in resistance device locations that occurs at mid-height can influence airflow exchange direction over the two halves of the building. In addition, zones 2 and 6 exhibit significantly reduced amounts of airflow
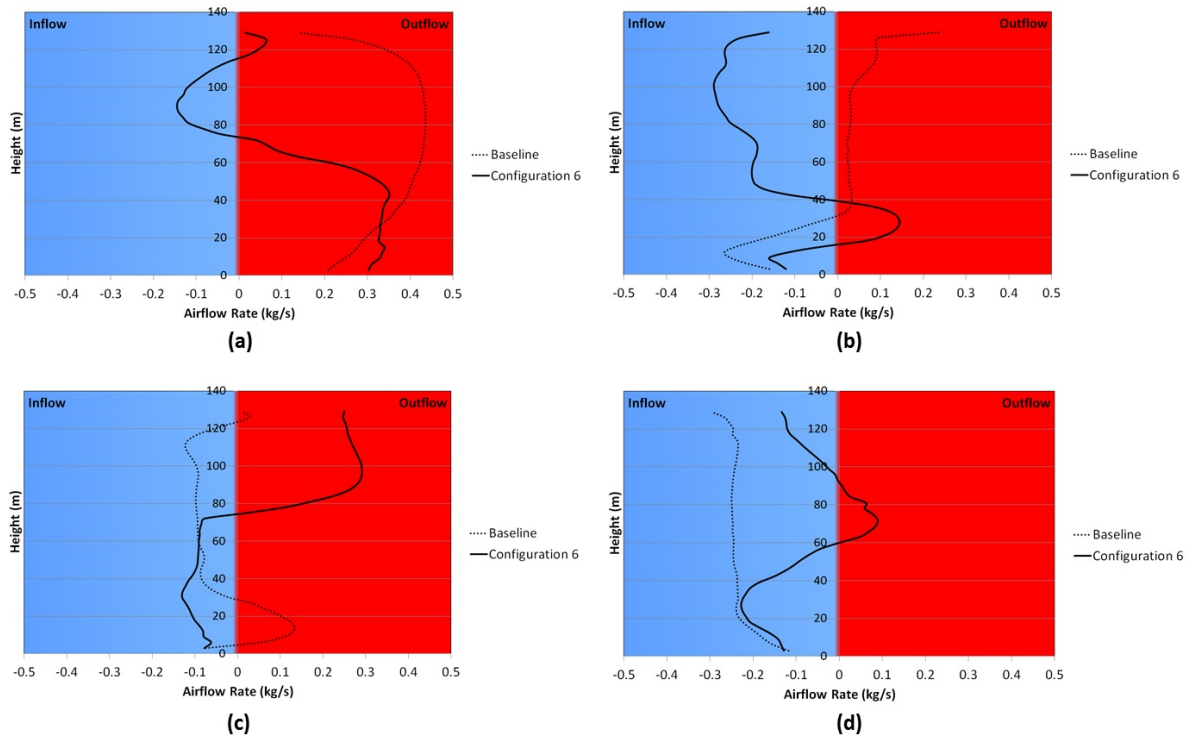
Figure 116: Variation of airflow direction with height for select zones (configuration 6) : (a) Zone 2 (b) Zone 3 (c) Zone 8 (d) Zone 6

exchange as compared to the baseline case. Also, the airflow exchange direction is reversed over most of the building height for zone 3 as compared to the baseline.

Figure 117 compares the airflow directions for four zones for configurations 6 and 7. Recall that for both configurations, the resistance device locations are the same in the upper and lower halves of the building. However, continuous resistance devices are employed in configuration 6, whereas configuration 7 uses discrete resistance devices separated by a vertical distance of 9 m. For all the zones examined, both configurations exhibit similar trends with regards to the airflow exchange direction.

Configuration 7 exhibits greater irregularity in the variation of the airflow exchange rate
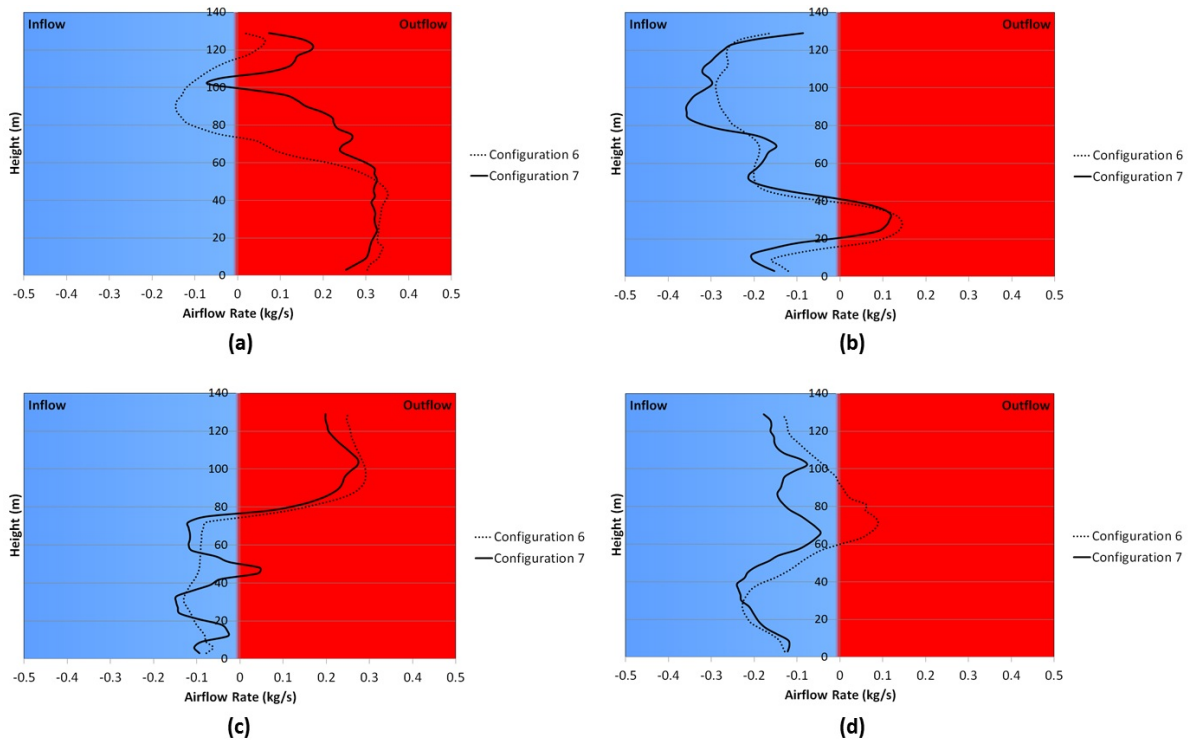
Figure 117: **Variation of airflow direction with height for select zones (configuration 7) : (a) Zone 2 (b) Zone 3 (c) Zone 8 (d) Zone 6**

with height, as can be seen from the vertical gradients. This can be expected on account of the discrete positioning of the resistance devices for this scenario. These results indicate that by suitably employing discrete resistance devices, it may be possible to vary the airflow exchange characteristics (amount/direction) over sub-sections of the building height (as can be observed for zone 8).

Based on the results presented it is seen that by appropriately employing resistance devices, it is possible to alter the airflow exchange characteristics of the zones in the elliptical cross-section building significantly as compared to the baseline case. In addition, it is also possible to have variation in the airflow direction (i.e. intake versus exhaust) for a given zone along the height of a building. It should be noted that the resistance device

configurations examined are not the only possible choices. These configurations were chosen for the purpose of a preliminary investigation of the resistance device concept applied to a full scale building. Practical implementation of the concept would involve conducting a detailed study of many more device configurations, and the effect that they have on the envelope pressure distribution, as well as the airflow distribution within the interior. Such information could then be used in order to develop a database relating required airflow distribution to the appropriate resistance device configuration, which could be used by a control algorithm. However, this is outside the scope of the present work.

4.6 Application of concept in control of natural ventilation

For model-predictive control, an objective function that serves as a metric to quantify the performance of the ventilation system is chosen. The role of the objective function is to combine multiple objectives (indoor air quality, thermal comfort, energy consumption) in multiple zones into a single computable quantity that helps determine the feasibility of the chosen ventilation configuration.

The choice of the objective function is dependent on the desired outcome. For instance, the objective function can either be based solely on IAQ, or solely on thermal comfort or energy consumption, or a combination of these. For a building in mild-weather locations, thermal comfort may be more important than energy consumption or IAQ, whereas a building in a cold-weather location will have equal emphasis on IAQ, thermal comfort and energy consumption. Furthermore, when combining multiple objectives, it is necessary to choose a common quantity such as monetary impact or human productivity to express these objectives.

In this work, an objective function that captures the deviation of the CO_2 concentrations in zones from those achieved by following ASHRAE standards is used. Thus, the goal is to use natural ventilation to match the IAQ conditions achieved by using ASHRAE standard 62. For this purpose, the concept of ASHRAE-relative airflow derived previously is employed.

Since the ASHRAE-recommended airflows (standard 62) are proportional to the occupancy, a candidate objective function is:

$$J = \frac{\sqrt{\sum_{n=1}^{N} \left(O_n \left[\left(\frac{Q_{SUP}}{Q_*} \right)_n - 1 \right] \right)^2}}{\sum_{n=1}^{N} O_n} \tag{40}$$

where O_n = Number of occupants in zone n and $\left(\frac{Q_{SUP}}{Q_*} \right)_n$ is the ASHRAE-equivalent airflow ratio for zone n.

This objective function represents the total percentage deviation of IAQ from ASHRAE-recommended values in the root mean square sense. Since the control algorithm attempts to minimize the objective function, employing the objective function shown in Equation (40) results in minimizing the deviation from ASHRAE standards. The objective function (40) penalizes both under-ventilation and over-ventilation equally. The rationale behind penalizing over-ventilation is that over-ventilation increases energy required to condition the supply air, along with draft discomfort associated with increased ventilation rate. As stated previously, a value of $Q_{SUP}/Q_* = 1$ corresponds to an IAQ equivalent to that achieved by matching ASHRAE recommended ventilation rates. Therefore, when ASHRAE recommendations are exactly met, the objective function value is equal to zero, and any deviation from ASHRAE results in a positive value.

In mild-weather locations, or when the energy costs associated with conditioning the supply air are negligible, one may not wish to penalize over-ventilation. In this case, the objective function can be chosen to be

$$J = \frac{\sqrt{\sum_{n=1}^{N} \min \left[\left(O_n \left[\left(\frac{Q_{SUP}}{Q*} \right)_n - 1 \right] \right), 0 \right]^2}}{\sum_{n=1}^{N} O_n} \qquad (41)$$

Finally, it should be noted that the objective function can be easily modified to reflect various scenarios and goals. For instance, if the goal is to maintain a specified level of IAQ, a simple objective function such as

$$J = \max_n \left| \left(\frac{Q_{SUP}}{Q*} \right) - 1 \right|, \qquad 1 \leq n \leq N \qquad (42)$$

can be used. This objective function focuses on the zone with the maximum deviation from the specified ventilation rate $\left[\left(\frac{Q_{SUP}}{Q*} \right) = 1 \right]$, that is, the zone which is over-ventilated or under-ventilated by the largest amount.

For numerical results presented here, the objective functions defined in Equations (40), (41) and (42) are used. Thus, the focus of this work is only on IAQ within the building interior. Another goal for a ventilation system is to satisfy the thermal comfort requirements of the occupants. However, as discussed previously in Chapter 2, it is difficult to describe the parameters that influence the perception of thermal comfort. In particular, in naturally ventilated buildings, the occupants may be willing to accept a larger range of temperature variation, especially for buildings in temperate climatic locations. As this is the focus of the present work, we choose to neglect the thermal comfort requirement, and instead focus solely on IAQ. Finally, it is noteworthy that the logic and approach in

choosing the objective function are applicable to a wide range of problems beyond natural ventilation and tall aerodynamic buildings.

In this section, numerical results comparing a few candidate strategies for controlling natural ventilation for the building with an elliptical cross-section described earlier are presented. Throughout this section, it is assumed that the openings between zones are fixed in size and fully open. The ventilation ports to the ambient are 0.05 m^2 in the fully open mode, but they can be adjusted. On account of the quasi-steady state assumption made previously, the results presented here are for the steady-state. In all the simulations, airflow results from CONTAM are used to calculate ASHRAE-equivalent airflows as detailed earlier.

First, a uniform occupant distribution with five occupants in each zone, except for the unoccupied central passage is assumed. For this case, three different scenarios are looked at, namely, no control, control over resistance location and control over individual ventilation-port openings. In the first scenario, the baseline pressure distribution around building envelope (no resistance devices employed) is assumed, and all openings of the ventilation ports are set to be equal in size. The goal is to choose the opening size to be such that the user-chosen objective function is minimized within the above-mentioned constraints. Figure 118 shows the variation of the objective function (Equation (40)) as a function of the opening of ventilation ports.

It is observed that the value of objective function is minimal when the ventilation ports are 25% open, that is, a 25% opening for all the ventilation ports leads to airflows that are closest to ASHRAE recommendations. Recall that the ventilation port size (i.e., 100% open) is 0.05 m^2. When the ports are more than 25% open, the airflows in the zones are
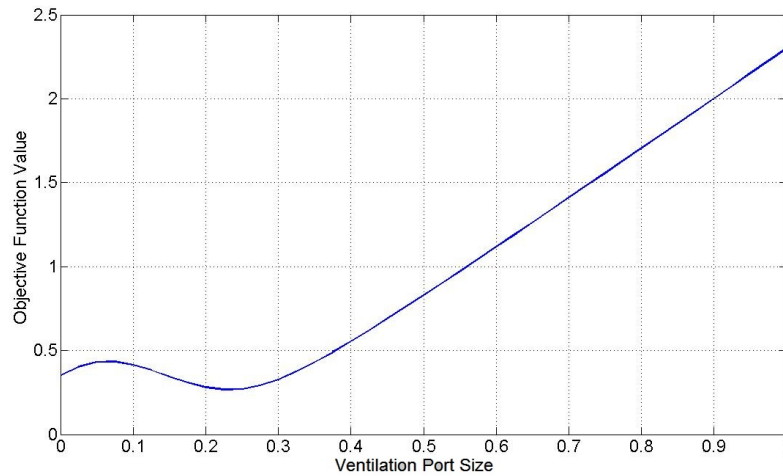
Figure 118: Effect of ventilation port opening size on the objective function defined in (Equation 40) for the case with uniform occupancy

larger, and since (40) penalizes over ventilation, larger airflows lead to an increased value of the objective function. We note here that the optimal objective function value of less than 0.26 corresponds to less than a 26% deviation from ASHRAE-recommended airflows in the root-mean square sense.

In the second scenario, all the ventilation-port openings are set to their optimal value of 25%, and the location of the resistance device is controlled along the building perimeter. Figure 120 shows values of the objective function for various locations of the resistance device shown in Figure 119.

From the figure, location 3 appears to be the optimal location for the resistance device. However, although there are variations in the objective function value between different resistance locations, the variations are small and within 0.1 or 10% of ASHRAE-recommended airflows. Therefore, the conclusion is that in this case (uniform occupancy), controlling the resistance location has a limited effect in helping to meet
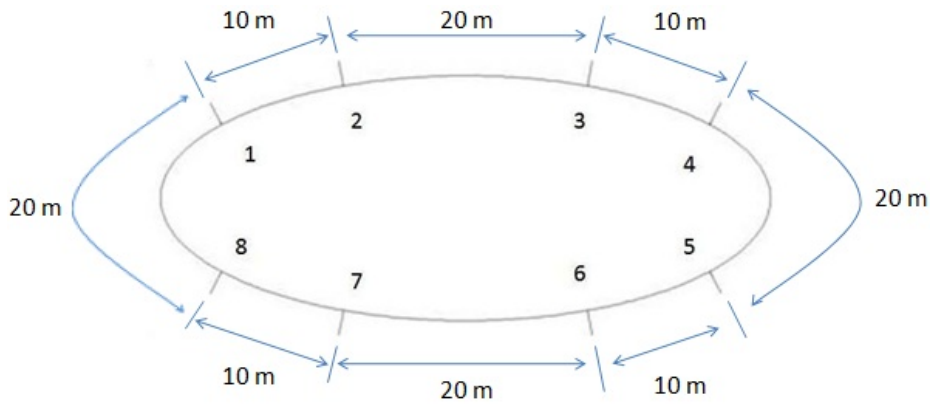
Figure 119: Location of resistance devices

ventilation requirements.
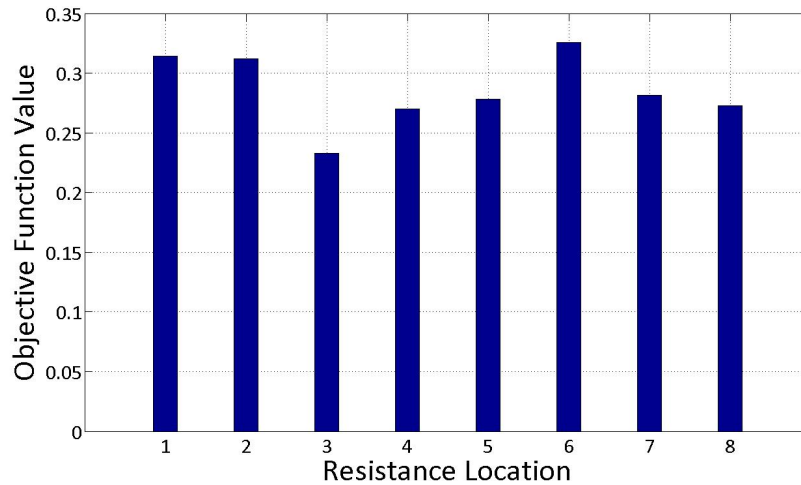
Figure 120: Values of the objective function (Equation 40) for various locations of the resistance device for the case with uniform occupancy

In order to verify whether the port size used in this scenario is optimal, a simple two degree of freedom (DOF) control scenario is investigated, in which the ventilation port size and resistance location are the controlled parameters. First, all the ventilation ports are set to be equal in size. Then, the opening size is allowed to take various values ranging from fully closed to fully open, and the variation in the objective function is observed. This

procedure is then repeated for all possible resistance locations. This process gives us the entire function space for the described two DOF system. Figure 121 illustrates the function space for this particular scenario. It is seen that the minimum possible cost is obtained at a ventilation port size of about 25%, and a resistance location of around 50 m, which corresponds to the resistance location 3. This is in agreement with our earlier results with one DOF.
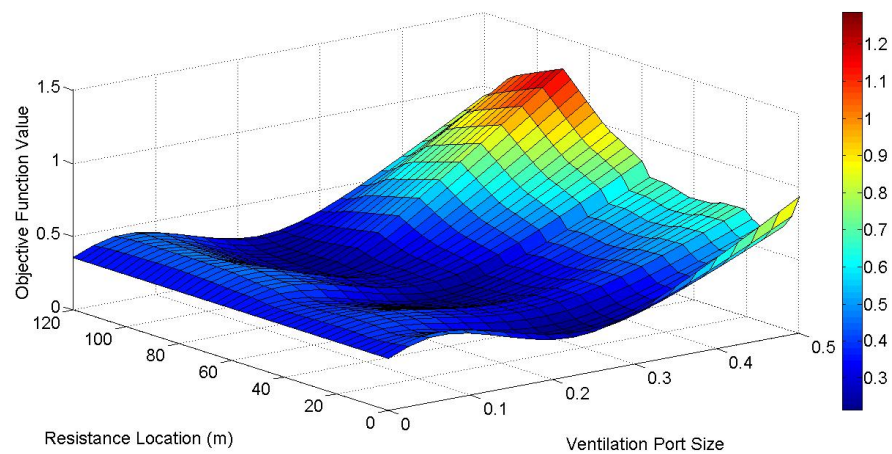
Figure 121: Variation in objective function (Equation 40) for the 2 DOF scenario with uniform occupancy

In the third scenario, independent control over individual ventilation port openings is allowed, and the pressure distribution is kept fixed (baseline pressure distribution). In this scenario, the controller has eight degrees of freedom as there are eight ventilation ports. Optimization is then performed within the model-predictive framework with the objective function (Equation (40)) to determine the ventilation-port openings configuration that allows us to satisfy the ventilation requirements as closely as possible. With independent control over all eight ventilation ports, the model-predictive control algorithm yields a configuration of ventilation port openings that result in an objective function value of 0.12

or roughly within 12% deviation from ASHRAE-recommended airflows.

Table 4 compares the ASHRAE-equivalent airflows for the optimal configurations from all three scenarios in terms of amount of airflows in L/s per person for each zone. Recall that the ASHRAE recommended airflow (standard 62) is 8.5 L/s per person. From Table 4, it is apparent that despite having uniform conditions of occupancy and window size, the amount of airflow received by each zone varies significantly. This is mainly due to the local pressure difference, which may be vastly different for each zone for a building. Some zones like zone 5, which is located near the stagnation point, receive large amounts of fresh air from the ambient, whereas other zones such as zone 1 are primarily ventilated by airflow from adjacent zones and receive almost no fresh air. In fact, in the first scenario, the ASHRAE-equivalent airflow for zone 1 is negative, indicating that Q_{SUP}/Q^* is less than one or equivalently the effective CO_2 concentration of the supply air to zone 1 is greater than C_{ASH}. Large variations are observed in the scenario with no control, with zones 4, 5

	No Control	Resistance-location control	Ventilation-port control
Objective-function value	0.26	0.21	0.12
Zone 1	-0.59	2.97	3.57
Zone 2	4.93	9.77	10.71
Zone 3	7.82	6.46	3.48
Zone 4	14.02	12.66	9.01
Zone 5	17.93	16.32	10.71
Zone 6	5.01	3.48	10.20
Zone 7	17.59	13.68	9.86
Zone 8	4.33	1.78	10.03

Table 4: Optimal objective-function values and ASHRAE-equivalent airflows in L/s per person for the case with uniform zone occupancy

and 7 receiving much more airflow than is required, whereas zones 1, 2, 6, and 8 receive

inadequate airflow. The scenarios involving control over resistance location and control over ventilation port size perform better than the scenario with no control. For the scenario with control over ventilation port size, it is apparent that most zones are supplied with close to the required amount of airflow, which means that the IAQ in most zones is close to that corresponding to ASHRAE Standard 62. This is reflected in the fact the value of the objective function associated with this scenario is the least among all the scenarios considered.

Furthermore, due to the inter-connections between the different zones, any change in airflow patterns in one zone will also affect several other zones. This further highlights the necessity for the centralized controller as discussed earlier. Although the scenario with no control and with control over the resistance location provide acceptable airflows for most zones, independent individual control of ventilation-port openings is shown to provide the most control over IAQ in various zones. The individual port sizes obtained in the results shown for this scenario are shown in Figure 122. It is to be noted that since there may be multiple airflow paths that lead to similar AHSRAE-equivalent airflows in a zone, there may be other combinations of port sizes that result in similar ventilation performance.

Next, a non-uniform occupant distribution is studied, in which zone 2 has 10 occupants, zone 7 has 1 occupant and all other zones are unoccupied. This occupant distribution is chosen such that a zone with a need for large airflow (zone 2) is on the suction side and hence represents a difficult case. Again, the three scenarios described previously are considered, namely, no control, control over resistance location, and control over ventilation port openings.

For the first scenario, again the opening of all ventilation ports are kept identical. As seen
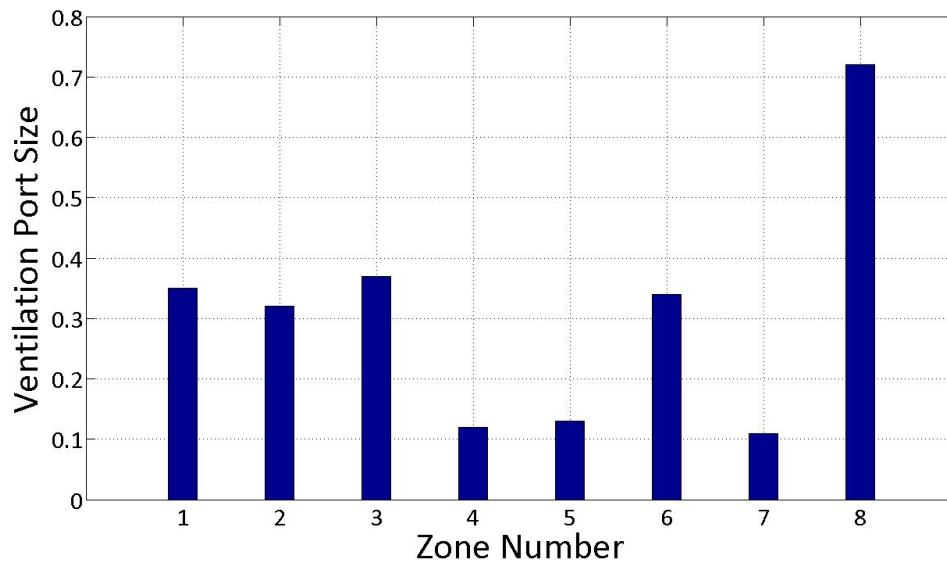
Figure 122: Ventilation port sizes for scenario with independent control over port size

in Figure 123, the objective function is minimized when all ventilation ports are 15% open as opposed to 25% for the uniform occupant distribution case. This is attributed to the fact that 7 out of 8 zones have a smaller airflow requirement in comparison to the uniform occupancy case.

Next, for the second scenario, the procedure for the two DOF system described previously is followed, and the function space for this configuration is obtained. Figure 124 shows the variation in the objective function as the resistance location and ventilation port size are varied.

In this case, a significant variation of more than an order of magnitude in the objective function is observed as the resistance location is varied. In this scenario, changing the resistance location and thus the pressure distribution around the building envelope is an effective strategy as it helps supply different quantities of air to different zones. Figure 125
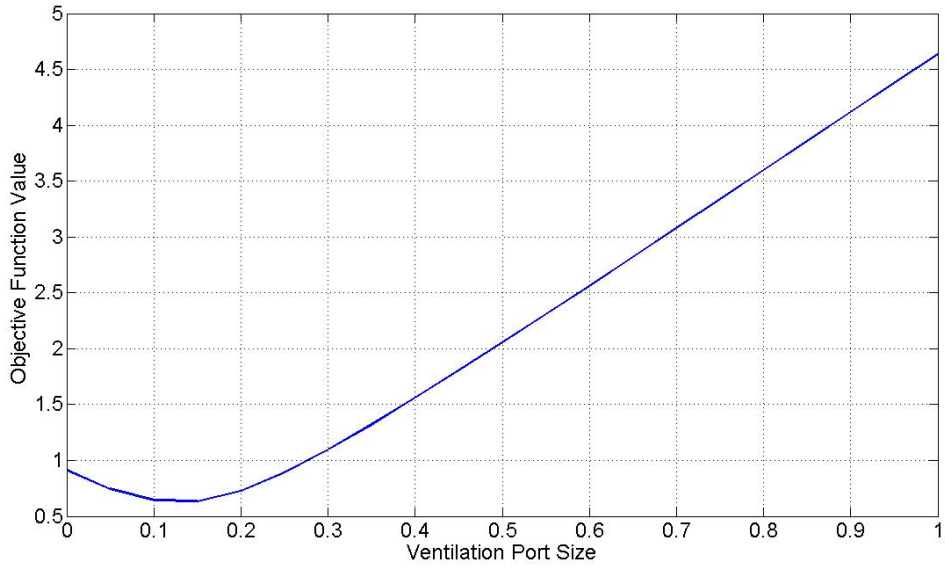
Figure 123: Variation of the objective function (Equation 40) with opening of the ventilation ports with all ports equal in size and non-uniform occupancy
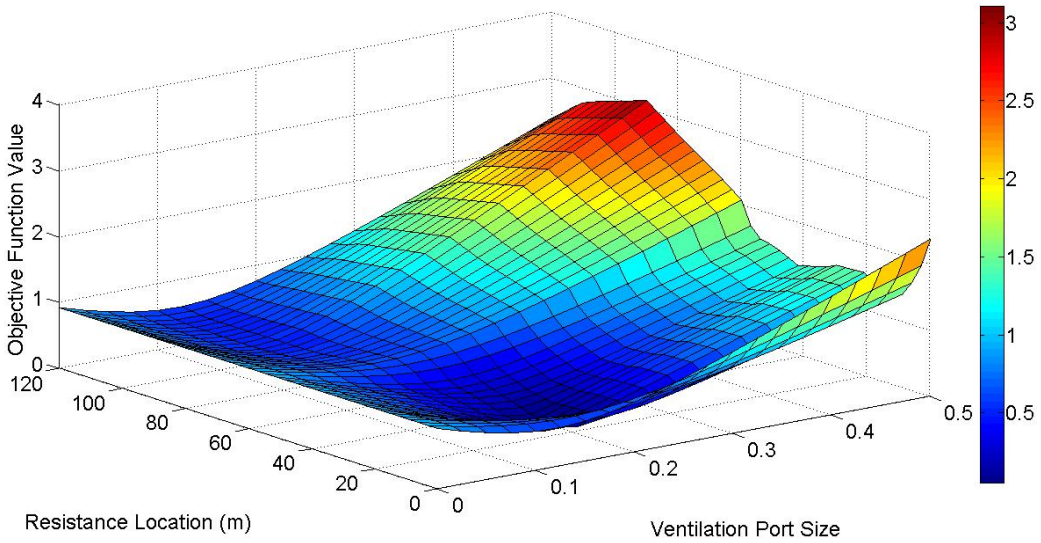
Figure 124: Variation in objective function (Equation 40) for the 2 DOF scenario with non-uniform occupancy.

shows the breakdown of the ASHRAE-equivalent airflows in L/s per person for both zones 2 and 7 for various locations of the resistance device. Clearly locations 1 and 2 for the resistance device results in significantly smaller objective-function values and thus significantly better IAQs than other locations. As seen from Figure 125, placing the resistance device at various locations result in large variation of ASHRAE-equivalent airflow for both zones. Since the ASHRAE recommended airflow (Standard 62) is 8.5 L/s per person, some locations of the resistance device such as location 6 yields a ten-fold over-ventilation for zone 7.

Cost	0.05
Zone 2	8.97
Zone 7	9.24

Cost	0.34
Zone 2	7.77
Zone 7	39.48

Cost	0.06
Zone 2	9.09
Zone 7	9.43

Cost	0.72
Zone 2	6.48
Zone 7	73.43

Cost	0.75
Zone 2	8.03
Zone 7	78.83

Cost	0.80
Zone 2	9.81
Zone 7	82.14

Cost	0.80
Zone 2	9.98
Zone 7	82.45

Cost	0.90
Zone 2	11.15
Zone 7	88.44
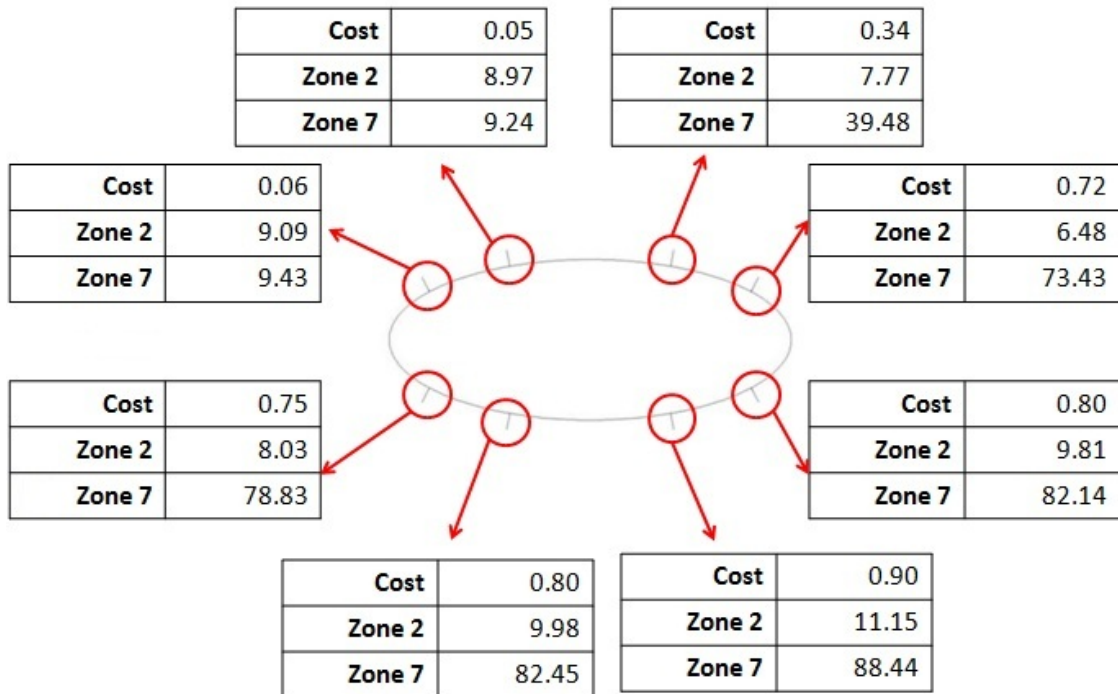
Figure 125: ASHRAE-equivalent airflows for zones 2 and 7 in L/s per person for various locations of the resistance device with non-uniform occupancy.

In the third scenario, with independent control of individual ventilation port openings, the objective function is further minimized to 0.005. It should be noted however, that the order of magnitude difference in the objective function value between the second and third

scenarios does not necessarily reflect the superiority of one technique over the other, as both strategies perform very well and provide almost the exact amount of supply airflow to the occupied zones. Table 5 compares the ASHRAE-equivalent airflows in L/s per person for the occupied zones for all three scenarios. It is to be noted that the scenario with no control does not perform well as large deviations are observed in the airflows as compared to the required amount. In comparison, it is again seen that having independent individual

	No Control	Resistance-location control	Ventilation-port control
Objective-function value	0.63	0.05	0.005
Zone 2	4.83	8.97	8.52
Zone 7	17.10	9.24	8.00

Table 5: Optimal objective-function values and ASHRAE-equivalent airflows in L/s per person for the case with non-uniform occupancy.

control over port openings is an effective strategy for meeting ASHRAE recommendations. Control over the resistance location is also very effective in satisfying the ventilation requirements closely. It is noteworthy that by letting each ventilation port be independently controlled, the airflow pattern within the building can be modified, leading to a high degree of control of the airflows in various zones. Furthermore, it can be concluded that in the case with non-uniform occupancy, controlling location of resistance device is also an effective strategy for controlling the airflows in the zones.

Finally, to illustrate the effect of the choice of objective function on the optimal solution, the scenario with non-uniform occupant distribution where all ventilation ports are set to be 15% open is considered. The objective functions defined in Equations (41) and (42) are used, and the values of the objective function obtained for different locations of the resistance device are compared.

Figure 126 represent values of the objective function (Equation41), while Figure 127 represents the values of objective function (Equation42) for various locations of the resistance device. In Figure 126, the objective function for several resistance locations is zero.
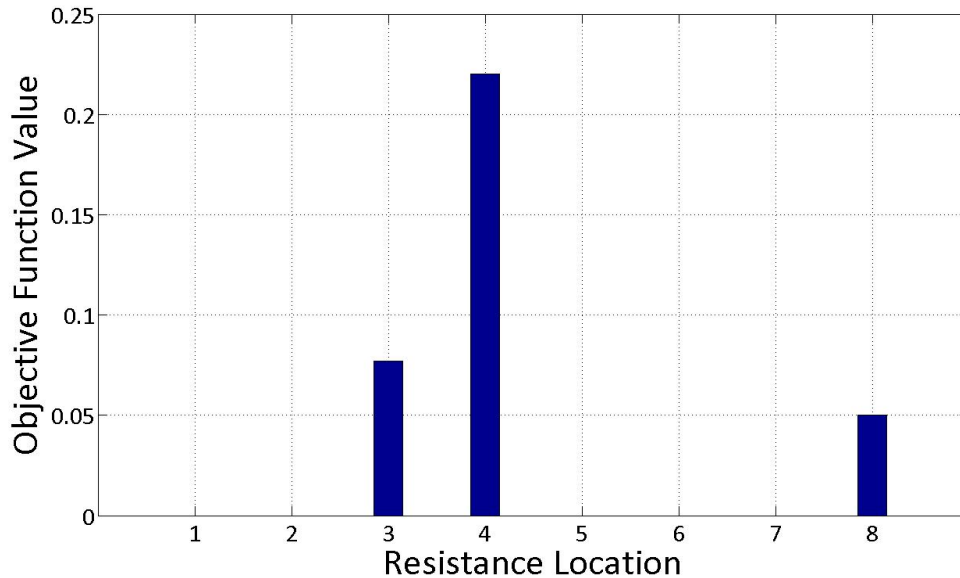
Figure 126: Values of the objective function (Equation 41) for various locations of resistance devices with non-uniform occupancy

This is due to the fact that these locations of the resistance device yield over ventilation in all zones, and (41) does not penalize over ventilation. Therefore, from the point of view of objective function (41), locations 1, 2, 5, 6, and 7 of the flow resistance device are all optimal and thus acceptable choices for the resistance device. Therefore, the objective function defined in Equation (41) may be employed in mild-weather locations or when energy is cheap, in which case over-ventilation may not be an issue. When the objective function defined in Equation (42) is used, it follows from Figure 127 that locations 1 and 2 have the lowest values of the objective function. Thus the same scenario yields different
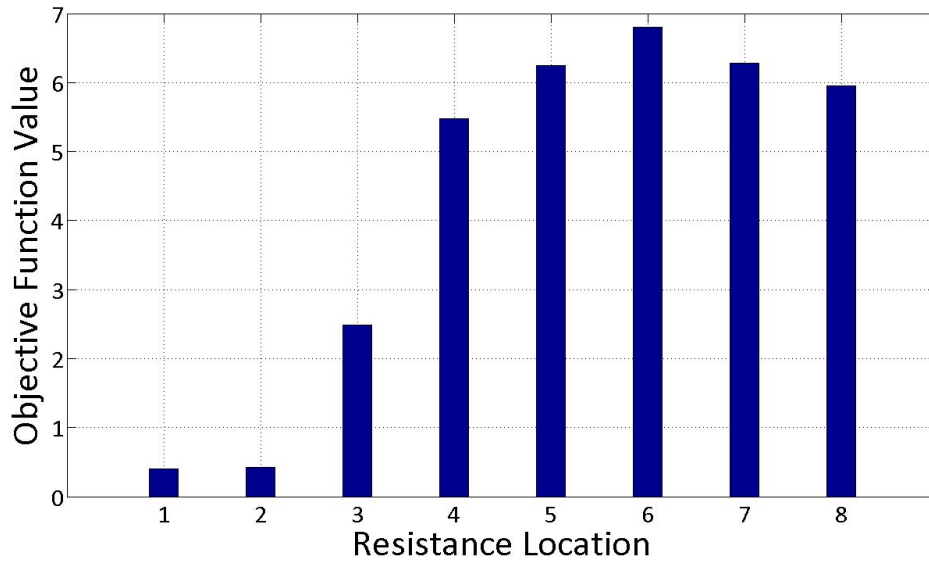
Figure 127: Values of the objective function (Equation 42) for various locations of resistance devices with non-uniform occupancy

optimal locations depending on the objective function employed. Not surprisingly, the choice of objective function is crucial and must be chosen to reflect specific goals of the ventilation system and can be modified to account for additional factors such as weather conditions, thermal comfort, and energy consumption.

5   Energy Considerations

In the preceding chapters, various techniques for manipulating building envelope wind pressure distribution were explored, followed by a discussion of how these techniques could be applied for the natural ventilation of high-rise buildings. The airflow rates considered in these sections were relatively low, on the order of 1 ACH. The underlying assumption is that the naturally ventilated building is geographically located in a region where the external temperature is relatively low (i.e., in the heating season). In this case, the amount of airflow exchange is minimized in order to reduce the amount of energy that is required to condition the ventilation airflow, while satisfying IAQ requirements. It is therefore useful to obtain an estimate of the energy requirements associated with the conditioning of the ventilation airflow. In this section, a brief investigation of the energy requirements associated with the application of natural ventilation in buildings is conducted. In addition, we also explore other energy related issues such as the amount of potential wind power generation using turbines.

First, we calculate the energy requirements for both heating and cooling of a typical floor for a building in two geographical locations, namely, San Francisco and San Diego. For this purpose, a steady state analysis is performed, and the well-mixed assumption is used, wherein the internal conditions within a floor are taken to be spatially homogeneous. Under such conditions, the energy balance for the floor can be described by the following equation,

$$\dot{m}C_p\left(T_i - T_o\right) = \dot{q}_i + \dot{q}_s + \dot{q}_{cond} + \dot{q}_e \tag{43}$$

where $\dot{m}$ is the mass flow rate of the ventilation airflow (in kg/s), C_P is the specific heat

capacity of air (in J/kg-K), T_i is the temperature of the interior of the building (in K), T_o is the temperature of the surroundings, $\dot{q}_i$ is the internal heat gain (due to equipment, occupants etc.) (in W), $\dot{q}_s$ is the heat gain due to solar radiation, $\dot{q}_{cond}$ is the rate at which cooling (or heating) needs to be supplied, and $\dot{q}_e$ represents the heat transfer across the building envelope by a combination of conduction and convection. This heat transfer is calculated by the following equation,

$$\dot{q}_e = UA\,(T_o - T_i) \tag{44}$$

where U is the overall conductance of the building envelope (in W/m^2-K) and A is the area of the building envelope (in m^2).
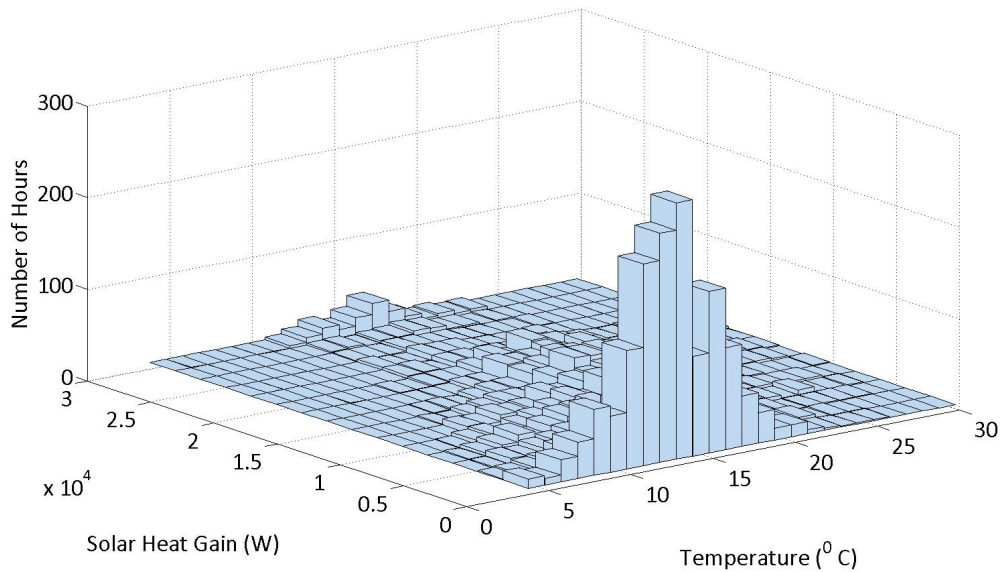
Figure 128: 2-D histogram plot showing temperature and solar heat gain for San Francisco

The calculation procedure is as follows. First, weather data for a typical meteorological year (TMY) is obtained for the chosen geographical locations. The variables of interest in

the data are the distribution of the dry bulb temperature, and the amount of solar irradiation. The data chosen covers a 12 hour occupancy period (i.e., from 7 a.m. to 7 p.m.). Next, the total amount of radiation (both direct and diffuse) incident on the building envelope is calculated following the procedures detailed in [66]. In order to calculate the amount of incident radiation, it is first necessary to determine the orientation of the building, as the amount of incident radiation changes according to the orientation of the building surfaces. For this purpose, the orientation of the major axis of the building is again chosen to be along the same direction indicated in Figure 107. Then, this radiation data and temperature data are sorted into bins, which correspond to the number of hours in a year that particular combinations of incident radiation and ambient temperature are prevalent in the surroundings. A graphical representation of these bins is shown in Figure 128, which is a 2-D histogram plot.

For the energy calculations, the indoor set point temperature (T_i in Equation 43) is chosen to be 22^0 C. The value of the overall envelope conductance (U) is obtained from the ASHRAE Handbook of Fundamentals for a glazed glass envelope, which is a typical material chosen for the façades of high-rise buildings. Then, for each bin of data in the histogram (i.e. for paired values of $\dot{q}_s$ and T_o), the value of $\dot{q}_{cond}$ is calculated. A positive value indicates that the floor needs to be heated under the prevailing conditions, whereas a negative value indicates that cooling needs to be provided. Then, the calculated value of $\dot{q}_{cond}$ is multiplied by the number of hours in a year that the chosen combination of $\dot{q}_s$ and T_o is prevalent, and this gives us the amount of energy required for heating (or cooling) the floor under the given ambient conditions. Finally, the efficiencies associated with the mechanical equipment used to provide heating/cooling is considered. The boiler efficiency is taken to be 90% and the coefficient of performance (COP) of the refrigeration unit is

assumed to be 5. Therefore, the amount of energy that needs to be provided can be calculated by,

$$
Q = \begin{cases} \dot{q}_{cond}/0.9 & \textit{For heating} \\ \dot{q}_{cond}/5 & \textit{For cooling} \end{cases} \tag{45}
$$

The indoor heat load ($\dot{q}_i$) is dependent upon the occupancy and the equipment installed. This quantity is estimated using the following procedure. It is assumed that each occupant generates heat at a rate of 100 W. It is further assumed that each occupant is assigned a computer which generates 100 W, and has lighting equipment which generates a further 100 W. Thus, each occupant is associated with a total heat load of 300 W. The typical amount of space assigned to an occupant in an office building is around 200 ft^2 ($\sim$ 18.5 m^2). The elliptical cross-section building considered has a floor area of 785 m^2. Based on this data, the floor is assumed to have 40 occupants, thus giving a total internal heat load of 120,000 W.
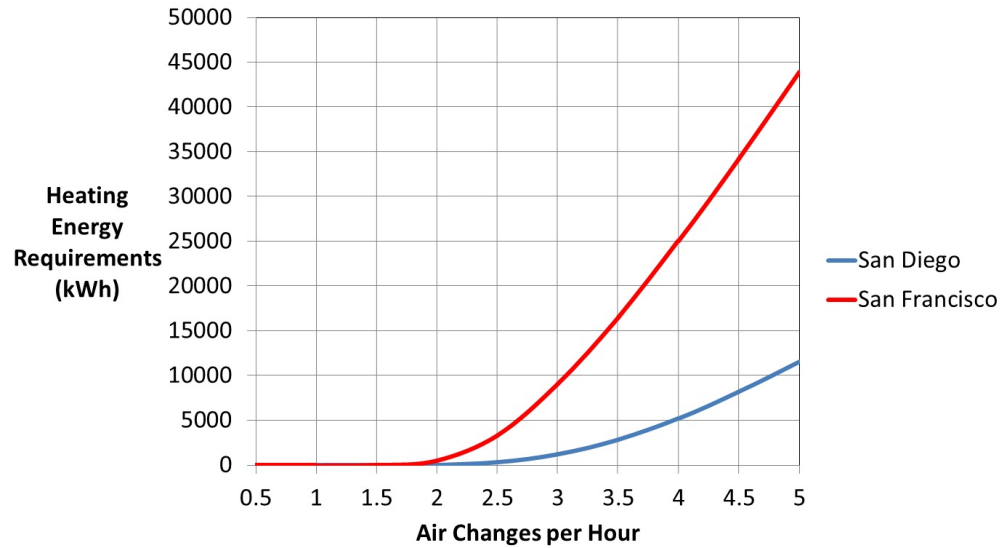
Figure 129: Comparison of heating energy requirements

Figure 129 details the heating energy expenditure for a floor in the building under

consideration under the climatic conditions of San Francisco and San Diego. This figure shows that for low airflow rates (< 2 ACH), it is not required to heat the ventilation airflow. The heat gains present in the system are sufficient to ensure that the set-point temperature of 22^0 C is achieved. In fact, it is necessary to provide cooling under such conditions. As the flow rate increases, it becomes necessary to provide heating to the incoming airflow. It can be seen that the heating energy expenditure for San Francisco is much larger than that for San Diego.
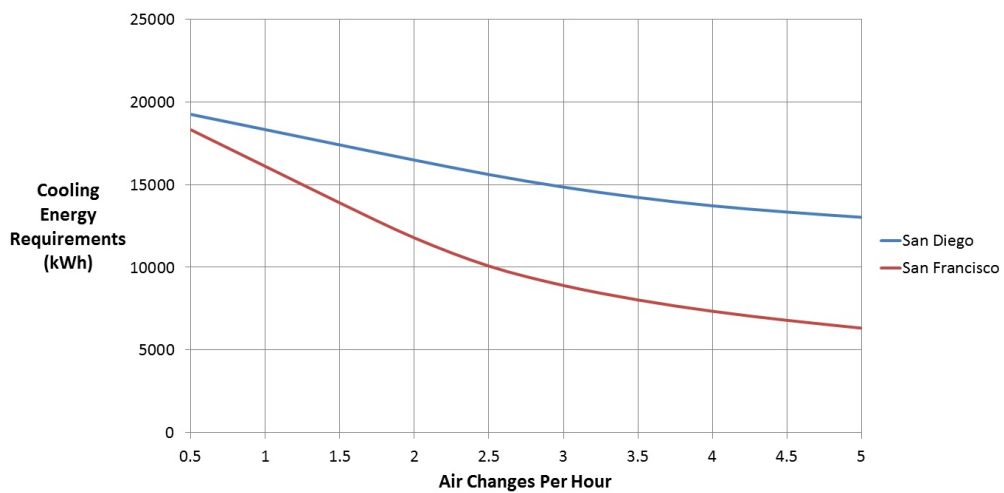
Figure 130: Comparison of cooling energy requirements

Figure 130 details the cooling energy expenditure for the building under the conditions described. In contrast with the heating energy requirements seen in Figure 129, the amount of energy spent on cooling the ventilation airflow decreases as the flow rate increases. This suggests that by increasing the flow rate still further, it may be possible to eliminate the necessity for cooling altogether. Therefore, it may be prudent to choose a ventilation flow rate that minimizes the total amount of heating and cooling energy requirements. One method to achieve this goal is by increasing the amount of ventilation airflow during the cooling season, while reducing the amount of airflow during the heating

season, subject to satisfying IAQ requirements. However, it is difficult to compare heating and cooling requirements directly, as the relevant parameter for cooling requirements is the amount of electricity used, whereas that for heating is the amount of fuel (typically, natural gas) used. It may then be useful to convert the energy requirements into dollar value equivalents by considering the price of electricity and natural gas respectively.

In the preceding chapters, the application of the resistance device concept to manipulate the building envelope wind pressure distribution was explored in detail. One of the possible methods of implementing this concept in practice is by mounting wind turbines on the building exterior. By this method, it is possible to generate electrical power which can then be used to offset some of the energy consumed during the operation of the building. It is then of interest to estimate the amount of energy that may be generated by the use of such devices.

For a turbine of cross-section area A, the total power content of the wind passing through the turbine can be expressed by,

$$P_{wind} = \frac{1}{2}\rho A V^3 \tag{46}$$

where ρ is the air density (in kg/m^3), and V is the wind speed. Then, assuming a turbine efficiency η, the total amount of power generated by a turbine can be expressed as,

$$P_{turbine} = \eta \left(\frac{1}{2}\rho A V^3 \right) \tag{47}$$

For the purposes of wind energy calculations, two turbine locations are considered, namely, one which is 60 m away from the ground, and another which is 120 m away from the ground. Recall that the wind speeds at these two heights are different due to the presence
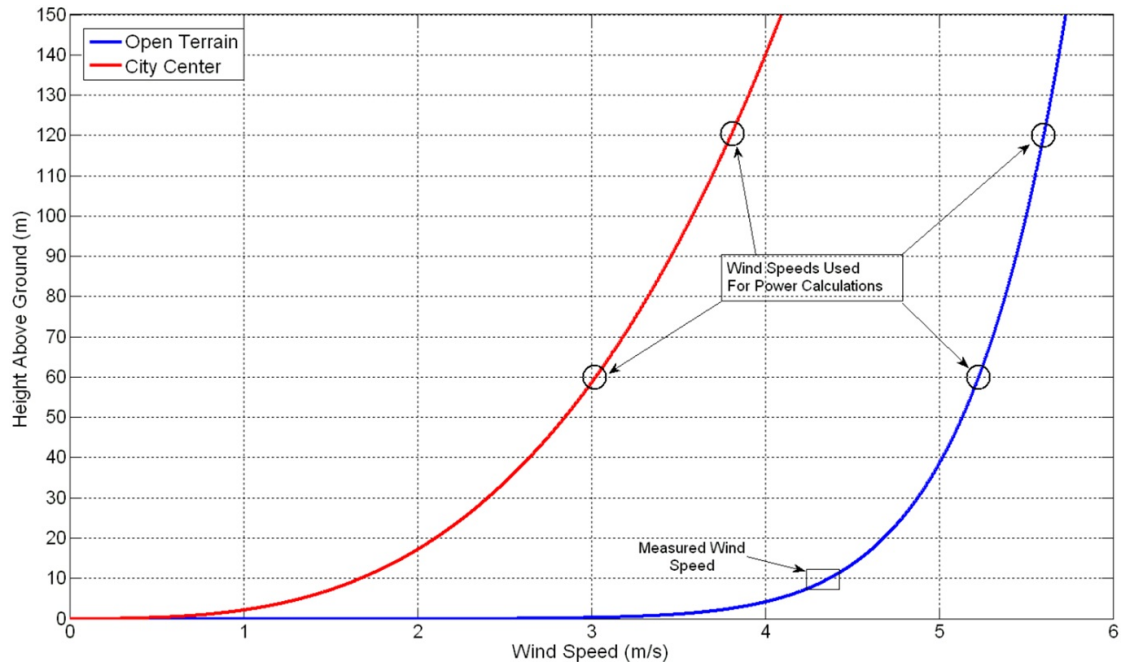
Figure 131: ABL profiles used for wind energy calculations

of the ABL. Here, two ABL velocity profiles are considered. One profile is used for a building located in flat, open terrain, while the other is for a building located in a city center. The wind data for San Francisco obtained from Figure 107 is again used for the purposes of these calculations. As the wind rose is plotted in terms of ranges of wind speed, we take the average of each wind speed range as a representative measured wind speed for the purposes of generating the ABL velocity profiles. Figure 131 shows two ABL profiles used for this purpose, as well as the locations of the wind turbines along the height of the building. The width of the turbine is 2 m and the height of the turbine is 3 m, giving a cross-sectional area of 6 m^2. These dimensions are chosen as the resistance devices explored previously are assumed to be the same height as a typical floor (3 m), and project 2 m normal to the surface of the building envelope. The turbine efficiency is assumed to be 30% ($\eta = 0.3$).

	60 m level	120 m level
Urban Terrain	942	1871
Open Terrain	4863	5986

Table 6: Wind energy generation (in kWh)

Table 9 presents the results of the wind energy calculations. It can readily be seen that turbines located on a building situated in open terrain generate a lot more power than those on a building located in the city center. This is expected on account of the difference in the ABL profiles or the two scenarios. It is also observed that for both locations, the turbines located at 120 m generate more power than those at 60 m. Again, this is expected as the wind speed increases with the height. The relative difference in power generation between the two heights is much more pronounced for the city center location as the difference in velocity is more significant ($\sim$ 1 m/s as opposed to $\sim$ 0.3 m/s for the open terrain case).

With reference to Figure 130, we see that the wind turbines can potentially offset a significant percentage of the energy required to cool the ventilation airflow. For instance, at large airflow rates, a wind turbine mounted on a building located in open terrain can contribute as much as 50% of the energy required to provide cooling. Even at low airflow rates, such a turbine can provide about 20% of the energy required to run the refrigeration equipment. However, for a building located in an urban center, the amount of energy extracted is not large enough to make a significant contribution towards cooling energy requirements.

In a naturally ventilated building, fans are not required in order to provide the ventilation airflow. On account of this, there are some energy savings, which we now estimate. For this purpose, the results for the elliptical building are considered, where the wind is at a

10^0 angle of incidence, and the wind speed is 5 m/s. For these conditions, as seen previously, the amount of airflow exchange can be calculated using CONTAMW. In addition, we can also obtain the pressure drops across the ventilation openings. We then seek to estimate the amount of energy that would be required if fans were used to supply the calculated amount of airflow across the pressure drops specified. For a given fan efficiency η, the fan power requirement can be calculated by,

$$P_{fan} = \frac{Q \Delta P_0}{\eta} \tag{48}$$

where Q is the volume flow rate (in m^3/s) through an opening, and ΔP_0 is the total pressure drop (in Pa) across the opening. ΔP_0 is calculated using,

$$\Delta P_0 \approx \Delta P + \frac{1}{2}\rho \left(\frac{Q}{A}\right)^2 \tag{49}$$

where ΔP is the static pressure drop across the opening (in Pa), and A is the area of the opening (in m^2). The total energy requirement is calculated by adding the fan power requirements for all 8 openings in the building, and multiplying by the total time of operation during the year (for 12 hours of daily operation). The fan efficiency is assumed to be 50% ($\eta = 0.5$).

	Baseline	Case 1	Case 2	Case 3
ACH	0.76	0.69	1.16	0.41
Energy Requirements	438	342	885	114

Table 7: Annual fan energy requirements (in kWh)

Table 5 displays the fan energy requirements under these conditions. For the airflow rates considered here, it is apparent that during the heating season, the fan energy requirements

outweigh the energy requirements for conditioning the supply airflow, which are essentially zero. However, during the cooling season, the fan energy is a negligible fraction of the energy required for conditioning the airflow. For a building located in a city center, it can also be observed that a significant fraction of the energy output of building mounted VAWT's may be consumed by fans utilized for providing the ventilation airflow.

6 Conclusions

The wind pressure distribution around a building envelope is an important factor influencing the quality of the ventilation provided in a naturally ventilated building. It is possible to increase or decrease the amount of airflow supplied to the building interior by changing the sizes of the ventilation openings accordingly, however, it is not possible to control the distribution of the airflow in the interior (or the airflow direction through a given opening), as this is controlled by pressure distribution around the building envelope (which is determined by the wind speed and direction). In this work, various techniques to manipulate the building envelope wind pressure distribution such as jet flaps and resistance devices are discussed. The scope of application of these techniques is limited to buildings of streamlined cross-section.

The resistance device technique is seen to be a particularly effective method of manipulating the envelope wind pressure distribution. It does not require an external power source for its operation, and in fact, it may even be used for power generation by employing VAWT's. The concept may be implemented in practice by installing an array of fixed devices around the building perimeter at specified locations. Alternatively, it is also possible to reduce the number of devices around the perimeter by ensuring that these may be moved around the perimeter (e.g., by mounting them on rails). The mechanism of action of this technique relies on the presence of streamline curvature near the surface, and the resulting normal pressure gradients. For this reason, this technique is effective for buildings with curved surfaces, such as the elliptical cross-section building investigated in this work. This technique is seen to be particularly effective when applied to the elliptical cross-section building considered in this research.

The primary advantage of manipulating the building envelope pressure distribution is that it allows for controlling the direction of airflow exchange with the ambient for the various zones within the building. For example, at low angles of incidence of the wind ($\sim 10^0$), it is possible to control the direction of airflow exchange for 6 out of the 8 zones for the floor plan studied. Therefore, depending upon the prevalent ventilation requirements within the building, it is possible to specify the zones that receive air from or exhaust air to the ambient. As the angle of incidence of the wind increases, the level of control over the airflow exchange direction decreases. At an angle of incidence of 45^0, it is no longer possible to control the direction of airflow exchange for any zone within the building. At this incidence angle, a cross-ventilation flow pattern is established, in which it is a trivial problem to supply the required amount of ventilation, and in which it is not possible to have any control over the direction of these airflows.

By employing continuous banks of resistance devices on a full-scale 3D building, it is possible to exert significant control over the pressure distribution, and consequently, the direction of airflow exchange over the entire height of the building. By choosing a suitable resistance device configuration, it is seen that for a particular zone, it is not only possible to change the direction of airflow exchange with respect to the baseline, but, that it is possible to reverse the direction of the airflows along the height of the building. This indicates by dividing the building into discrete vertical blocks, it may be possible to control the direction of airflow exchange in these blocks independently. Furthermore, it is observed that a vertical spacing of around 10 m between discrete resistance devices is sufficient to obtain similar results as with continuous banks of devices. A potential method of implementing the resistance device technique discussed is by mounting vertical axis wind turbines (VAWT) around the building perimeter. This implementation has the added

advantage of being able to harvest energy from the wind. Wind power generation by the use of VAWT's may help offset a significant portion of the electrical energy consumption of a building.

In a conventionally ventilated building, all the zones are supplied with airflow of the same quality (i.e., a mixture of outdoor and recirculated airflow). However, in a naturally ventilated building, it may not always be possible to supply fresh (i.e., outdoor) air to all the zones. Outdoor air entering a given zone may become partially polluted on account of pollutant sources present in the zone. This partially polluted air may then be used to ventilated other zones in the building before being exhausted to the ambient. Therefore, it is difficult to assess whether this partially polluted airflow is sufficient to meet the ventilation requirements of the other zones it may pass through. The ASHRAE-equivalent airflow metric developed in this work allows for the quantification of the ventilation quality provided to various zones of a building. Using this metric, it is possible to make a comparison with the well-established ASHRAE guidelines related to the amount of ventilation provided using a conventional HVAC system.

A potential method for optimal control of natural ventilation is demonstrated using a control framework consisting of two software packages coupled using a bridge developed at Syracuse University. The role of an objective function for this purpose is explained, and the ASHRAE-equivalent airflow metric developed is utilized in the definition of a few example objective functions. The simple control problems considered in this work demonstrate the utility of the resistance device concept for controlling the amount of ventilation provided to various zones in a building. It is observed that using this concept, it may be possible to satisfy ventilation requirement purely by manipulating the wind pressure distribution on

the envelope when the internal occupant distribution is non-uniform. However, sole use of this technique may be less effective for a uniform occupant distribution. Under such conditions, the optimization results suggest that it is advantageous to also exert control over the ventilation ports in the building envelope. It is possible to satisfy ventilation requirements very closely by allowing independent control over the port sizes.

The energy analysis performed for the cities of San Francisco and San Diego indicates that for airflow rates less than 2 ACH, it is not required to heat the ventilation airflow. For larger airflow rates, the heating energy requirements for San Francisco are significantly larger than those for San Diego. This is due to the fact that the external temperature in San Francisco is lower than that in San Diego for most of the year. Conversely, it is seen that the amount of cooling required decreases as the airflow rate increases. This is due to the fact that increasing the amount of airflow helps offset the internal heat gains within the building. The lower temperatures prevalent in San Francisco help reduce the amount of cooling to be provided in comparison to San Diego. These results indicate that a suitable strategy that may be implemented to reduce energy consumption is to reduce the amount of ventilation airflow while maintaining adequate IAQ during the cooling season, while increasing the amount of airflow provided during the cooling season, subject to concerns such as draft.

7   Future Work

The present work demonstrates the feasibility of utilizing various means of pressure manipulation for application in the natural ventilation of streamlined cross-section buildings. The resistance device concept is explored in detail, and is utilized in the simple problem explored for the purpose of studying control of natural ventilation. There are several aspects of this problem that may be explored in more detail.

The analysis performed to evaluate the presented techniques of building envelope wind pressure manipulation is purely computational. The validation of the CFD model conducted indicates that it is possible to predict pressure distribution for airfoils with uniform incoming flow. For a complete study, it is necessary to perform validation using the building cross-sections considered. Therefore, wind tunnel models of the cross-sections considered should be used to obtain experimental data for validation of the CFD model. In addition, the validation presented in this work does not address the issue of the resistance device concept. Therefore, it is necessary to incorporate these resistance devices in the wind tunnel model and validate the computational results obtained using this experimental data. The implication of unsteadiness due to vortex shedding along with wind fluctuations on the effectiveness of the proposed concept of controlling ventilated airflows should also be checked experimentally. In addition, the experimental work should include measurement of the airflows between zones, as well as between the zones and ambient. This aspect of the work may be challenging as it is difficult to obtain accurate estimates of inter-zonal airflows based on measurements of the airflow velocity between the zones.

An important question that arises is the applicability of the pressure manipulation

concepts discussed here for conventional building designs(i.e., rectangular cross-sections). The flow separation that is expected to occur at the sharp corners of such buildings may present a challenge in the implementation of these techniques. One potential method that may be investigated to address (mitigate) this phenomenon is the use of pressure manipulation techniques such as synthetic jets or vanes as disccused previously.

The quasi-steady assumption is made while performing the analysis in much of the present work. A more detailed study needs to account for transient behavior as well. For instance, the effect that resistance devices have on the envelope pressure distribution has been explored in detail, however, another factor that is of interest is the time that is taken for the envelope pressure distribution to change on introduction of the resistance devices. This is of interest as it is necessary to have an estimate of the time taken for the effects of the chosen control actions to manifest themselves. On a related note, it is also interesting to explore the effect of fluctuating wind on the performance of the concept. Similarly, in order to properly model the thermal behavior of the building interior, it is necessary to account for the thermal mass of the building. This can affect the rate at which the internal temperature changes during the occupied period, and therefore, can influence the thermal comfort. In addition, night cooling of the thermal mass is a technique that is widely used for the purposes of thermal regulation during the occupied period.

The control problem studied in the present work is a simple formulation that considers only the IAQ in the occupied spaces of the building. In practice, the thermal comfort of the occupants is another important factor determining the performance of the ventilation system. Therefore, for a more detailed study, this parameter should also be considered while judging the optimality of a chosen control action. This may be incorporated by

including a term related to the thermal comfort in an objective function, in addition to a term related to the prevalent IAQ. However, combining these parameters in a single objective function is complicated by the fact they are not directly comparable. One possible avenue to resolve this issue is by judging the effect that changes in these factors have on occupant productivity. There are some studies in the literature that aim to establish correlations between changes in productivity and changes in both IAQ and thermal comfort. As occupant productivity may be expressed in monetary terms, it then becomes possible to combine thermal comfort and IAQ in a single objective function, by comparing dollar values instead. However, productivity is a parameter that is difficult to quantify, and it may therefore be difficult to obtain an accurate picture of the manner in which it is affected by changes in IAQ and thermal comfort.

An alternative formulation that may be more appropriate is to incorporate the costs associated with conditioning the supply airflow. It is always possible to maintain good IAQ within a building by increasing the ventilation flow rate. However, as seen previously, depending upon the ambient conditions, this may increase the amount of energy consumption for heating/cooling the ventilation airflow, which is necessary for maintaining thermal comfort. Thus, the goals of providing good IAQ, and reducing energy consumption may conflict with each other. Therefore, this provides us with an alternative formulation wherein the goal is to minimize energy consumption for conditioning the ventilation airflow with the constraint that IAQ requirements within the building are satisfied.

Furthermore, the control problem considered utilizes a rather simple method for finding appropriate control actions (namely, using optimization routines in MATLAB). This technique involves exploring a large set of control actions, and choosing the action that

results in the lowest objective function value. This method is inefficient and does not guarantee a globally optimal solution. A more sophisticated approach might be to include information about the behavior of the system. An example of such a method is the linear quadratic regulator (LQR), which is used for the optimal control of a dynamic system [67]. This technique is applicable to systems governed by linear differential equations, with cost functions that are quadratic functions of the states of the system and the inputs. For example, the evolution of the CO_2 concentration in a well-mixed zone may be modeled by a first order differential equation. In this scenario, an objective function may be formulated by combining the zone CO_2 concentration and the ventilation airflow provided to the zone (input) with suitable weights. Then, the LQR method provides a sequence of control actions that is theoretically optimal (i.e., results in the minimum cost). It is of course necessary to supply weights that reflect the goals of the control problem. For instance, in this example, it may be useful to provide the input (airflows) with weights that reflect the costs associated with conditioning the supply airflows.

References

[1] US Department of Energy. Buildings energy data book. `http://www.wbdg.org/resources/psychspace_value.php`, May 2008.

[2] S. Roaf. Innovative approaches to the natural ventilation of buildings : the imperative for change. *Architectural Science Review*, 55(1):1–3, 2012.

[3] F. Allard, M. Santamouris, and S. Alvarez. *Natural ventilation in buildings : a design handbook.* James & James (Science Publishers) Ltd., 1998.

[4] W.J. Fisk and A.H. Rosenfeld. Estimates of improved productivity and health from better environments. *Indoor Air*, 7(3):158–172, 1997.

[5] R. Djukanovic, P. Wargocki, and P.O. Fanger. Cost-benefit analysis of improved air quality in an office building. In *Proceedings of Indoor Air*, Monterey, California, USA, 2002.

[6] O. Seppanen, W.J. Fisk, and Q.H. Lei. Ventilation and performance in office work. *Indoor Air*, 16(1):28–36, 2006.

[7] J. Cermak. Aerodynamics of buildings. *Annual Review of Fluid Mechanics*, 8:75–106, 1976.

[8] M.E. Fountain and E.A. Arens. Air movement and thermal comfort. *ASHRAE Journal*, 35(8):26–30, 1993.

[9] M.D. Ruud, J.W. Mitchell, and S.A. Klein. Use of building thermal mass to offset cooling loads. *ASHRAE Transactions*, 96(2):820–829, 1990.

[10] P. Heiselberg. Principles of hybrid ventilation. Technical Report ISSN 1395-7953 R0207, IEA ECBCS-Annex 35, 2002.

[11] D.W. Etheridge and B. Ford. Natural ventilation of tall buildings - options and limitations. In *CTBUH 8th World Congress*, Dubai, UAE, 2008.

[12] G. Brager, S. Borgeson, and Y.S. Lee. Control strategies for mixed-mode buildings. Technical report, Center for the Built Environment, University of California, Berkeley, 2007.

[13] C. Ghiaus, F. Allard, M. Santamouris, C. Georgakis, C.-A. Roulet, M. Germano, F. Tillenkamp, N. Heijmans, F. Nicol, E. Maldonado, M. Almeida, G. Guarracino, and L. Roche. Natural ventilation in urban buildings - summary of urbvent project. In *Proceedings of Passive and Low Energy Cooling for the Built Environment*, Santorini, Greece, 2005.

[14] R.J. DeDear and G.S. Brager. Thermal comfort in naturally ventilated buildings: revisions to ashrae standard 55. *Building and Environment*, 34(6):549–561, 2002.

[15] J.F. Nicol and M.A. Humphreys. Adaptive thermal comfort and sustainable thermal standards for buildings. *Energy and Buildings*, 34(6):563–572, 2002.

[16] J.W. Axley and S.J. Emmerich. A method to assess the suitability of a climate for natural ventilation of commercial buildings. In *Proceedings of Indoor Air*, Monterey, California, USA, 2002.

[17] J.S. Emmerich, A.K. Persily, W.S. Dols, and J.W. Axley. Impact of natural ventilation strategies and design issues for california applications, including input to ashrae standard 62 and california title 24. Technical Report 7062, 2003.

[18] S. J. Emmerich and J. Crum. Simulated performance of natural and hybrid ventilation systems in an office building. Technical Report 611-40076-01, Air Conditioning and Refrigeration Technology Institute, 2005.

[19] P. Heiselberg. The hybrid ventilation process - theoretical and experimental work. *Air Infiltration Review*, 21(1):1–4, 1999.

[20] M. Liddament, J. Axley, P. Heiselberg, Y. Li, and T. Stathopoulos. Achieving natural and hybrid ventilation in practice. *International Journal of Ventilation*, 5(1), 2006.

[21] T. Pasquay. Natural ventilation in high-rise buildings with double facades, saving or waste of energy. *Energy and Buildings*, 36(4):381–389, 2004.

[22] E. Ring and G.S. Brager. Occupant comfort, control, and satisfaction in three california mixedmode office buildings. In *Proceedings of the ACEEE Summer Study on Energy Efficiency in Buildings*, Pacific Grove, California, USA, 2000.

[23] Y. Jiang, D. Alexander, H. Jenkins, R. Arthur, and Q. Chen. Natural ventilation in buildings: Measurement in a wind tunnel and numerical simulation with large eddy simulation. *Journal of Wind Engineering and Industrial Aerodynamics*, 91(3):331–353, 2001.

[24] D. Etheridge and J. Nolan. Ventilation measurements at model scale in a turbulent flow. *Building and Environment*, 14(1):53–64, 1979.

[25] P. Karava, T. Stathopoulos, and A.K. Athienitis. Wind-induced natural ventilation analysis. *Solar Energy*, 81(1):20–30, 2007.

[26] A. Mochida, H. Yoshimoto, T. Takeda, T. Kakegawa, and S. Miyauchi. Methods for controlling airflow in and around a building under cross-ventilation to improve indoor

thermal comfort. *Journal of Wind Engineering and Industrial Aerodynamics*, 93(6):437–449, 2005.

[27] P. Heiselberg, E. Bjorn, and P.V. Nielsen. Impact of open windows on room airflow and thermal comfort. *International Journal of Ventilation*, 1(2):91–100, 2001.

[28] ASHRAE. Handbook of fundamentals. Technical report, ASHRAE, 2005.

[29] M. Deru and P. Burns. Infiltration and natural ventilation model for whole-building energy simulation of residential buildings. In *ASHRAE Conference*, Kansas City, Missouri, USA, June 28 - July 2 2003.

[30] M. Orme. Applicable models for air infiltration and ventilation calculations. Technical Report AIC-TN-51-1999, Air Infiltration and Ventilation Centre, 1999.

[31] M.H. Sherman and D.T. Grimsrud. Infiltration-pressurization correlation: Simplified physical modeling. Technical Report LBL-10163, Lawrence Berkeley National Laboratory, 1980.

[32] G. Walton and W.S. Dols. Contam 2.4 user guide and program documentation. Technical report, National Institute of Standards and Technology, 2005.

[33] G. Binder. *Tall buildings of Europe, the Middle East and Africa*. Images Publishing Group, 2006.

[34] J.W. Axley. Application of natural ventilation for u.s. commercial buildings - climate suitability, design strategies & methods, modeling studies. Technical Report GCR-01-820, National Institute of Standards and Technology, 2001.

[35] P.F. Linden. The fluid mechanics of natural ventilation. *Annual Review of Fluid Mechanics*, 31:201–238, 1999.

[36] P. Irwin, J. Kilpatrick, J. Robinson, and A. Frisque. Wind and tall buildings : Negatives and positives. *The Structural Design of Tall and Special Buildings*, 17(5):915–928, 2008.

[37] S. Aggerholm. Control of hybrid ventilation systems. *International Journal of Ventilation*, 1(4), 2003.

[38] G. Carrilho da Graca, P.F. Linden, and P. Haves. Design and testing of a control strategy for a large, naturally ventilated office building. *Building Services Engineering Research and Technology*, 25(3):271–287, 2004.

[39] A. Mahdavi and C. Proglhof. A model-based approach to natural ventilation. *Building and Environment*, 43(4):620–627, 2008.

[40] M. Kummert and P. Andre. Simulation of a model-based optimal controller for heating systems under realistic hypotheses. In *Ninth International IBPSA conference*, Montreal, Quebec, Canada, 2005.

[41] M. Mozer, L. Vidmar, and R. Dodier. The neurothermostat : Predictive optimal control of residential heating systems. *Adv. in neural info. proc. systems*, 9:953–959, 1997.

[42] H.C. Spindler and L. Norford. Naturally ventilated and mixed-mode buildings - part ii: optimal control. *Building and Environment*, 44(4):750–761, 2009.

[43] A.I. Dounis, M.L. Bruant, G. Guarracino, and M. Michel. Indoor air-quality control by a fuzzy reasoning machine in naturally ventilated buildings. *Applied Energy*, 54(1):11–28, 1996.

[44] D. Kolokotsa, K. Niachou, V. Geros, K. Kalaitzakis, G.S. Stavrakakis, and M. Santamouris. Implementation of an integrated indoor environment and energy management system. *Energy and Buildings*, 37(1):93–99, 2005.

[45] R. Alcala, J. Casillas, O. Cordon, A. Gonzalez, and F. Herrera. A genetic rule weighting and selection process for fuzzy control of heating, ventilating and air conditioning systems. *Engineering Applications of Artificial Intelligence*, 18(3):279–296, 2005.

[46] A. Shepherd and W. Batty. Fuzzy control strategies to provide cost and energy efficient high quality indoor environments in buildings with high occupant densities. *Building Services Engineering Research and Technology*, 24(1), 2003.

[47] D. Kolokotsa, A. Pouliezos, G. Stavrakakis, and S. Lazos. Predictive control techniques for energy and indoor environmental quality management in buildings. *Building and Environment*, 44(9):1850–1863, 2009.

[48] A.I. Dounis and C. Caraiscos. Advanced control systems engineering for energy and comfort management in a building environment – a review. *Renewable and Sustainable Energy Reviews*, 13(6-7):1246–1261, 2009.

[49] J.K. Ward, J. Wall, and C. Perfumo. Environmetally active buildings : the controls challenge. *Architectural Science Review*, 55(1):26–34, 2012.

[50] H.B. Rijal, P. Tuohy, M.A. Humphreys, J.F. Nicol, A. Samuel, and J. Clarke. Using results from field surveys to predict the effect of open windows on thermal comfort and energy use in buildings. *Energy and Buildings*, 39(7):823–836, 2007.

[51] M. El Mankibi and P. Michel. Development and assessment of hybrid ventilation

control strategies using a multicriteria approach. *Internation Journal of Ventilation*, 4(3), 2005.

[52] P. Blondeau, M. Sperandio, and F. Allard. Multicriteria analysis of ventilation in summer period. *Building and Environment*, 37(2):165–176, 2002.

[53] A. Glezer and M. Amitay. Synthetic jets. *Annual Review of Fluid Mechanics*, 34:503–529, 2002.

[54] G.D. Shrewsbury. Numerical study of a research circulation control airfoil using navier-stokes methods. *AIAA Journal of Aircraft*, 26(1):29–34, 1989.

[55] N.A. Dimmock. An experimental introduction to the jet flap. Technical Report 344, Aeronautical Research Council, 1957.

[56] P.M. Pelken. Research agenda: Integrierte wind technologien. *XIA Intelligente Architektur, Zeitschrift fuer Architektur und Technik*, July-September 2009.

[57] P. Land. Innovations in sustainability at height: Experimental tall buildings. In *CTBUH 8th World Congress*, 2008.

[58] H.K. Versteeg and W. Malalasekara. *An introduction to computational fluid dynamics : the finite volume method*. Prentice Hall, 2007.

[59] J. Anderson. *Computational fluid dynamics*. McGraw-Hill, 1995.

[60] Ansys Fluent. Fluent user guide. Technical report, Ansys, 2011.

[61] N. Gregory and C.L. O'Reilly. Low-speed aerodynamic characteristics of naca 0012 aerofoil section, including the effects of upper surface roughness simulating hoar frost. Technical Report ARC R & M 3726, NASA Ames Research Center, 1970.

[62] K.W. Bullivant. Tests of the naca 0025 and 0035 airfoils in the full-scale wind tunnel. Technical Report 708, Langley Memorial Aeronautical Laboratory, NACA, 1940.

[63] A. Roshko. Experiments on the flow past a circular cylinder at very high reynolds number. *Journal of Fluid Mechanics*, 10(3):345–356, 1961.

[64] D. Demetriou and H.E. Khalifa. Evaluation of distributed environmental control systems for improving iaq and reducing energy consumption in office buildings. *Building Simulation*, 2(3):197–214, 2009.

[65] P.M. Pelken. Manipulation of air flow around high-rise structures through the integration of flow resistance devices. Private communication, 2012.

[66] F.C. McQuiston, J.D. Parker, and J.D. Spitler. *Heating, ventilating, and air conditioning : analysis and design.* J. Wiley & Sons, 2005.

[67] J.S. Bay. *Fundamentals of Linear State Space Systems.* McGraw-Hill, 1999.

Prasad Sivakumar

Curriculum Vitae

Mechanical and Aerospace Engineering
Syracuse University
263 Link Hall
Syracuse, NY 13210

902 Ivy Ridge Rd.,
Syracuse, NY 13210
315-420-2621 (cell)
prasad.sivakumar@gmail.com
DOB: April 30, 1984

Research Interests
: Computational fluid dynamics, natural ventilation of buildings, fluid mechanics, heat transfer, thermodynamics

Education

Doctor of Philosophy, Mechanical and Aerospace Engineering — *December 2012*
Syracuse University, Syracuse NY
Thesis: Building envelope wind pressure manipulation for application in streamlined high-rise buildings
Advisor: Dr. Thong Q. Dang

Master of Science, Mechanical and Aerospace Engineering — *May 2008*
Syracuse University, Syracuse, NY
Advisor: Dr. Thong Q. Dang

Bachelor of Engineering, Mechanical Engineering — *June 2006*
University of Mumbai, Mumbai, India

Experience

Syracuse University — 2008-2012

Teaching assistant, MAE 571 : Computational Fluid Dynamics	*Spring 2012*
Teaching assistant, AEE 343 : Compressible Flow	*Spring 2012*
Teaching assistant, MAE 341 : Fluid Mechanics	*Fall 2012*
Teaching assistant, MAE 571 : Computational Fluid Dynamics	*Spring 2011*
Teaching assistant, AEE 343 : Compressible Flow	*Spring 2011*
Teaching assistant, MAE 341 : Fluid Mechanics	*Fall 2011*
Teaching assistant, MAE 571 : Computational Fluid Dynamics	*Spring 2010*
Teaching assistant, AEE 342 : Aerodynamics	*Spring 2010*
Teaching assistant, MAE 341 : Fluid Mechanics	*Fall 2009*
Teaching assistant, MAE 571 : Computational Fluid Dynamics	*Spring 2009*
Teaching assistant, ECS 104 : Engineering Computational Tools	*Spring 2009*
Teaching assistant, MAE 341 : Fluid Mechanics	*Fall 2008*

Doctoral Research — *2008 - 2012*

Investigated potential for manipulating wind pressure distribution around the perimeters of buildings of different cross-sections using CFD studies

Investigated performance of model predictive control strategies for natural ventilation by utilizing MATLAB and multi-zone airflow simulation packages

Technical Skills	*Computational fluid dynamics:* Fluent, Gambit, Pointwise, Gridgen	
	Solid modeling: AutoCAD, Solidworks	
	Computer programming: Matlab, Fortran, C/C++	
Professional Activities	Paper peer-reviewer, IAQVEC Conference	*2010*
Journal Publications	**Sivakumar, P.**, Palanthandalam-Madapusi, H.J., Dang, T.Q. "Control of natural ventilation for aerodynamic high-rise buildings", Building Simulation, Vol. 3(4), pp. 311-325.	*2010*
	Sivakumar, P., Dang, T.Q. "Building envelope wind pressure manipulation for streamlined high-rise buildings", *to be submitted to the International Journal of Ventilation.*	*2010*
Conference Publications (Peer-Reviewed)	Dang, T.Q., Khalifa, H.E., Pai, N., **Sivakumar, S.** "Manipulation of building envelope wind pressure loading via moveable flow-resistance devices", In Proceedings of the 11th International Conference of Indoor Air Quality and Climate, Copenhagen, Denmark, August 17 -22.	*2008*
	Sivakumar, P., Palanthandalam-Madapusi, H.J., Dang, T.Q., Khalifa, H.E., "Performance criteria for an intelligent centralized controller for natural ventilation", In Proceedings of the 9th International Conference and Exhibition: Healthy Buildings, Syracuse, NY, September 13 - 19.	*2009*
	Sivakumar, P., Palanthandalam-Madapusi, H.J., Dang, T.Q., "Centralized optimal model-predictive control for natural ventilation", In Proceedings of 7th International Conference on Indoor Air Quality, Ventilation and Energy Conservation in Buildings, IAQVEC, Syracuse, NY, August 15 - 18.	*2010*